Université de Montréal

Relevé polarimétrique d'étoiles candidates pour des disques de débris

par

Amélie Simon

Département de physique

Faculté des arts et des sciences

Mémoire présenté à la Faculté des études supérieures

en vue de l'obtention du grade de

Maître ès sciences (M.Sc.)

en physique

Août, 2010

Université de Montréal

Faculté des études supérieures

Ce mémoire intitulé:

Relevé polarimétrique d'étoiles candidates pour des disques de débris

présenté par:

Amélie Simon

a été évalué par un jury composé des personnes suivantes:

Serge Demers,	président-rapporteur
Pierre Bastien,	directeur de recherche
Gilles Fontaine,	membre du jury

Mémoire accepté le: _____

Sommaire

Le relevé DEBRIS est effectué par le télescope spatial Herschel. Il permet d'échantillonner les disques de débris autour d'étoiles de l'environnement solaire. Dans la première partie de ce mémoire, un relevé polarimétrique de 108 étoiles des candidates de DEBRIS est présenté. Utilisant le polarimètre de l'Observatoire du Mont-Mégantic, des observations ont été effectuées afin de détecter la polarisation due à la présence de disques de débris. En raison d'un faible taux de détection d'étoiles polarisées, une analyse statistique a été réalisée dans le but de comparer la polarisation d'étoiles possédant un excès dans l'infrarouge et la polarisation de celles n'en possédant pas. Utilisant la théorie de diffusion de Mie, un modèle a été construit afin de prédire la polarisation due à un disque de débris. Les résultats du modèle sont cohérents avec les observations.

La deuxième partie de ce mémoire présente des tests optiques du polarimètre POL-2, construit à l'Université de Montréal. L'imageur du télescope James-Clerk-Maxwell passe de l'instrument SCUBA à l'instrument SCUBA-2, qui sera au moins cent fois plus rapide que son prédécesseur. De même, le polarimètre suit l'amélioration et un nouveau polarimètre, POL-2, a été installé sur SCUBA-2 en juillet 2010. Afin de vérifier les performances optiques de POL-2, des tests ont été exécutés dans les laboratoires sub-millimétriques de l'Université de Western Ontario en juin 2009 et de l'Université de Lethbridge en septembre 2009. Ces tests et leurs implications pour les observations futures sont discutés.

Mots clés : diffusion — étoiles : individuelles (HR 8799, HD 115404) — instrumentation : polarimètres — matière circumstellaire — polarisation — relevés

Abstract

The DEBRIS survey, being performed by the space telescope Herschel, is an unbiased sampling of the debris disks candidates in the solar neighbourhood. In the first part of this thesis, a ground-based polarimetric survey of 108 DEBRIS candidate stars is presented. Using the polarimeter, "La Belle et la Bete," at the Mont-Megantic Observatory, observations were carried out in order to detect polarization induced by the presence of a debris disk. Due to a low rate of detection, a statistical analysis was performed to compare the polarization between stars owning a debris disk with stars without one. Using Mie scattering theory, a basic model was constructed to estimate the level of polarization produced by dust grains in a debris disk. The results of this model are consistent with our observations.

The second part of the thesis presents the optical tests of the polarimeter POL-2, built at Université de Montréal. The James Clerk-Maxwell-Telescope imager SCUBA has been upgraded to SCUBA-2, which is more than one hundred times faster than its predecessor with 500 times more pixels. Likewise, the polarimeter follows the improvement as a new polarimeter, POL-2, was installed on SCUBA-2 in July 2010. In order to verify the optical performance of POL-2, tests were completed at the submillimeter laboratories at the University of Western Ontario in June 2009, and the University of Lethbridge in September 2009. These tests and their implications for future observations are discussed.

Key words : circumstellar matter — instrumentation: polarimeters — scattering — stars: individual (HR 8799, HD 115404) — surveys — polarization

Table des matières

Liste des tableaux

Table des figures

Abréviations

CCD	Charged Coupled Device
CHARA	The Center for High Angular Resolution Astronomy
DEBRIS	Disc Emission via a Bias-free Reconnaissance in the Infrared/Submillimetre
FTS	Fourier Tranform Spectrometer
FWHM	Full Width at Half Maximum
HDPE	High Density PolyEthylene
IRAS	Infrared Astronomical Satellite
ISO	Infrared Space Observatory
JCMT	James Clerk Maxwell Telescope
PACS	Photodetector Array Camera and Spectrometer
RPM	Rotation Per Minute
SCUBA	Submillimetre Common-User Bolometer Array
SPIRE	Spectral and Photometric Imaging Receiver
STIS	Space Telescope Imaging Spectrograph
SUNS	SCUBA-2 Unbiased Nearby Stars
UOL	University of Lethbridge
UWO	University of Western Ontario

Sigles

Å	Ångström
M_d	Mass du disque
M_J	Masse de Jupiter
M_T	Masse terrestre
$M_\odot$	Masse solaire

A Pierre Olivier, Nicole et Guillaume

Remerciements

Je tiens à remercier tous mes collègues de travail : Rémi Fahed pour avoir répondu avec brio à toutes mes questions, Noemi Giammichele pour son aide généreuse, Cassandra Bolduc pour sa bonne humeur, Marie-Michèle Limoges pour avoir donné de son temps si généreusement, Sandie Bouchard pour son aide précieuse en galactique, Mathieu Vick pour ses bleuets frais, Antoine de la Chevrotière pour ses décorations d'un goût certain, Patrick Ingraham pour avoir patiemment corrigé mon anglais, Lison Malo pour la générosité de son temps, Marilyn Latour d'être ma colocataire durant les conférences, Marie-Eve Naud pour ses bons conseils, ainsi que tous les autres qui ont pris le temps de répondre à mes questions et qui m'ont aidée à avancer ce projet. Merci à Emilie Storer pour son excellent travail. Merci aux techniciens de l'Observatoire du Mont-Mégantic : Pierre-Luc Lévesque, Ghislain Turcotte, Bernard Malenfant. Merci à Pierre Bastien pour sa disponibilité, sa patience et merci de m'avoir permis de faire cette maîtrise.
Merci à mes proches qui m'ont encouragée tout au long de cette maîtrise. Merci à mes parents qui m'ont permis d'avoir un rêve et de le poursuivre. Merci à Volny de m'avoir encouragée à faire des études, mais qui viendrait me voir même si j'étais devenue coiffeuse à Carpentras. Merci à ma famille pour leur compréhension lors de mes nombreuses absences aux évènements familiaux pour cause d'observations, de conférences... Merci tout particulièrement à ma grand-mère Denise pour sa bonne humeur, son grand coeur. Merci à mes grands-parents Mitsou et André qui me suivent de loin mais auxquels je pense beaucoup. Et enfin, un grand merci à Pierre Olivier, attentionné, sensible, drôle, généreux. Merci de m'aider à atteindre mon rêve, merci d'être à mes côtés quand j'en ai le plus besoin, merci pour tous les moments de bonheur partagés.

Chapitre 1

Introduction

1.1 Relevé polarimétrique d'étoiles candidates pour des disques de débris

Les disques de débris sont des disques circumstellaires formés de particules de poussières, éventuellement de planétésimaux et ils ne contiennent que peu ou pas de gaz. Ils sont typiquement constitués de grains de poussière de 1 à 100 μm et sont situés entre 10 et 100 UA de leur étoile hôte. Ils absorbent une partie de l'énergie stellaire dans l'UV et irradient celle-ci dans l'infrarouge, ayant des températures à l'équilibre entre 50 et 120 K.

1.1.1 Les disques de débris du système solaire

Le système solaire possède trois disques de ce type : la ceinture de Kuiper, la ceinture d'astéroïdes et le nuage zodiacal. La ceinture de Kuiper s'étend au delà de l'orbite de Neptune, entre 30 et 55 UA. Elle est principalement composée de petits corps et trois planètes naines y ont été détectées : Pluton, Matemake et Haumea. Sa masse est estimée à 10^{-1}M$_\oplus$ (Delsanti & Jewitt 2006). La ceinture d'astéroïdes est située entre l'orbite de Mars et celle de Jupiter à environ 3 UA. Elle est constituée de la majorité des astéroïdes connus. Elle possède une planète naine : Cérès. Sa masse totale est évaluée à 6×10^{-4} M$_\oplus$ (Krasinsky et al. 2002). Le nuage zodiacal, responsable de la lumière zodiacale, s'étend jusqu'à environ 3 UA et a une masse d'approximativement 10^{-9} M$_\oplus$ (Ipatov & Mather 2006). La plupart des disques extra-solaires

détectés jusqu'à présent ressemblent à la ceinture de Kuiper, mais avec plusieurs magnitudes de poussières en plus. Les instruments actuels ne nous permettent pas de détecter des disques de débris aussi ténus que ceux du système solaire.

1.1.2 Véga, première étoile extra-solaire possédant des corps solides

Le premier disque de débris extra-solaire a été découvert autour de Véga en 1984 par Aumann et al. (d'où le nom d'étoiles de type Véga pour les étoiles possédant un disque de débris). C'est lors d'observations routinières de calibration de Véga, que l'équipe d'IRAS découvrit que cette étoile avait une émission dans les longueurs d'ondes infrarouges bien supérieures à l'émission due à la photosphère uniquement. IRAS est un télescope spatial de 0.57 m lancé en 1983, ayant pour mission de réaliser un relevé complet du ciel dans les bandes infrarouges centrées sur 12, 25, 60 et 100 μm. Véga (aussi nommée α Lyrae) est une étoile A0V d'environ 10 000 K, c'est une étoile de calibration photométrique de l'hémisphère nord. Elle a été observée comme telle par IRAS, dans un mode de calibration qui était plus précis que dans le cas d'observations faites lors du relevé du ciel.

En extrapolant l'émission d'un corps noir à 10 000 K, Aumann et al. (1984) ont conclu que l'excès observé par rapport à l'émission de la photosphère seule est de 16 à 100 μm. Aucun excès n'avait été détecté jusqu'à des longueurs d'ondes de 20 μm jusqu'alors. Puisque la perte de masse de l'étoile est inférieure à $10^{-12}\mathrm{M}_{\odot}\mathrm{an}^{-1}$, ils ont déduit que la source de cet excédent était des poussières en équilibre thermique avec l'étoile. En modélisant cet excès, ils ont conclu que les grains de poussière étaient à 85 UA de l'étoile, qu'ils avaient un rayon de l'ordre du millimètre et qu'ils possédaient une température de 85 K. Ils ont d'abord inféré que cet excès provenait d'un disque protoplanétaire mais une étude plus approfondie des étoiles Véga, Fomalhaut et β Pictoris a résulté en l'excitante découverte que ces objets étaient les premières étoiles de la séquence principale, mis à part notre soleil, qui possèdent des matériaux solides, sans avoir une perte de masse significative (Gillett 1986).

Le disque de débris de Véga a été résolu grâce au télescope spatial Spitzer, voir l'article

de Su et al. (2005). Ils en ont déduit qu'il s'étend de 70 à 815 UA, les particules ont une taille entre 1 et 50 μm et la masse totale des poussières du disque serait de 3×10^{-3} $M_{\oplus}$. Il est intéressant de noter qu'environ dix ans avant la première détection de planètes extra-solaires nous avions des preuves indirectes de la présence de corps rocheux autour d'étoiles autre que le soleil.

1.1.3 La formation de disques de débris

Une partie de la lumière de l'étoile est absorbée par les particules de poussière et ré-émise sous forme de radiation infrarouge. Cette émission provoque une chute en spirale des particules vers le Soleil et leur destruction, connue sous le nom d'effet Poynting-Robertson. Lorsque le disque de débris est dense, ce qui est le cas pour la plupart des disques détectés jusqu'à ce jour, les grains de poussières ont une grande probabilité d'entrer en collision les uns avec les autres. Si la trajectoire d'un grain de poussière est trop perturbée, il sera éjecté du disque par la pression de radiation. Ainsi, les disques de débris ont une durée de vie courte, jusqu'à dix millions d'années. Cependant, ils sont présents autour d'étoiles de tout âge, ce qui implique la présence d'un mécanisme continuel de remplissage du disque (Backman & Paresce 1993). Celui-ci est la collision de planétésimaux et la sublimation de comètes (Williams & Wetherill (1994), Wyatt & Dent (2002), Thébault & Augereau (2007)). Ces processus dynamiques créant ces disques contiennent des informations sur la présence de corps rocheux. La distribution spatiale du disque, sa forme et les caractéristiques des poussières le constituant sont autant d'informations sur les planétésimaux, sur l'évolution du système et sur la possible présence de planètes.

Observer des disques de débris est un outil précieux pour étudier les corps solides autour d'étoiles et pour comprendre la dynamique des systèmes planétaires (voir Wyatt (2008), Krivov (2010) pour des revues récentes). Par exemple, s'il y avait une production continue de poussières formant un disque tel qu'observé autour de Véga durant l'intégralité de sa vie, une masse initiale de planétésimaux de plusieurs centaines de fois la masse de Jupiter serait nécessaire. Il est plus probable que la poussière observée autour de Véga provienne d'une collision récente

de comètes ou d'astéroïdes de masses moyennes. Le disque de Véga serait donc relativement jeune par rapport à l'étoile et devrait disparaître en l'absence de nouvelles collisions (Su et al. 2005).

1.1.4 Planètes et disques de débris

Il est possible d'utiliser les disques de débris résolus pour inférer la présence de planètes qui perturbent le disque. Des observations de Véga au télescope CHARA, réseau de six télescopes de 1 m de diamètre, au Mont Wilson (USA), ont permis de détecter un anneau intérieur de poussières, à 8 UA. Ces poussières seraient la preuve de perturbations dynamiques existant au sein du système. Ce qui pourrait être dû à un intense bombardement cométaire ou météoritique, comparable au grand bombardement tardif et pourrait donc être la preuve de la présence d'un système planétaire (Absil et al. 2006). De plus, des irrégularités dans le disque suggèrent la présence d'au moins une exoplanète, probablement de la taille de Neptune, en orbite autour de l'étoile. Celle-ci aurait migré de 40 UA à 65 UA en 56 millions d'années et aurait alors perturbé le disque en y créant des surdensités (Wyatt 2003). Le disque de β Pictoris a été résolu par l'instrument STIS du télescope spatial Hubble (Heap et al. 2000). Le disque est gauchi, ce phénomène peut être expliqué par la présence d'une planète, d'une masse de 4 M_J, si elle est à 10 UA et si l'étoile a 20 millions d'années. Une conclusion équivalente peut être produite pour l'étoile Fomalhaut (Kalas et al. 2005).

Beichman et al. (2005) ont décelé une corrélation entre la présence de planètes et celle de disques de débris. Cependant, ce résultat est controversé car il n'a pas été confirmé par Kóspál et al. (2009) ou Bryden et al. (2009). Dans tous les cas, pour les disques résolus, leur grande extension suggère la présence de planétésimaux qui perturbent le disque (Backman & Paresce 1993). Puisque la formation planétaire a une incidence sur les disques de débris (Wyatt 2008), dans le cas de notre système solaire, les disques de la ceinture de Kuiper et de la ceinture d'astéroïdes ont évolué avec le temps : ils étaient beaucoup plus massifs par le passé (Stern (1996), O'Brien et al. (2007)) et leur position aurait pu changer à travers les âges (Gomes et al. (2005), Thommes et al. (2007)).

Afin d'aiguiser les modèles de disques de débris, de contraindre leur évolution, et de connaître leurs caractéristiques, nous avons besoin d'un relevé non-biaisé. Ce sera possible grâce au relevé DEBRIS du télescope spatial Herschel.

1.1.5 Relevés de disques de débris

Entre la parution de la découverte du disque de débris autour de Véga en 1984 et la parution de la première revue sur les disques de débris en 1993 par Backman, environ 100 étoiles, de tous types et de tous âges, étaient déjà cataloguées comme possédant des disques circumstellaires. En 2002, dernière date à laquelle la base de données de disque de débris de l'Observatoire Royal d'Edimbourg a été mis à jour, 900 étoiles possédaient un disque de débris. Des relevés effectués dans les longueurs d'ondes infrarouges, principalement grâce aux télescopes IRAS, ISO et Spitzer, il est apparu qu'environ 15% des étoiles de la séquence principale possède un disque circumstellaire (Backman & Paresce (1993), Plets & Vynckier (1999)). Cependant, cette fraction pourrait être aussi grande que 25% car il existe des évidences de la présence de disques de débris trop froids pour avoir été détectés par les relevés dans les longueurs d'ondes infrarouge. Par exemple, Wyatt (2003) ont observé 22 étoiles dans les longueurs d'ondes sub-millimétriques, à 850 μm, au télescope du JCMT. Trois d'entre elles possèdent des disques de débris, disques qui n'avaient pas encore été détectés par les télescopes IRAS et ISO. Selon leur estimation, 9 à 14% des étoiles pourraient posséder des disques non détectables dans les longueurs d'ondes infrarouges. Lestrade et al. (2006) sont arrivés à une conclusion équivalente. Une telle proportion d'étoiles qui possèdent des disques de débris en font un sujet incontournable.

1.1.6 Le télescope spatial Herschel

Herschel est un télescope spatial de l'Agence Spatiale Européenne, il possède le plus grand miroir construit pour un télescope spatial, avec un diamètre de 3.5 m. Lancé avec succès le 14 mai 2009, il est désormais au deuxième point de Lagrange du système Terre-Soleil. Observant dans les longueurs d'ondes infrarouges et sub-millimétriques, entre 55 et 671 μm, il est refroidi

de manière passive à une température de 85 K. Les principaux objectifs scientifiques de Herschel sont : l'examen de la formation des galaxies dans l'univers primitif et de son évolution, l'examen de la création des étoiles et de leur interaction avec le milieu interstellaire, l'observation de la composition des atmosphères à la surface des comètes, des planètes et des satellites et l'examen de la chimie moléculaire de l'univers. Herschel possède trois instruments, un spectromètre à haute résolution : HIFI et deux caméras/spectrographes à résolution moyenne : PACS et SPIRE (Pilbratt et al. 2010).

1.1.7 Les instruments PACS et SPIRE

PACS est à la fois un spectromètre et un imageur. Il utilise deux grilles de photoconducteurs de 16×25 pixels pour de la spectroscopie de champ intégral et deux grilles de bolomètres de 16×32 et de 32×64 pixels pour de l'imagerie photométrique. Dans le mode photométrique, il observe simultanément dans deux bandes : à 60-85 μm ou à 85-125 μm et à 125-210 μm avec un champ de $1.75' \times 3.5'$(Poglitsch et al. 2010).

L'instrument SPIRE est un spectromètre et un photomètre. Le spectromètre a un champ d'opération allant de 194 à 671 μm. Le champ est presque circulaire, avec un diamètre de 2.6'. Le mode photométrique opère simultanément dans trois bandes spectrales à 250, 350 et 500 μm, il utilise des bolomètres qui sont refroidis à 0.3 K. Le champ de vue est de $4' \times 8'$(Griffin et al. 2010).

Ce sont les modes photométriques qui vont être utilisés pour le relevé DEBRIS.

1.1.8 Le relevé DEBRIS

Un des projets clés d'Herschel est le relevé DEBRIS, relevé limité par le flux. Il consiste en 446 étoiles de l'environnement proche du Soleil. Les cibles ont été sélectionnées selon leur distance et leur type spectral, ce sont les ≈90 étoiles les plus proches, dans le champ d'Herschel, de chaque type spectral A, F, G, K et M. Pour une description du relevé DEBRIS voir : Matthews et al. 2010b, en préparation, pour la sélection des cibles voir Phillips et al. (2010). Les

observations sont réalisées à 100 μm et 160 μm utilisant l'instrument PACS (Poglitsch et al. 2010) avec un suivi d'environ 100 cibles à 250, 350 et 500 μm avec l'instrument SPIRE (Griffin et al. 2010). Les cibles ont été sélectionnées de la même façon pour le relevé SUNS du JCMT (à 850 μm) et le relevé DEBRIS, 356 étoiles sont en commun entre ces deux relevés (Phillips et al. (2010), Matthews et al. (2007)). Le télescope spatial Spitzer a déjà permis d'observer 196 des cibles de DEBRIS (Matthews et al. 2010b, en préparation). Ainsi, la couverture spectrale peut aller de 24 à 850 μm pour certaines étoiles. Les étoiles les plus éloignées sont à 9, 16, 21, 24 et 46 pc pour les étoiles M, K, G, F et A respectivement.

Observer dans l'environnement proche du soleil fournit un échantillon qui couvre une large gamme de paramètres stellaires pour lesquels une littérature riche existe déjà. La probabilité de trouver des disques sera plus grande, ainsi que de les résoudre dans l'espace. Puisque les cibles sont seulement sélectionnées grâce à leur distance et leur type spectral, l'échantillon DEBRIS n'est pas biaisé. Il permettra de contraindre les propriétés des disques en fonction de l'âge de l'étoile, de sa masse stellaire, de sa métallicité, de la présence de planètes, de la morphologie du système, de la multiplicité... Les premiers résultats de DEBRIS sont donnés dans l'article de Matthews et al. (2010a) qui rend compte de disques résolus spatialement par Herschel.

Nous avons utilisé la liste des cibles de DEBRIS pour le relevé polarimétrique effectué à l'Observatoire du Mont-Mégantic. Ainsi, nous tirons partie de la sélection minutieuse des étoiles faite par l'équipe de DEBRIS et l'observation en polarimétrie peut apporter des contraintes supplémentaires sur les disques.

1.1.9 La polarimétrie de disques de débris

La plupart des disques de débris ont été détectés grâce à un excès de flux dans les longueurs d'ondes infrarouge/sub-millimétrique par rapport au flux photosphérique de l'étoile. L'excès de flux provient des poussières chauffées par l'étoile qui vont émettre de la radiation thermique. Cependant, les disques de débris peuvent aussi être détectés par polarimétrie car la poussière

du disque diffuse la lumière et la polarise. La polarisation est un indicateur de la forme, de la taille et de la composition des grains. Une telle polarisation a déjà été trouvée autour de disques résolus, tel le disque de l'étoile β Pictoris (Gledhill et al. (1991), Wolstencroft et al. (1995), Tamura et al. (2006)) et celui de AU Microscopii (Graham et al. 2007). La polarisation de disques de débris a aussi été détectée autour d'étoiles possédant des disques circumstellaires non résolus : Bhatt & Manoj (2000) ont comparé la polarisation d'étoiles avec de la matière circumstellaire avec celles qui n'ont pas de disques. Oudmaijer et al. (2001), Eritsyan et al. (2002), Tamura & Fukagawa (2005), Chavero et al. (2006) et Wiktorowicz et al. (2010) ont présenté des mesures polarimétriques d'étoiles avec des excès dans l'infrarouge.

1.2 POL-2, un nouveau polarimètre pour le JCMT

La partie instrumentale de ce mémoire consiste en des tests optiques effectués pour vérifier le bon fonctionnement du polarimètre POL-2. Les tests en laboratoire et la rédaction des rapports de ces tests ont été effectués dans le cadre de ma maîtrise.

1.2.1 Le relevé SUNS

La sélection des cibles pour les relevés SUNS du télescope JCMT et DEBRIS du télescope Herschel a été faite de la même manière. Le relevé SUNS devait initialement comprendre les 100 étoiles les plus proches, dans le champ du JCMT, de chaque type spectral A, F, G, K et M. Cependant, la construction et la mise en route de SCUBA-2 ont été retardées et il est possible qu'une partie des cibles du relevé SUNS ne puisse être observée par manque de temps. Pour les cibles observées par le JCMT et Herschel, une large couverture spectrale allant de 100 à 850 μm permettra d'avoir de précieuses contraintes sur les disques de débris. De plus, le JCMT a été doté d'un polarimètre : POL-2, construit à l'Université de Montréal. Il sera possible de détecter la polarisation de la lumière due aux poussières des disques de débris, si ce dernier est assez massif.

1.2.2 L'instrument POL-2

POL-2 est un polarimètre constitué de deux polariseurs en grilles et d'une lame demi-onde achromatique. Les polariseurs servent d'analyseur et de calibrateur. La lame demi-onde tourne continuellement permettant de faire des observations rapides et de s'affranchir des fluctuations de l'atmosphère. Ceci est possible grâce à SCUBA-2, qui peut observer jusqu'à 500 fois plus rapidement que son prédecesseur SCUBA et qui possède un détecteur de type CCD avec environ 10 000 pixels.

Des tests optiques du polarimètre POL-2 ont été effectués afin de vérifier s'il satisfaisait les attentes portées aux instruments du JCMT. Ces tests ont fait parti de ma maîtrise et ils sont présentés dans les annexes C et D.

1.3 Présentations des articles et des annexes

Dans ce mémoire, nous présenterons dans une première partie les aspects observationnel et théorique qui constituent ma maîtrise : l'article rendant compte des observations polarimétriques d'étoiles du relevé DEBRIS, au télescope de l'Observatoire du Mont-Mégantic (Québec, Canada), voir la section 2. Une mise en contexte est donnée dans la section 2.2, les observations sont présentées dans la section 2.3.1. Les résultats sont donnés dans la section 2.3.2, ils seront discutés dans la section 2.4. Une étude de la littérature a été effectuée afin de comparer la polarisation d'étoiles avec des disques de débris et celles sans détection d'excès dans l'infrarouge, voir la section 2.6. Une étude équivalente avait déjà été effectuée par Bhatt & Manoj (2000). L'annexe A est un guide pour analyser des données polarimétriques et dans l'annexe B le cas particulier des données du polarimètre la Belle et la Bête est discuté.

Nous poursuivrons par la partie instrumentale du mémoire qui consiste aux tests en laboratoire du polarimètre POL-2, qui est installé au JCMT, voir section 3. POL-2 est présenté dans la section 3.1. Les tests sont décrits dans les sections 3.2, 3.3 et 3.4. Les annexes C et D consistent aux rapports des tests optiques effectués dans les laboratoires sub-millimétriques

de l'Université de Western Ontario (UWO) et de l'Université de Lethbridge (UOL).

1.4 Contributions à l'article et aux rapports

Avant d'observer avec le polarimètre la Belle et la Bête, il a fallu remonter l'instrument, activité à laquelle j'ai participé, et faire quelques réparations. Lors de ma maîtrise, j'ai observé à l'Observatoire du Mont-Mégantic en trois séries, totalisant 25 nuits, dont 5 nuits claires. J'ai été accompagnée du Pr. Pierre Bastien durant la première série, puis j'ai observé seule pour les autres. J'ai créé un programme IDL pour analyser les données. Il pourra être utilisé dans le futur, notamment par M. Daniel Sarrazin qui continuera le projet et observera le reste des cibles de DEBRIS que je n'ai pu observées durant ma maîtrise. J'ai écrit des guides pour analyser les données, ils sont donnés dans les annexes A et B. Ils ont été utilisés par Mlle Kirthika Mohan pour analyser des observations que le Pr. Pierre Hily-Blant de l'Université de Grenoble et le Pr. Edith Falgarone de l'Ecole Normale Supérieure de Paris sont venus prendre au télescope du Mont-Mégantic avec la Belle et la Bête, en mars 2010.

J'ai produit la totalité de l'article, avec l'aide du Pr. Pierre Bastien, principalement sur les questions de modélisation de la polarisation dû à la présence d'un disque de débris. La recherche dans la littérature d'articles portant sur les étoiles possédant une polarisation importante et sur les relevés de disques de débris a été faite par Mlle Emilie Storer, notamment pour permettre la comparaison statistique donnée dans la section 2.6.

J'ai participé aux tests à l'UWO et l'UOL en 2009 et j'ai écrit les rapports donnés en annexes C et D avec l'aide du Pr. Pierre Bastien et du Pr. Martin Houde de l'UWO pour modéliser les ondes stationnaires présentes dans POL-2. J'ai participé à l'installation de POL-2 sur SCUBA-2, au JCMT à Hawaï, en juillet 2010.

Chapitre 2

Polarimetric Survey of Candidate Stars for Debris Disks

A. Simon [1], P. Bastien[1], E. Storer[1]

To be submitted to *The Astronomical Journal*

August 2010

1. Département de Physique, Université de Montréal, C.P. 6128, Succ. Centre-Ville, Montréal, Québec H3C 3J7, Canada.

2.1 Abstract

We present the first part of a polarimetric survey done at the 1.6 m Ritchey-Chrétien telescope of the Mont-Mégantic Observatory. We observed 109 stars with the purpose of finding polarization due to circumstellar matter. The observations were done in a wide band centered on 7660 Å. Our targets, which are a sample of the Herschel telescope survey DEBRIS, are the closest stars evenly distributed along the spectral types A, F, G, K and M (furthest one at 46 pc). They were selected only according to their distance, the survey is then unbiased as the neighbouring stars span all existing characteristics of main-sequence stars. We also observed HR 8799 since it is a star of particular interest (three resolved planets, two circumstellar disks and a halo). Of all the stars we observed, only one had a polarization detected above 3σ (HD 115404) and 14 stars were measured with a polarization between 2σ and 3σ. This lack of detection can be explained by the expected low polarization induced by debris disks, by the fact that polarization diminishes when inclination decreases (face-on disks do not polarize light) and by the fraction of expected debris disks (25%).

Key words: circumstellar matter — scattering — stars: individual (HR 8799, HD 115404)

— surveys — polarization

2.2 Introduction

The first large unbiased survey of debris disks was carried out by the Infrared Astronomical Satellite (IRAS). It was found that $\approx 15\%$ of main-sequence stars host debris disks (Backman & Paresce (1993), Plets & Vynckier (1999)). However, this fraction might be as high as 25% since there is evidence for a population of disks too cold to have been detected in the infrared (Wyatt (2003), Lestrade et al. (2006), Rhee et al. (2007)). Such a high proportion of stars hosting disks makes them a necessary subject of study. Their shape is indicative of the history of the system. Disks are found around stars at every age but their lifetime is shorter than that of the hosting star, due to the Poynting-Robertson effect and radiation pressure. However,

debris disks are still present due to replenishment mechanisms that continuously feed dust to the debris disks (Backman & Paresce 1993). These mechanisms are collisions between planetesimals and sublimation of comets (Williams & Wetherill (1994), Wyatt & Dent (2002)). Hence, observing debris disks is an important way to infer the presence of solid bodies around stars and to understand the dynamics of planetary systems (see Wyatt (2008), Krivov (2010) for recent reviews). Moreover, Beichman et al. (2005) found a correlation between the presence of debris disks and the presence of planets. However, it is still a subject of debate as this trend was not confirmed by Kóspál et al. (2009). In any case, for spatially-resolved disks, their wide extension indicates that planetesimals are present and perturb the disk (Backman & Paresce 1993). To clarify this question and to sharpen models of debris disks, an unbiased survey is needed, and should give us useful information about the characteristics of debris disks and their host stars. Such a survey is being carried out by the Herschel telescope with DEBRIS (Disc Emission via a Bias-free Reconnaissance in the Infrared/Submillimeter).

The space telescope Herschel observes at submillimeter wavelengths. Its Open Time Key Program DEBRIS is a flux-limited survey which consists of the 446 nearest stars, evenly distributed along the spectral types A, F, G, K and M. For a description of the DEBRIS survey see: Matthews et al. (2010b, in preparation), for the target selection, see: Phillips et al. (2010). The observation runs at 100 μm and 160 μm using the PACS instrument (Photodetector Array Camera and Spectrometer, Poglitsch et al. (2010)) with follow-up of around 100 targets at 250, 350 and 500 μm with the SPIRE instrument (Spectral and Photometric Imaging Receiver, Griffin et al. (2010)). As many as 356 stars are in common with the JCMT (James Clerk Maxwell Telescope) SCUBA-2 Unbiased Nearby Stars (SUNS) survey at 850 μm (Phillips et al. (2010), Matthews et al. (2007)). To date, 196 of the targets have been observed with the MIPS or IRS instrument of Spitzer (Matthews et al. 2010b, in preparation). Hence the spectral coverage would span from 24 to 850 μm for these stars. Distances of the farthest stars are 9, 16, 21, 24 and 46 pc for the M, K, G, F and A stars respectively. Observing in the close environment around the sun provides a sample covering a wide range of stellar parameters for which a rich literature already exists. It also maximizes the possibility of finding disks and spatially resolving

them. As the targets are only selected by their distances, the DEBRIS sample is unbiased and it will give us statistical information about how debris disks properties vary as a function of age, stellar mass, metallicity, presence of planets, system morphology, multiplicity, etc. The firsts results of DEBRIS are given in: Matthews et al. (2010a) with spatially resolved disks observed.

Most disks are found by an excess of flux in the infrared/submillimeter wavelengths compared to the stellar photospheric flux. This flux excess comes from dust heated by the star and that emits thermal emission (first discovery was made with IRAS around Vega (Aumann et al. 1984)). But debris disks can also be detected by polarimetry as dusty disks scatter and polarize stellar light. Polarization is an indicator of shape, size and composition of the grains. Such polarization has already been measured in spatially resolved disks such as the Beta Pictoris disk (Gledhill et al. (1991), Wolstencroft et al. (1995), Tamura et al. (2006)) and the AU Microscopii disk (Graham et al. (2007)). Polarization has also been observed on non-spatially resolved disks: Bhatt & Manoj (2000) compared polarization of stars with circumstellar matter and those that are devoid of such matter ; Oudmaijer et al. (2001), Eritsyan et al. (2002), Tamura & Fukagawa (2005), Chavero et al. (2006) and Wiktorowicz et al. (2010) presented polarization measurements of stars with infrared excess.

In this paper we present the first part of a polarimetric survey of the DEBRIS stars in order to get useful information provided by detection in polarization (orientation of the disk on the plane of the sky, information about the grains...). We will discuss the observations and the data reduction in section 2.3, we will then look at the properties of the stars with the highest polarization in section 2.4. By a search of polarization and infrared measurements in the literature, we will statistically compare polarization of stars with debris disks with stars without such disks in section 2.6. A model of polarization induced by dust is given in section 2.5. We will end with a discussion on the results we found in section 2.7.

2.3 Observational Results

2.3.1 Observations

The observations were made at the 1.6 m Ritchey-Chrétien telescope of the Mont-Mégantic Observatory (OMM), based in Quebec, Canada. We observed during three runs between 2009 December 1 and 2010 March 3. We used a 8.18″ aperture, all multiple stars we observed were integrated at the same time in the 8.18″ aperture. We used a broadband red filter, RG645 which yields a bandpass centered on 7660 Å and with a FWHM of 2410 Å. Polarization was measured with "La Belle et la Bête" instrument which is a two-channel photoelectric polarimeter. It uses a Wollaston prism as analyzer, a Pockels cell operated at 125 Hz as modulator, and a quarter wave plate.

The data were calibrated for polarization efficiency with a prism (between 75% and 83%), for instrumental polarization using unpolarized standards and for the zero point of position angle, using polarized standard stars. More information about the instrument and the method of observation can be found in Manset & Bastien (1995). We observed unpolarized standards for each run and we used the same ones as PlanetPol (Lucas et al. 2009). The polarized standards we observed come from Turnshek et al. (1990) and from the PlanetPol polarized standard stars (Hough et al. 2006).

In order to have a sigma error of 0.04%, we adjusted the integration time according to the magnitude of the star. Errors were calculated from photon statistics and also include the error due to calibration mentioned above. The errors are in the range 0.02% to 0.12% (with a mean of 0.04%). The uncertainty on the angle of the polarization vector was computed with:

$$\Delta_\theta = 28.65 \frac{\Delta_P}{P}.$$

The data were pre-analyzed by the computer "La Belle" while observing. The rest of the analysis was automated using IDL programs created for this purpose. Of the 297 stars that are visible from the observatory, 108 were observed for this analysis. We also observed the

star HR 8799 even if it is not included in the DEBRIS survey, as it is a target of particular interest: it hosts three resolved planets (Marois et al. 2008) and debris disks (Su et al. (2009), Reidemeister et al. (2009)).

2.3.2 Results

All targets from the DEBRIS survey are nearby stars and the furthest one is at 46 pc. The interstellar polarization is negligible for such distances (Piirola (1977), Leroy (1993), Lucas et al. (2009)), hence the polarization we measured is intrinsic to the stars. Column 1 of Tables 2.1 and 2.2 is the identification given for the SUNS and DEBRIS surveys, the first letter represents its spectral type and the number is a zero-padded running number increasing with distance in each subsample, these identifiers are referred to by the acronym UNS, standing for Unbiased Nearby Stars, as in the SUNS survey name. Column 2 is the name of the primary star, the choice of name is generally in the order of preference: HD, HIP, GJ, LHS, NLTT, TYC, PPM, CCDM , other catalogue name, 2MASS (Phillips et al. 2010). The other columns represent the polarization measured, its uncertainty, the position angle of the polarization vector and its uncertainty. When the error on the angle of the polarization vector is larger than 52°, it is in fact undefined. Finally, the last column of the tables is the date when the polarization was measured. When we observed a certain star many times, the result given is the weighted mean of the measurements. A database with other informations on the targets (magnitude, distance, spectral type, etc) will be available online (Matthews et al., 2010b in preparation).

We found 15 stars with a polarization between 2 and 3σ (see Table 2.1). The stars with an observed polarization under 2σ are given in Table 2.2. The instrument works in such a way that there is a redundancy in the measurements of the Stokes parameters: measurements were done at 0°, 45°, 90° and 135° from a certain reference. Hence measurements at 0° and 90° for example should give approximately the same results. We compared the data between 0° and 90° and between 45° and 135°, for the measurement detected above 3σ and the ones between 2

and 3σ. Measurements are coherent, but not strongly correlated. We are looking at very small polarization and additional observations of HD 115404 and of the measurements between 2 and 3σ should be done to confirm these results.

We plotted the number of stars with a given Q/I and U/I, see figures 2.1 and 2.2. Firstly, we can verify that the instrumental polarization is well determined, if such is the case, we should have a peak around 0. We see that it is the case for U/I but Q/I has an offset of -0.01%. It is nonetheless smaller than the error on the determination of the instrumental polarization, therefore it is compatible with 0%. A very strong peak around 0 is seen in both figures, with two bumps around that peak. This indicates that the errors were larger on certain nights than on others. It is indeed the case as we had some problems with one of the two photomultipliers during some nights and we had to use only half of the data. Finally, we can not clearly conclude about the presence of polarized stars which would stand in the wings of the peak.

We observed the star HR 8799 even if it is not a target of the DEBRIS survey. Results are given in Table 2.3.

2.4 Discussion

We have made a coherent census of polarization due to debris disks for 109 stars. We have only one detection above 3σ and 14 measurements above 2σ. This low rate of detection could be explained by many factors: only 25% of stars of the DEBRIS survey are expected to have debris disks (Matthews et al. 2010b, in preparation) ; in a face-on disk the polarization vector will cancel out (small fraction of disks have favourable inclination for detection) and we have error on the measurement of around 0.04%, which seems to be at the limit of detection (see section 2.5). Moreover, we used an $8.18''$ aperture centered on the star, therefore the unpolarized light from the star is integrated at the same time as the polarized light from the disk. That decreases very significantly the polarization detected, for example β Pictoris has been found to be 15% polarized if the star is hidden (Gledhill et al. 1991) but through a whole

aperture, the intrinsic polarization was measured to be 0.2% (Krivova et al. 2000). Hence, we might overlook debris disks because of the mean error on polarization in our survey is too large.

2.4.1 HD 115404

The only detection we found is on HD 115404, which is a K2.5 V star (Gray et al. 2003). No debris disks have been found around that star by infrared/submillimeter excess yet.

2.4.2 Stars with Detected Polarization Over 2σ and Known Debris Disks or Planets

HD 75732, also known as 55 Cancri hosts five planets: 55 Cnc b (Marcy & Butler 1996), 55 Cnc c (Marcy et al. 2002), 55 Cnc d (Marcy et al. 2002), 55 Cnc e (McArthur et al. 2004) and 55 Cnc f (Fischer et al. 2008). A debris disk has been reported by Trilling & Brown (1998), but its existence has been put into question by Schneider et al. (2001).

HD 120136, also known as τ Bootis, hosts one planet (Butler et al. 1997).

Lucas et al. (2009) have made polarization measurements of these two stars in order to find a variable polarization due to the presence of planets very close to the host stars. They found a polarization around 10^{-6}. Hence, HD 75732 and HD 120136 are very likely not polarized at the level measured in this survey. They found that the polarization of HD 75732 is very stable at a level of 10^{-6}, showing no sign of the periodic variations that would be expected if a short-period planet were detected. They also found large scatter, 7.0×10^{-6} in the Stokes parameter U/I for HD 120136, but no indication for the expected periodicity. The polarization induced by a hot Jupiter is expected to be at the level of 10^{-5} - 10^{-6} (Hough et al. 2006).

HD 106591 has a debris disk: Su et al. (2006) found an infrared excess at 24 and 70 μm, four times higher than the flux coming only from the photosphere, using the Multiband Imaging Photometer for Spitzer (MIPS). Unfortunately no model has been computed yet to deduce the

distance of the dust from the star or its mass.

HD 98231 is a double star, it has already been observed by Herschel, which found a submillimeter excess on the primary star (Brenda Matthews, private communication). The preliminary models of blackbody leads to a disk with a radius of 0.021 AU.

HD 60179 is also a double star with a debris disk detected by Herschel (Brenda Matthews, private communication). The radius of the disk would be of 0.067 AU.

2.4.3 HR 8799

We observed the star HR 8799 and found a small polarization of 0.07% at 2.8 times the error. This star is particularly interesting since it hosts three resolved planets (Marois et al. 2008) and three debris disks. Confirmation of this detection and observations in other wavelength bands would give us better constraints on the debris disks.

Su et al. (2009) and Reidemeister et al. (2009) modeled the infrared/submillimeter excess of HR 8799 and found that this star hosts three debris disks: an inner warm disk, a planetesimal disk and a halo. For the characteristics of the disks in the preferred model of Su et al. (2005), see Table 2.4. The first column represents the parameters of the disks: R_{in} and R_{out} stand for the inner and outer radii of the ring respectively, a_{min} and a_{max} for the minimum and maximum radii of the grains and M_d for the mass of the disk.

Using the model described in section 2.5, we estimate the polarization expected for such disks. For the inner disk, the polarization would be 0.02%, supposing that all the dust grains are at a distance of 6 AU and have a radius of 0.1 μm. For the planetesimal disk, the polarization could be as high as 1% if all particles have a radius of 1 μm and are at a distance of 90 AU. If the halo is totally symmetric around the star, it would not polarize the light. For the variation of polarization as a function of the radius of the grains in the planetesimal disk, see Figure 2.3.

In that figure, all grains are assumed to be astronomical silicates of a certain radius, at 90 AU from the star with a scattering angle of 90°. For future work, a model with a ring and a distribution of grain radius should be used. The small inclination of the ring should also be taken into account as it has a strong impact on polarization. For the same debris disk, we would see a different polarization for an inclined disk than for an edge-on disk; the polarization of a disk inclined at 23° is 15% of the value of the polarization of the same disk seen edge-on (see equation 2.6).

2.5 Models

Using the Mie scattering theory, we were able to constrain the mass of the disks. For all models, we assumed that: all grains are astronomical silicates, they are at a certain distance from the star; they have a certain radius and that the scattering angle is 90°. This angle is approximately the angle at which the polarization is maximal and corresponds to all grains being at 90° from the line of sight. We should keep in mind that the dust is in reality distributed along a ring and that the angle of inclination of the disk has a strong influence on the polarization we would detect.

We modeled the grains with astronomical silicates and took the complex refractive index given in Draine (1985), at 0.80 μm: m = n + ik with n = 1.71 and k = 0.0297. We computed numerically the Van de Hulst intensities, i_1 and i_2 for each grain radius and scattering angle.

Having those, we can estimate the polarization with:

$$P = P_{dust}\ N \frac{I_c}{I_\star + I_c}. \tag{2.1}$$

Knowing that the polarization of one grain is given by:

$$P_{dust} = \frac{i_1 - i_2}{i_1 + i_2} \tag{2.2}$$

and:

$$I_c = I_\star \, \frac{i_1 - i_2}{2k^2R^2}. \tag{2.3}$$

Combining equations 2.1 and 2.3, we then have:

$$P = P_{dust} \; N\left(\frac{\frac{i_1 - i_2}{2k^2R^2}}{1 + \frac{i_1 - i_2}{2k^2R^2}} \right), \tag{2.4}$$

with: I_c and $I_\star$ the intensities of the cloud and the star respectively, k the wavenumber, R the distance from the star and N the number of grains. The number of grains and the mass M of the disk are linked by:

$$M = \rho \, VN, \tag{2.5}$$

with ρ the density of the grain (we used the value of 3 g.cm^{-3} for astronomical silicates) and V the volume of a grain.

To put upper limit constraints on the mass of the disk, we assume a polarization detected at a level of 0.1%, which is the upper limit that we have on most of our measurements. The polarization induced by debris disks will approximately decrease as the square of their distance from the star, see equation 2.4. Therefore, in this survey we are more sensitive to hot debris disks such as the zodiacal cloud in our solar system. Fixsen & Dwek (2002) estimated that the grain radii of the zodiacal cloud range from 0.01 μm to 1 cm, decreasing exponentially. We then use a grain radius of 0.1 μm (but see Figure 2.4 for the influence of grain radius on the mass, for a debris disk at 1 AU).

We assume that all grains are at 1 AU, as for the zodiacal cloud the density of grains decreases quickly when the distance from the star is superior to 3 AU (Ipatov & Mather 2006) (but see Figure 2.5 for the influence of the distance on the mass of the disk.

With all these assumptions, we found a mass of the disk of 4.5×10^{-9} M$_\oplus$. The model was computed with conservative assumptions that would tend to find the disk massive, in order to

have a realistic mass upper limit. As the zodiacal cloud mass is between 0.33 - 1.81 $\times$ 10^{-9} $M_{\oplus}$, we indeed are at the limit of sensitivity of the instrument, if extrasolar hot debris disks resemble the zodiacal cloud.

Single scattering by Mie particles in optically thin envelopes around a star has been considered in the past and can be applied in the context of our paper. Bastien (1987) analytically studied the properties of different geometries. For an azimuthally symmetric but otherwise arbitrary density distribution, the polarization is proportionnal to $\sin^2 i$ as long as grains are relatively small compared to the wavelength, i.e., $x = ka = 2\pi/\lambda a < 2.0$, where a is the grain radius. For a plane disk, the polarization is given by (Bastien 1987):

$$P \propto \frac{15}{4}[N'(\sin i)^2]\bar{F_{22}}, \tag{2.6}$$

where N' is an integral over the radial density distribution in the disk, and $\bar{F_{22}}$ is real and depends on the scattering phase function (Simmons 1982). $\bar{F_{22}}$ also determines the wavelength dependence of the polarization. The position angle normally is perpendicular to the disk, except for a possible change by $\pi/2$ when $\bar{F_{22}}$ changes sign. In all cases, we see that there is a strong, sine square, dependence on the inclination.

2.6 Statistical Comparison

Since we measured small polarization levels in our sample of debris disks candidates, we compare statistically the distributions of two samples: 1) polarization measurements from the Heiles catalogue, and 2) our measurements including 4 stars observed by Bhatt & Manoj (2000) (hereafter B&M). As we are looking at nearby stars, the submillimeter/infrared excess measured, compared to the photosphere, comes from dust around those stars. We assume that the presence of submillemeter/infrared excess is a reliable indicator of the presence of debris disks.

1) For the comparison, we queried the polarization catalog of Heiles (2000) for all stars

from the DEBRIS and SUNS surveys (629 stars). We found polarization measurements for 189 stars. We searched for infrared measurements for these 189 stars in the following papers: Su et al. (2006), Beichman et al. (2006), Trilling et al. (2008). We then compared the polarization between stars that are known to have debris disks with the ones where no debris disks have been found. The results are given in Figure 2.6. No significant differences have been found on the polarization between stars with and without infrared excess. The mean polarization of stars that are known to host debris disks and for stars where no debris disks have been detected is given in table 2.5. No significant difference has been found between the two groups.

B&M did the same comparison for 61 stars and they found a greater polarization for vega-like stars. They observed 27 stars and 34 come from the Heiles catalog (2000). Error on measurements in the Heiles catalog are around 0.1% and could be as high as 0.3%. For that matter, as the error on the polarizarion measurements of B&M are small (mean: 0.06%), we include them in the following analysis:

2) We made the same comparison for our polarization sample, adding 4 stars observed by B&M that are parts of the DEBRIS sample. Three of them have been detected in polarization: HD 102647 at 0.15±0.05%, HD 109085 at 0.38±0.04% and HD 115892 at 0.18±0.06%. In addition to the stars observed in submillimeter/infrared in papers: Su et al. (2006), Beichman et al. (2006), Trilling et al. (2008), we add the preliminary measurements by Herschel (Brenda Matthews, private communication). Of the 108 stars of the DEBRIS sample we observed, 17 stars have already been observed with Herschel. The preliminary results show that 2 of these 17 stars have a debris disk. Only 10 stars we observed have infrared/submillimeter excess, for the other 98, no excess have been discovered yet. Hence, we compared the polarization of 14 stars with infrared/submillimeter excess with 98 stars where no excess have been found (see Figure 2.7). In that figure, we see a difference in polarization between stars having an infrared excess and those which have none. We used an extension of the chi-square goodness-of-fit test in order to test if the two samples are statistically different. The coefficient of contingency, ranging from 0 to 1 measures the degree of dependence between two samples, the larger the

value, the greater the degree of dependance. We found 0.08 within our sample. The mean polarization for stars without detected infrared excess and for those with a debris disk is given in table 2.5. The mean polarization is greater for stars having infrared excess compared to stars having none, but the deviation on the mean does not permit us to conclude that there is a statistically significant difference between the two samples. These results are an indication that more detections should be found with a small increase on the measurement precision and with observing the remaining 186 stars of the DEBRIS sample visible from the OMM.

2.7 Conclusion and Further Prospects

We performed a coherent census of polarization due to debris disks for 109 stars. Only one detection over 3σ and 14 measurements between 2σ and 3σ have been found. This low rate of detection could be explained by many factors: the small fraction of expected debris disks, their random inclination that will not always be favourable and the error on the measurements. By modeling polarization due to debris disks, we have found upper limit constraints on the mass of the debris disks. We did a statistical comparison of polarization of stars that have debris disks with stars where none have been found, we see a statistical difference between the two samples. We can conclude that we are at the limit of the sensitivity to detect polarization due to debris disks and increasing the precision on future measurements should lead to more detections.

The authors wish to sincerely thank the telescope operators at the Mont-Mégantic Observatory, Pierre-Luc Lévesque, Bernard Malenfant and Ghislain Turcotte. We also would like to thank Rémi Fahed and Lison Malo for their precious help, Marie-Michèle Limoges for a careful reading of this manuscript and David Lafrenière for insightful discussions on HR 8799. This research has made use of the SIMBAD database and the VizieR catalog access tool, operated at CDS, Strasbourg, France.

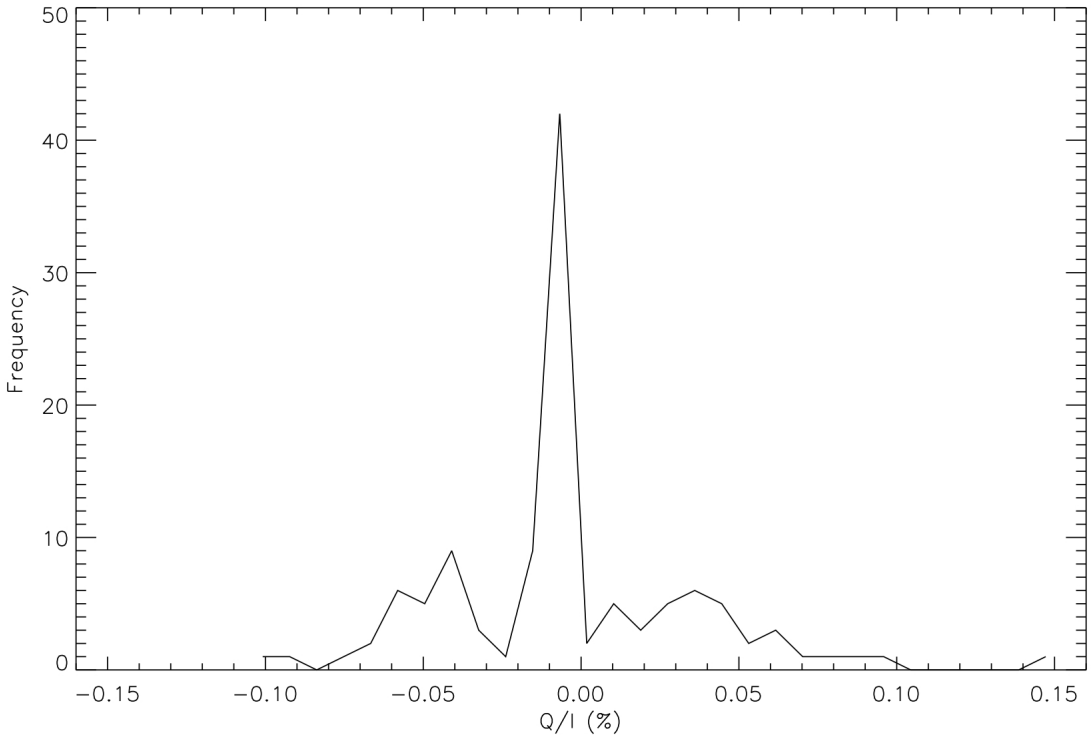

FIGURE 2.1 – Frequency distribution of the normalized Stokes parameter Q/I, for all stars.

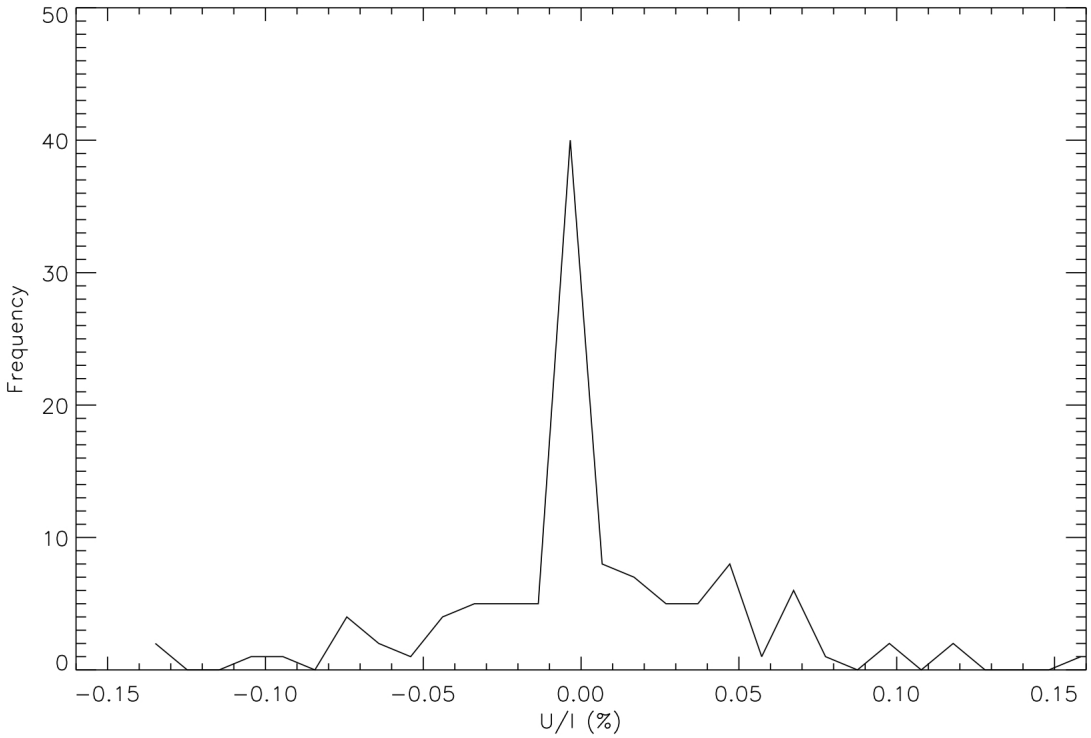

FIGURE 2.2 – Frequency distribution of the normalized Stokes parameter U/I, for all stars.

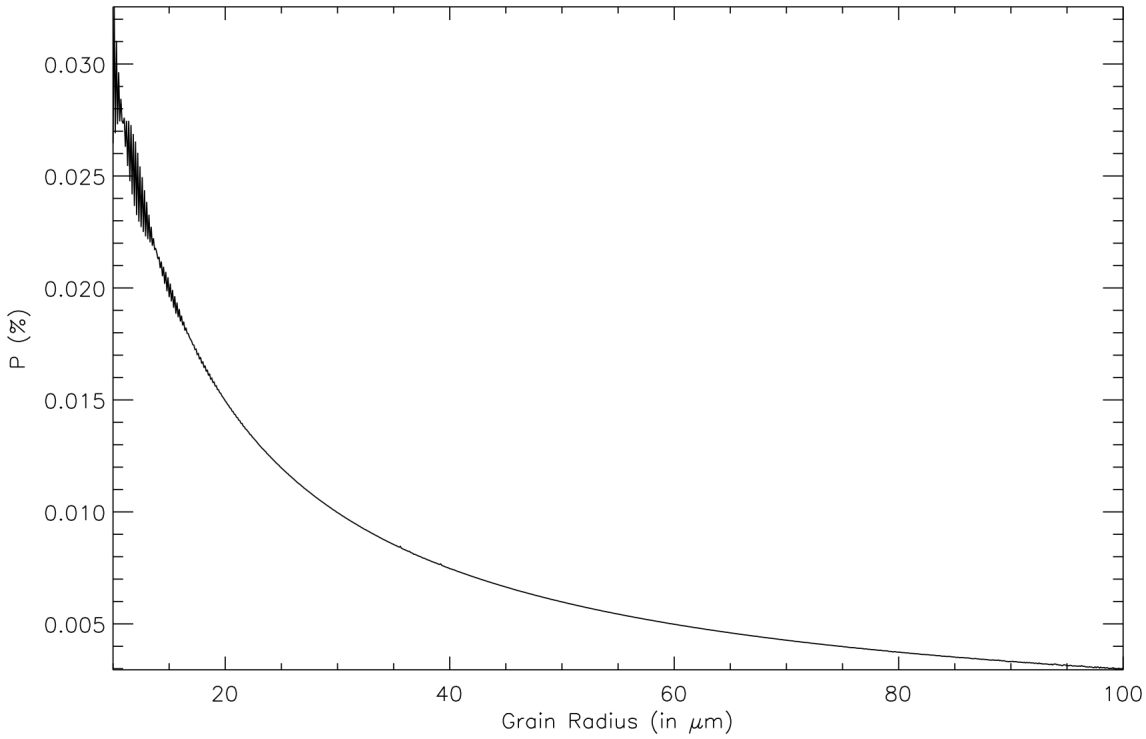

FIGURE 2.3 – Polarization as a function of the grain radius for HR 8799. We used characteristics of the preferred model of Su et al. (2005).

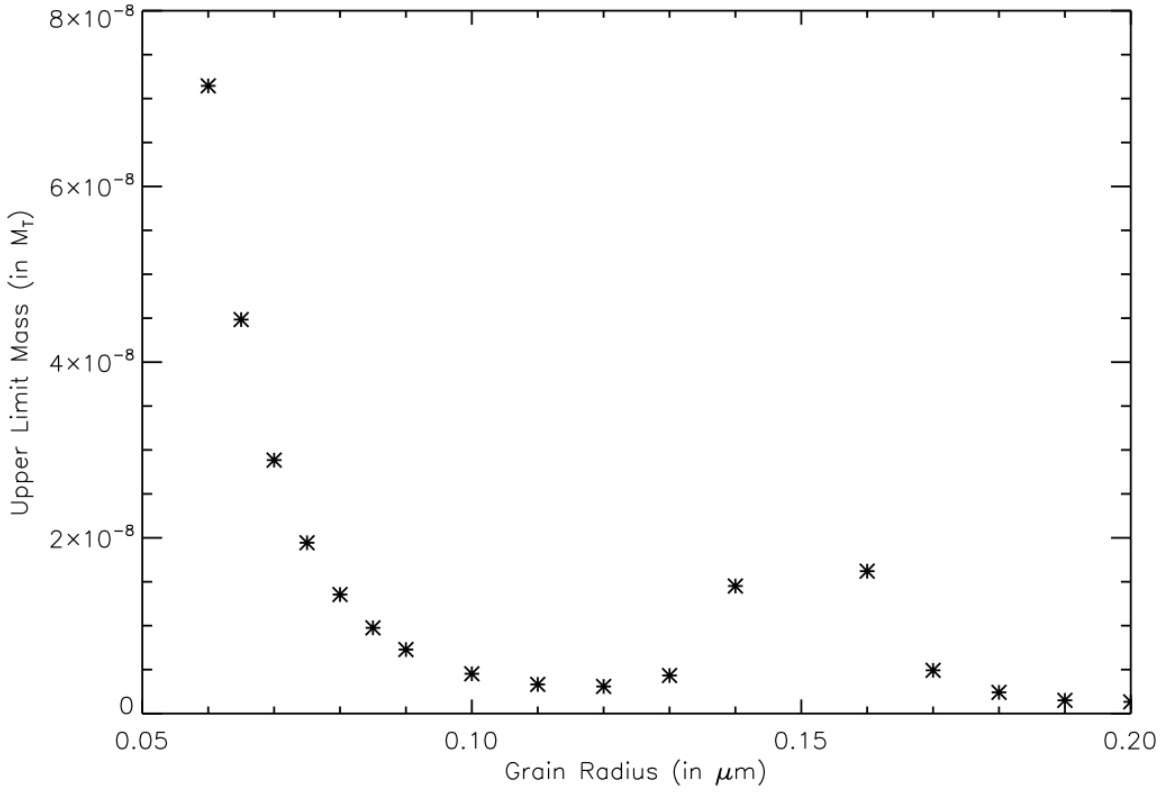

FIGURE 2.4 – Mass of the disk determined as a function of the grain radius, for an assumed observed polarization of 0.1%. Other assumptions are given in the text.

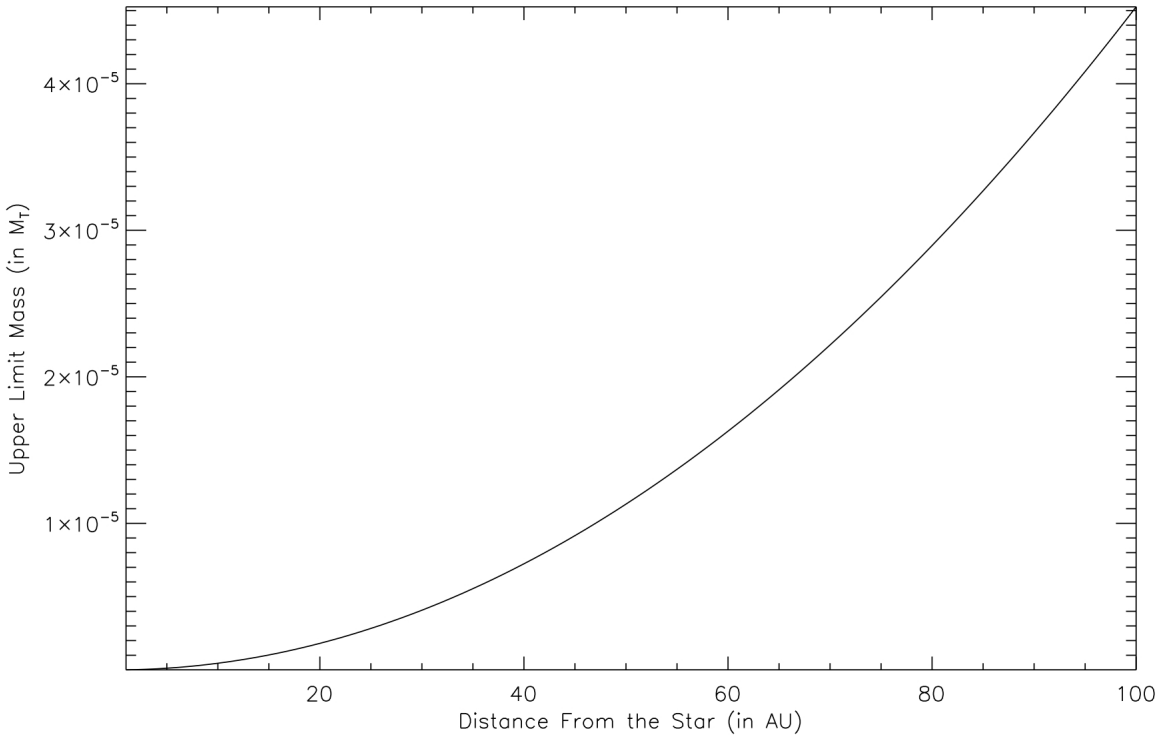

FIGURE 2.5 – Mass of the disk determined as a function of the distance of silicate grains of 0.1 μm. Other assumptions are given in the text.

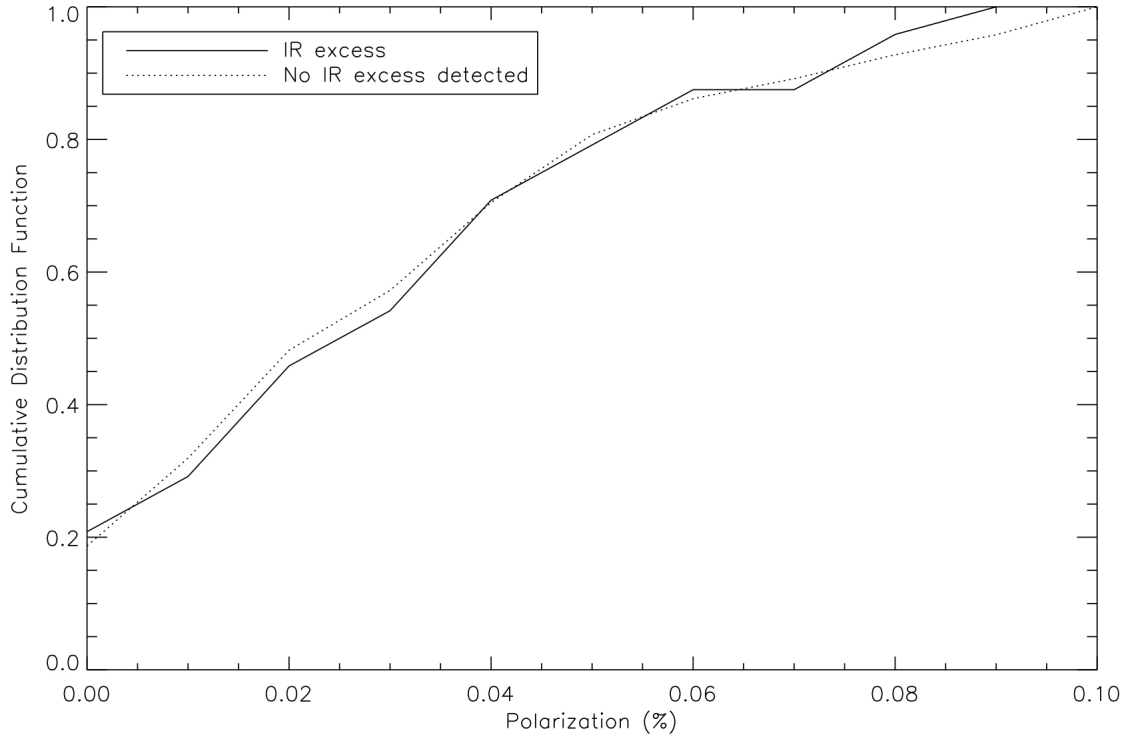

FIGURE 2.6 – Comparison of polarization in the Heiles Catalog for stars with and without infrared excess. The polarization is given as a function of the fractional number of stars with observed polarization lower than a given value. Solid line represents stars with infrared excess and dashed line stars without.

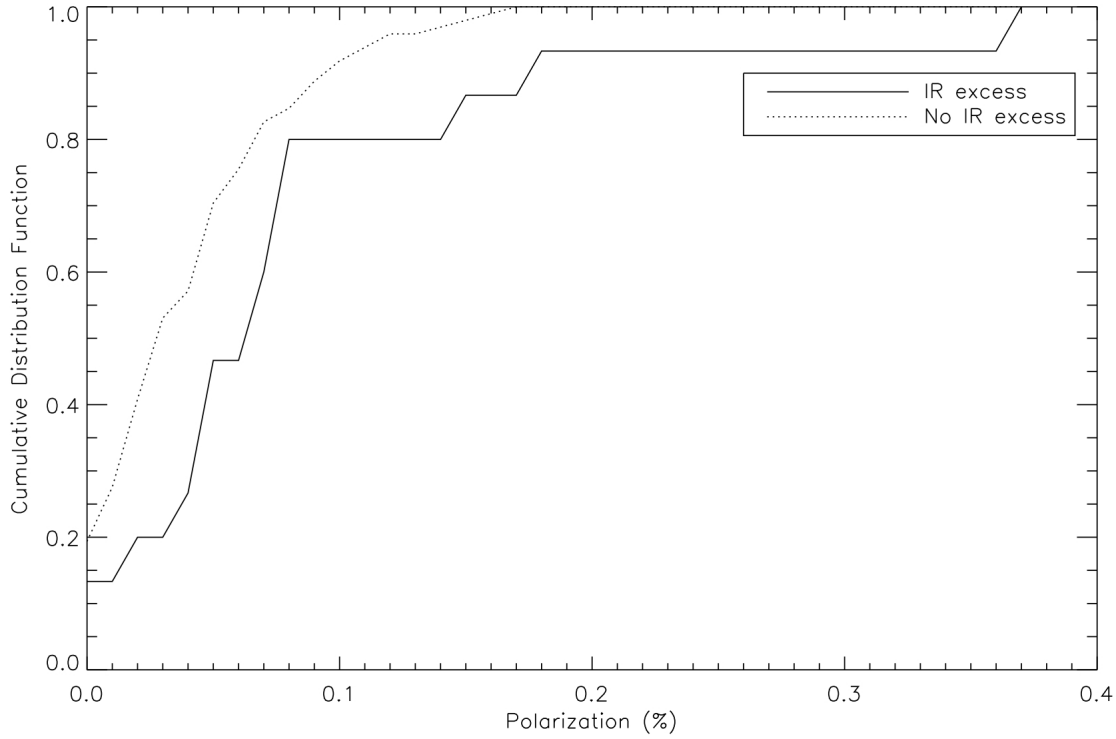

FIGURE 2.7 – Comparison of polarization for stars with and without infrared excess in this survey and the one of B&M. The polarization is given as a function of the fractional number of stars with observed polarization lower than a given value. Solid line represents stars with infrared excess and dashed line stars without.

TABLE 2.1 – Stars Observed with a Polarization Over 2σ.

UNS ID	Name (Primary)	P(%)	ΔP(%)	$\theta(^\circ)$	$\Delta\theta(^\circ)$	P/ΔP	Distance (pc)	Date
K046	HD 115404	0.152	0.043	8.4	7.4	3.5	11.095 ± 0.090	22Jan.
M069	GJ 3522	0.103	0.036	79.	11.	2.8	6.772 ± 0.091	02Mar.
K056	HD 97101	0.053	0.024	135.	10.	2.2	11.96 ± 0.12	04Dec.
K060	HD 75732	0.099	0.042	136.	11.	2.4	12.46 ± 0.10	21Jan.
K086	GJ 400 A	0.070	0.029	132.	13.	2.4	13.90 ± 0.32	04Dec.
K092	HD 110315	0.098	0.049	88.	14.	2.0	19.18 ± 0.12	22Jan.
G094	HD 78366	0.166	0.075	150.	14.	2.2	8.368 ± 0.055	21Jan.
F004	HD 98231	0.070	0.032	28.	15.	2.2	15.622 ± 0.049	04Dec.
F036	HD 120136	0.079	0.038	74.	15.	2.1	6.772 ± 0.091	22Jan.
F040	GJ 332 A	0.071	0.028	54.	13.	2.6	16.06 ± 0.17	08Dec.
F120	HD 101177	0.145	0.049	45.	10.	2.9	23.20 ± 0.39	22Jan.
F121	HD 100180	0.124	0.063	47.	17.	2.0	23.33 ± 0.66	08Dec.
A006	HD 60179	0.067	0.025	179.	10.	2.7	14.01 ± 0.41	08Dec.
A026	HD 106591	0.084	0.033	169.	13.	2.5	24.688 ± 0.085	23Jan.
A032	HD 103287	0.058	0.027	170.2	9.0	2.1	25.51 ± 0.26	23Jan.

TABLE 2.2: Stars Observed with a Polarization Under 2σ

UNS ID	Name (Primary)	P(%)	ΔP(%)	$\theta(^\circ)$	$\Delta\theta(^\circ)$	P/ΔP	Date
M003	HD 95735	0.047	0.031	177.	23.	1.5	02Mar.
M015	HIP 36208	0.011	0.030	26.	34.	0.4	02Mar.
M031	HIP 54211	0.032	0.035	und. [b]	52.	0.9	02Mar.
M032	GJ 388	0.078	0.050	54.	15.	1.6	23Jan.
M040	HD 119850	0.116	0.093	79.	20.	1.2	22Jan.
M042	HD 265866	0.000	0.036	und.	52.	0.0	21Jan.
M053	HIP 37766	0.000	0.031	130.	44.	0.0	02Mar.
M054	HIP 34603	0.000	0.046	und.	52.	0.0	22Jan.
M060	GJ 661 A	0.054	0.044	144.	20.	1.2	02Mar.
M067	HIP 53767	0.000	0.030	und.	52.	0.0	02Mar.
M070	HIP 53020	0.054	0.041	75.	18.	1.3	02Mar.
M076	HIP 51317	0.020	0.037	144.	23.	0.5	02Mar.
M090	GJ 1093	0.17	0.12	57.	19.	1.4	22Jan.
M095	HIP 49986	0.056	0.034	152.	22.	1.7	02Mar.
M100	HIP 86287	0.000	0.033	und.	52.	0.0	02Mar.
M109	HIP 38956	0.031	0.045	und.	52.	0.7	22Jan.
M110	GJ 1230 A	0.083	0.050	130.	16.	1.7	02Mar.
K005	HD 88230	0.082	0.048	160.	19.	1.7	22Jan.
K011	HD 79210	0.014	0.040	118.	22.	0.4	08Dec.
K017	HD 10476	0.055	0.030	166.	19.	1.8	23Jan.
K021	HD 157881	0.033	0.033	und.	52.	1.0	02Mar.
K028	HD 103095	0.049	0.049	177.	21.	1.0	22Jan.
K031	HD 151288	0.059	0.035	81.	18.	1.7	02Mar.
K041	HIP 66459	0.066	0.036	96.	12.	1.8	02Mar.
K055	CCDM 15009+4526 A	0.065	0.038	125.	15.	1.7	02Mar.
K064	HD 82106	0.031	0.032	und.	52.	1.0	02Mar.

TABLE 2.2: Stars Observed with a Polarization Under 2σ

UNS ID	Name (Primary)	P(%)	ΔP(%)	$\theta(^\circ)$	$\Delta\theta(^\circ)$	P/ΔP	Date
K070	HIP 67090	0.052	0.041	57.	16.	1.3	22Jan.
K072	HD 128165	0.000	0.037	175.	48.	0.0	02Mar.
K074	HD 120476	0.012	0.033	und.	52.	0.4	02Mar.
K082	HIP 27188	0.000	0.030	und.	52.	0.0	21Jan.
K096	HIP 70218	0.035	0.036	und.	52.	1.0	02Mar.
K098	HD 144579	0.000	0.046	und.	52.	0.0	02Mar.
K099	HIP 37288	0.000	0.031	und.	52.	0.0	02Mar.
K108	HIP 13375	0.000	0.064	und.	52.	0.0	23Jan.
K111	HD 110833	0.000	0.033	und.	52.	0.0	02Mar.
K121	GJ 319 A	0.000	0.029	105.	28.	0.0	02Mar.
G007	CCDM 12337+4121 A	0.038	0.029	67.	34.	1.3	02Mar.
G013	HD 101501	0.068	0.049	23.	26.	1.4	22Jan.
G016	HD 13974	0.024	0.041	51.	24.	0.6	23Jan.
G025	HD 133640	0.020	0.031	und.	52.	0.6	02Mar.
G029	HD 30495	0.055	0.035	129.	18.	1.6	08Dec.
G033	HD 95128	0.018	0.021	und.	52.	0.9	04Dec.
G040	HD 86728	0.016	0.046	und.	52.	0.3	22Jan.
G057	HD 111395	0.092	0.074	18.	20.	1.2	23Jan.
G061	HD 122742	0.089	0.051	38.	13.	1.8	22Jan.
G065	HD 50692	0.074	0.061	54.	19.	1.2	21Jan.
G081	HD 137108	0.012	0.035	und.	52.	0.3	02Mar.
G086	HD 84737	0.052	0.028	106.	15.	1.8	04Dec., 22Jan.
G088	HD 154345	0.000	0.055	und.	52.	0.0	02Mar.
G093	HD 52711	0.073	0.041	176.	17.	1.8	21Jan.
G100	HD 79028	0.000	0.044	und.	52.	0.0	22Jan.
G101	HD 136923	0.029	0.030	und.	52.	1.0	02Mar.

TABLE 2.2: Stars Observed with a Polarization Under 2σ

UNS ID	Name (Primary)	P(%)	ΔP(%)	$\theta(^\circ)$	$\Delta\theta(^\circ)$	P/ΔP	Date
G108	HD 89269	0.046	0.052	177.	22.	0.9	22Jan.
G109	GJ 337 A	0.118	0.061	118.	17.	1.9	23Jan.
F018	HD 90839	0.000	0.039	und.	52.	0.0	04Dec.
F019	HD 82328	0.000	0.049	und.	52.	0.0	22Jan.
F022	HD 22484	0.043	0.045	10.	24.	1.0	23Jan.
F024	HD 17206	0.060	0.034	170.	14.	1.8	23Jan.
F044	HD 48682	0.078	0.060	139.	29.	1.3	04Dec.
F045	HD 55575	0.018	0.033	161.	22.	0.5	22Jan.
F055	HD 114378	0.023	0.038	48.	32.	0.6	22Jan.
F058	HD 58946	0.053	0.034	11.	19.	1.6	22Jan.
F061	HD 69897	0.025	0.018	126.	21.	1.3	21Jan., 22Jan., 23Jan.
F067	GJ 271 A	0.046	0.024	147.	15.	1.9	21Jan., 22Jan.
F082	HD 58855	0.000	0.039	und.	52.	0.0	22Jan.
F084	GJ 335	0.054	0.054	171.	37.	1.0	22Jan.
F090	HD 33564	0.033	0.033	179.	26.	1.0	21Jan.
F097	HD 89449	0.000	0.035	und.	52.	0.0	23Jan.
F103	HD 108954	0.054	0.042	12.	16.	1.3	23Jan.
F113	HD 89125	0.064	0.033	151.	11.	1.9	23Jan.
A007	HD 76644	0.037	0.063	93.	26.	0.6	08Dec.
A011	HD 97603	0.090	0.055	175.	20.	1.6	23Jan.
A016	HD 38678	0.000	0.035	131.	26.	0.0	08Dec.
A028	CCDM 13240+5456 A	0.035	0.036	und.	52.	1.0	02Mar.
A042	HD 87696	0.010	0.039	32.	22.	0.3	04Dec.
A045	HD 78209	0.107	0.077	119.	19.	1.4	04Dec.
A048	HD 125161	0.024	0.028	und.	52.	0.9	02Mar.
A053	HD 125162	0.026	0.043	21.	22.	0.6	02Mar.

TABLE 2.2: Stars Observed with a Polarization Under 2σ

UNS ID	Name (Primary)	P(%)	ΔP(%)	$\theta(^\circ)$	$\Delta\theta(^\circ)$	P/ΔP	Date
A056	HD 56537	0.050	0.031	39.	12.	1.6	08Dec.
A065	CCDM 15278+2906 A	0.028	0.031	148.	56.	0.9	02Mar.
A066	HD 104513	0.025	0.042	und.	52.	0.6	22Jan.
A067	HD 14055	0.084	0.047	18.	21.	1.8	08Dec.
A068	HD 91312	0.029	0.040	122.	19.	0.7	04Dec.
A069	HD 112413	0.031	0.042	109.	22.	0.7	02Mar.
A074	HD 79439	0.124	0.071	60.	16.	1.7	08Dec.
A078	HD 184006	0.101	0.051	133.	16.	2.0	02Mar.
A079	HD 102124	0.020	0.029	8.	30.	0.7	02Mar.
A082	HD 71155	0.000	0.043	und.	52.	0.0	22Jan.
A083	HD 80081	0.029	0.031	und.	52.	1.0	21Jan.
A086	HD 13161	0.022	0.039	und.	52.	0.6	23Jan.
A087	HD 95608	0.033	0.032	86.	16.	1.0	23Jan.
A110	HD 89021	0.039	0.054	und.	52.	0.7	22Jan.
A127	HD 140436	0.000	0.033	und.	52.	0.0	02Mar.

[a]Angle is undefined when the ratio P/ΔP is too low.

TABLE 2.3 – Polarization Measurement of HR 8799.

Name	P(%)	ΔP(%)	$\theta(^\circ)$	$\Delta\theta(^\circ)$	P/ΔP	Distance(pc)	Date
HR 8799	0.070	0.025	95.5	8.9	2.8	39.4 $\pm$ 0.1	08Dec.

TABLE 2.4 – Parameters of the Disks in the Preferred Model of Su et al. (2005).

Parameters	Inner Warm Disk	Planetesimal Disk	Halo
R_{in} (AU)	6	90	300
R_{out} (AU)	15	300	1000
$a_{min}(\mu m)$	1.5	10	1
$a_{max}(\mu m)$	4.5	1000	10
$M_d(M_\oplus)$	1.1×10^{-6}	1.2×10^{-1}	1.9×10^{-2}

TABLE 2.5 – Results of the Comparison Between the Polarization of Stars Owning a Debris Disk with Stars without One.

	Heiles Catalog			OMM and B&M samples		
	Mean	σ	Number	Mean	σ	Number
With Debris Disks	0.034%	0.037%	24	0.092%	0.054%	14
Without Debris Disks	0.040%	0.043%	165	0.047%	0.039%	98

Bibliographie

Aumann, H. H., et al. 1984, ApJ, 278, L23

Backman, D. E., & Paresce, F. 1993, in Protostars and Planets III, ed. E. H. Levy & J. I. Lunine (Tucson, AZ: Univ. Arizona Press), 1253

Bastien, P. 1987, ApJ, 317, 231

Beichman, C. A., et al. 2005, ApJ, 622, 1160

Beichman, C. A., et al. 2006, ApJ, 652, 1674

Bhatt, H. C., & Manoj, P. 2000, A&A, 362, 978

Bryden, G., et al. 2006, ApJ, 636, 1098

Burns, J. A., Lamy, P. L., & Soter, S. 1979, Icarus, 40, 1

Butler, R. P., Marcy, G. W., Williams, E., Hauser, H., & Shirts, P. 1997, ApJ, 474, L115

Chavero, C., Gómez, M., Whitney, B. A., & Saffe, C. 2006, A&A, 452, 921

Dohnanyi, J. S. 1969, J. Geophys. Res., 74, 2531

DEBRIS Collaboration, et al. 2010, arXiv:1005.5147

Draine, B. T. 1985, ApJS, 57, 587

Eritsyan, M. A., Hovhannessian, R. K., & Hovhannessian, E. R. 2002, Astrophysics, 45, 25

Fischer, D. A., et al. 2008, ApJ, 675, 790

Fixsen, D. J., & Dwek, E. 2002, ApJ, 578, 1009

Gledhill, T. M., Scarrott, S. M., & Wolstencroft, R. D. 1991, MNRAS, 252, 50P

Graham, J. R., Kalas, P. G., & Matthews, B. C. 2007, ApJ, 654, 595

Gray, R. O., Corbally, C. J., Garrison, R. F., McFadden, M. T., & Robinson, P. E. 2003, AJ, 126, 2048

Griffin, M. J., et al. 2010, arXiv:1005.5123

Heiles, C. 2000, AJ, 119, 923

Høg, E., et al. 2000, A&A, 355, L27

Hough, J. H., Lucas, P. W., Bailey, J. A., Tamura, M., Hirst, E., Harrison, D., & Bartholomew-Biggs, M. 2006, PASP, 118, 1302

Ipatov, S. I., & Mather, J. C. 2006, Advances in Space Research, 37, 126

Korhonen, T., & Reiz, A. 1986, A&AS, 64, 487

Kóspál, Á., Ardila, D. R., Moór, A., & Ábrahám, P. 2009, ApJ, 700, L73

Krivov, A. V. 2010, Research in Astronomy and Astrophysics, 10, 383

Krivova, N. A., Krivov, A. V., & Mann, I. 2000, ApJ, 539, 424

Leroy, J. L. 1993, A&AS, 101, 551

Lestrade, J.-F., Wyatt, M. C., Bertoldi, F., Dent, W. R. F., & Menten, K. M. 2006, A&A, 460, 733

Lucas, P. W., Hough, J. H., Bailey, J. A., Tamura, M., Hirst, E., & Harrison, D. 2009, MNRAS, 393, 229

Mann, I., Köhler, M., Kimura, H., Cechowski, A., & Minato, T. 2006, A&A Rev., 13, 159

Manset, N., & Bastien, P. 1995, PASP, 107, 483

Marcy, G. W., & Butler, R. P. 1996, ApJ, 464, L147

Marcy, G. W., Butler, R. P., Fischer, D. A., Laughlin, G., Vogt, S. S., Henry, G. W., & Pourbaix, D. 2002, ApJ, 581, 1375

Marois, C., Macintosh, B., Barman, T., Zuckerman, B., Song, I., Patience, J., Lafrenière, D., & Doyon, R. 2008, Science, 322, 1348

Matthews, B. C., et al. 2007, PASP, 119, 842

Matthews, B. C., et al. 2010a, A&A, 518, L135

McArthur, B. E., et al. 2004, ApJ, 614, L81

Moro-Martín, A., et al. 2007, ApJ, 658, 1312

Najita, J., & Williams, J. P. 2005, ApJ, 635, 625

Oudmaijer, R. D., et al. 2001, A&A, 379, 564

Perry, C. L., & Johnston, L. 1982, ApJS, 50, 451

Phillips, N. M., Greaves, J. S., Dent, W. R. F., Matthews, B. C., Holland, W. S., Wyatt, M. C., & Sibthorpe, B. 2010, MNRAS, 403, 1089

Piirola, V. 1977, A&AS, 30, 213

Plets, H., & Vynckier, C. 1999, A&A, 343, 496

Poglitsch, A., et al. 2010, arXiv:1005.1487

Reidemeister, M., Krivov, A. V., Schmidt, T. O. B., Fiedler, S., Müller, S., Löhne, T., & Neuhäuser, R. 2009, A&A, 503, 247

Rhee, J. H., Song, I., Zuckerman, B., & McElwain, M. 2007, ApJ, 660, 1556

Schneider, G., Becklin, E. E., Smith, B. A., Weinberger, A. J., Silverstone, M., & Hines, D. C. 2001, AJ, 121, 525

Simmons, J. F. L. 1982, MNRAS, 200, 91

Smith, P. S., Hines, D. C., Low, F. J., Gehrz, R. D., Polomski, E. F., & Woodward, C. E. 2006, ApJ, 644, L125

Stern, S. A. 1995, AJ, 110, 856

Strubbe, L. E., & Chiang, E. I. 2006, ApJ, 648, 652

Su, K. Y. L., et al. 2005, ApJ, 628, 487

Su, K. Y. L., et al. 2006, ApJ, 653, 675

Su, K. Y. L., et al. 2009, ApJ, 705, 314

Tamura, M., & Fukagawa, M. 2005, in ASP Conf. Ser. 343, Astronomical Polarimetry: Current Status and Future Directions, ed. A. Adamson et al. (San Francisco, CA: ASP), 215

Tamura, M., Fukagawa, M., Kimura, H., Yamamoto, T., Suto, H., & Abe, L. 2006, ApJ, 641, 1172

Thébault, P., & Augereau, J.-C. 2007, A&A, 472, 169

Trilling, D. E., & Brown, R. H. 1998, Nature, 395, 775

Trilling, D. E., et al. 2008, ApJ, 674, 1086

Turnshek, D. A., Bohlin, R. C., Williamson, R. L., II, Lupie, O. L., Koornneef, J., & Morgan, D. H. 1990, AJ, 99, 1243

Wiktorowicz, S., Graham, J. R., Duchene, G., & Kalas, P. 2010, Bulletin of the American Astronomical Society, 41, 582

Williams, D. R., & Wetherill, G. W. 1994, Icarus, 107, 117

Wolstencroft, R. D., Scarrott, S. M., & Gledhill, T. M. 1995, Ap&SS, 224, 395

Wyatt, M. C. 2003, ApJ, 598, 1321

Wyatt, M. C. 2005, A&A, 433, 1007

Wyatt, M. C. 2008, ARA&A, 46, 339

Wyatt, M. C., & Dent, W. R. F. 2002, MNRAS, 334, 589

Wyatt, M. C., Dent, W. R. F., & Greaves, J. S. 2003, MNRAS, 342, 876

Chapitre 3

Tests optiques du polarimètre POL-2

3.1 Présentation de l'instrument

Observer dans les longueurs d'ondes sub-millimétriques nous permet de sonder les environnements froids de l'univers. Par exemple, un nuage à 10 K possède un pic d'émission à 300 μm. Les étoiles naissent dans de tels nuages moléculaires froids et denses. Les poussières interstellaires forment la matière solide du milieu interstellaire, dans les nuages moléculaires et dans les nuages ténus de la galaxie. Ces grains sont, en général, non sphériques et tournent rapidement, principalement dû à un couple radiatif qui est responsable de l'alignement des grains en présence d'un champ magnétique (Lazarian 2009). Les grains précessent de sorte qu'en moyenne leur axe de rotation sera parallèle au champ magnétique local et l'axe long y sera perpendiculaire. L'émission thermique des grains sera alors polarisée perpendiculairement à la projection du champ magnétique local sur le plan du ciel. Ainsi, étudier la polarisation de la lumière dans les longueurs d'ondes sub-millimétriques revient à étudier les champs magnétiques des milieux froids. Pouvant cartographier les champs magnétiques à différentes échelles, un polarimètre permet d'obtenir des observations pouvant tester les modèles de turbulence magnéto-hydrodynamique et les scénarios de formation d'étoiles. Par exemple, la densité d'énergie des champs magnétiques serait comparable aux densités d'énergie gravitationnelle et cinétique lors de l'effondrement d'un nuage moléculaire en proto-étoile, on pense que le champ magnétique joue un rôle déterminant dans la perte de l'énergie angulaire de la proto-étoile.

Utiliser un polarimètre dans les longueurs d'ondes sub-millimétriques permettrait de vérifier cette hypothèse. De plus, avoir un spectre polarimétrique permet d'obtenir de précieux renseignements sur les grains de poussière.

La partie instrumentale de ma maîtrise porte sur le polarimètre POL-2, qui est installé sur l'imageur SCUBA-2 au télescope du JCMT. Avec un diamètre de 15 m, le JCMT est le plus grand télescope observant dans les longueurs d'ondes sub-millimétriques. Il est situé au sommet du Mauna Kéa, dans l'état d'Hawaii aux Etats-Unis, à environ 4100 m d'altitude.

L'imageur du JCMT est en cours de modernisation, il est passé de SCUBA, possédant 128 bolomètres (donc 128 pixels) à SCUBA-2, qui possède le premier détecteur de type CCD dans le sub-millimétrique, avec 10 000 pixels. Les observations à risques partagés débuteront vers janvier 2011. SCUBA-2 observera simultanément dans deux bandes : à 450 et 850 μm.

POL-2 est le polarimètre associé à SCUBA-2, il est installé directement sur le cryostat (voir Figure 3.1) permettant ainsi au mode polarimétrique d'être mis en place rapidement. La Figure 3.2 est la photographie du polarimètre une fois que nous l'avons installé sur l'imageur en juillet 2010. POL-2 consiste en deux polariseurs en grille (le calibrateur et l'analyseur) et une lame demi-onde (voir Figure 3.3).

La lame demi-onde est achromatique, elle est faite de cinq plaques de saphirs biréfringentes collées, leurs axes rapides orientés selon des angles spécifiques afin d'augmenter la nature achromatique du délai de la lame demi-onde (Savini et al. 2009). Dans sa configuration d'observation, la lame demi-onde et l'analyseur seront dans le faisceau. La lame demi-onde tourne continuellement, à une vitesse typique de 2 Hz afin de contrer les effets de fluctuations de transparence de l'atmosphère. Des lectures rapides du détecteur permettront de connaître la valeur du flux en fonction de l'angle de la lame demi-onde.

Une lame demi-onde est un composé biréfringent, qui possède un axe privilégié, l'axe op-

tique. Une lumière polarisée peut être décomposée en deux axes, les axes perpendiculaire et parallèle à l'axe optique. Ces deux composantes ne vont pas se propager à la même vitesse dans le milieu biréfringent. Dans le cas d'une lame demi-onde, une des deux composantes va être retardée par rapport à l'autre de $\pi/2$. L'onde sortante d'une telle lame a une polarisation symétrique de l'onde entrante par rapport à l'axe optique. Lorsque la lame demi-onde tourne, le vecteur de polarisation va tourner avec elle, quatre fois plus vite (l'axe optique tourne deux fois plus vite que la lame, le vecteur de polarisation tourne deux fois plus vite que l'axe optique). Lorsque le vecteur de polarisation sortant de la lame est perpendiculaire aux grilles de l'analyseur, toute la lumière va passer et lorsque le vecteur de polarisation est parallèle aux grilles, la lumière sera bloquée.

La réponse typique de POL-2 à un objet partiellement polarisée est donnée dans la Figure 3.4. Notez que l'échelle n'est pas respectée, le flux du ciel est à environ 2000 Jy dans le régime sub-millimétrique et les sources astronomiques typiques pour lesquelles nous espérons déterminer les propriétés de polarisation ont un flux de 100 mJy à 850 μm et un pourcentage de polarisation de 1 à 5%. Ainsi le polarimètre doit être capable de mesurer un signal polarimétrique à un niveau de 1 mJy par rapport au signal du ciel de 2000 Jy.

Grâce au montage expérimental donné dans la Figure 3.3, nous pouvons déterminer toutes les caractéristiques de la lumière polarisée. Dans sa plus simple forme, POL-2 produit une onde sinusoïdale dont les trois observables sont l'amplitude (Ip sur la Figure 3.4), la phase et le décalage en ordonnée (sky + Imin sur la Figure 3.4). Elles sont reliées au pourcentage de polarisation, à l'angle de position du vecteur de polarisation dans le plan du ciel, et à l'intensité de l'émission non-polarisée, respectivement. Nous devons être capable de mesurer ces trois variables précisément.

3.2 Tests à l'UWO en 2007 et 2008

Afin de vérifier les performances de l'instrument POL-2, il a été testé au laboratoire d'astronomie sub-millimétrique de l'Université de Western Ontario (UWO) à London en Ontario en juin 2007. La réponse des composantes optiques (transmission, retardance et extinction) a été déterminée. L'analyseur et le calibreur étaient alors deux polariseurs constitués d'une fine membrane gravée par lithographie. Les composantes optiques présentaient une bonne réponse lorsque la lame demi-onde était fixe mais il existait un important problème de vibration lorsque la lame demi-onde tournait, ce qui rendait impossible l'observation d'un objet astronomique en rotation continue de la lame.

L'avantage de POL-2 est de pouvoir observer rapidement un objet grâce à cette rotation, avant même que des fluctuations atmosphériques ne perturbent les mesures. Une solution aux problèmes de vibration devait être trouvée. Le mécanisme de rotation a été amélioré et POL-2 a de nouveau été testé à l'UWO en avril 2008. Les vibrations étaient toujours présentes. Toutefois, une solution a été trouvée : en remplaçant la fine membrane polarisante par un petit polariseur en grille emprunté au laboratoire de l'UWO, le problème de vibration semblait résolu.

Cependant, il fallait vérifier que les polariseurs en grilles de la taille nécessaire pour POL-2 (30 cm de diamètre) réglerait totalement le problème. C'est ce que nous avons fait pendant ma maîtrise, nous avons testé POL-2 aux laboratoires de physique sub-millimétrique de l'UWO et à l'Université de Lethbridge (UOL). Deux rapports ont été produits pour ces tests (voir annexes A et B). Ils ont notamment servi pour l'acceptation du polarimètre comme instrument adéquat et remplissant les attentes du JCMT.

3.3 Tests à l'UWO en juin 2009

Nous avons testé les composantes optiques de POL-2 à l'UWO en juin 2009. L'émetteur d'ondes sub-millimétriques utilisé pour ces tests produit une onde polarisée avec une longueur

d'onde (ou fréquence) donnée, qui peut être ajustée dans une certaine gamme. Nous avons fait les tests à 450 μm et 850 μm, qui sont les longueurs d'ondes centrales des bandes passantes utilisées pour SCUBA-2.

Depuis les derniers tests faits en avril 2008, deux polariseurs en grilles et une nouvelle lame demi-onde avaient été reçus. Nous avons testé la réponse optique de ces composantes à l'UWO. Elles se comportent de manière satisfaisante. Un enregistrement quantitatif en continu du signal n'était pas réalisable avec le montage expérimental au laboratoire. Donc, lorsque la lame demi-onde tournait en continu, nous avions seulement accès à la réponse du polarimètre sur un oscilloscope. Nous ne voyions aucune vibration et nous avons pu vérifier de manière quantitative ce résultat grâce aux tests opérés à l'UOL (voir chapitre 3.4).

Cependant, il est apparu de ces tests que POL-2 ne se comporte pas comme un polarimètre parfait et des ondes stationnaires perturbent sa réponse. L'amplitude et la phase de ces ondes stationnaires ont été déterminées avec précision grâce aux tests qui ont été faits à l'UOL (voir chapitre 3.4). Nous avons ainsi corrigé pour les erreurs introduites par ces ondes afin d'obtenir les caractéristiques réelles de l'instrument. Le rapport des tests à l'UWO est donné dans l'annexe A.

3.4 Tests à l'UOL en septembre 2009

POL-2 a été testé à l'UOL en septembre 2009 car l'émetteur disponible en laboratoire reproduisait beaucoup mieux les bandes passantes centrées sur 450 μm et 850 μm, qui seront utilisées lors des observations. De plus, il était possible d'enregistrer le signal en fonction du temps. Ce qui nous a permis de mieux contraindre la réponse de POL-2 lorsque la lame demi-onde tournait en continu. Nous avons eu la confirmation que les problèmes de vibrations ont complètement été résolus grâce aux nouveaux polariseurs à grilles. De plus, les caractéristiques des ondes standards ont été déterminées, elles pourront ainsi être déduites lors de l'analyse des données. Nous avons produit un rapport des tests optiques, donné dans l'annexe B.

3.5 Acceptation finale de POL-2 comme instrument du JCMT et installation au télescope

En avril 2010, des membres du JCMT sont venus à l'Université de Montréal afin de vérifier que POL-2 satisfaisait leurs attentes concernant les instruments utilisés sur ce télescope. Ils ont vérifié le bon fonctionnement des logiciels disponibles pour contrôler POL-2, ses caractéristiques mécaniques et les rapports des tests leur ont permis de vérifier le bon comportement de ses composantes optiques. L'instrument a ainsi officiellement été accepté comme instrument du JCMT en mai 2010. Nous avons été au télescope du JCMT au Mauna Kea du 15 au 18 juillet 2010, pour installer POL-2 sur SCUBA-2. Ce qui a été fait avec succès comme nous le voyons sur la photo de la Figure 3.2.

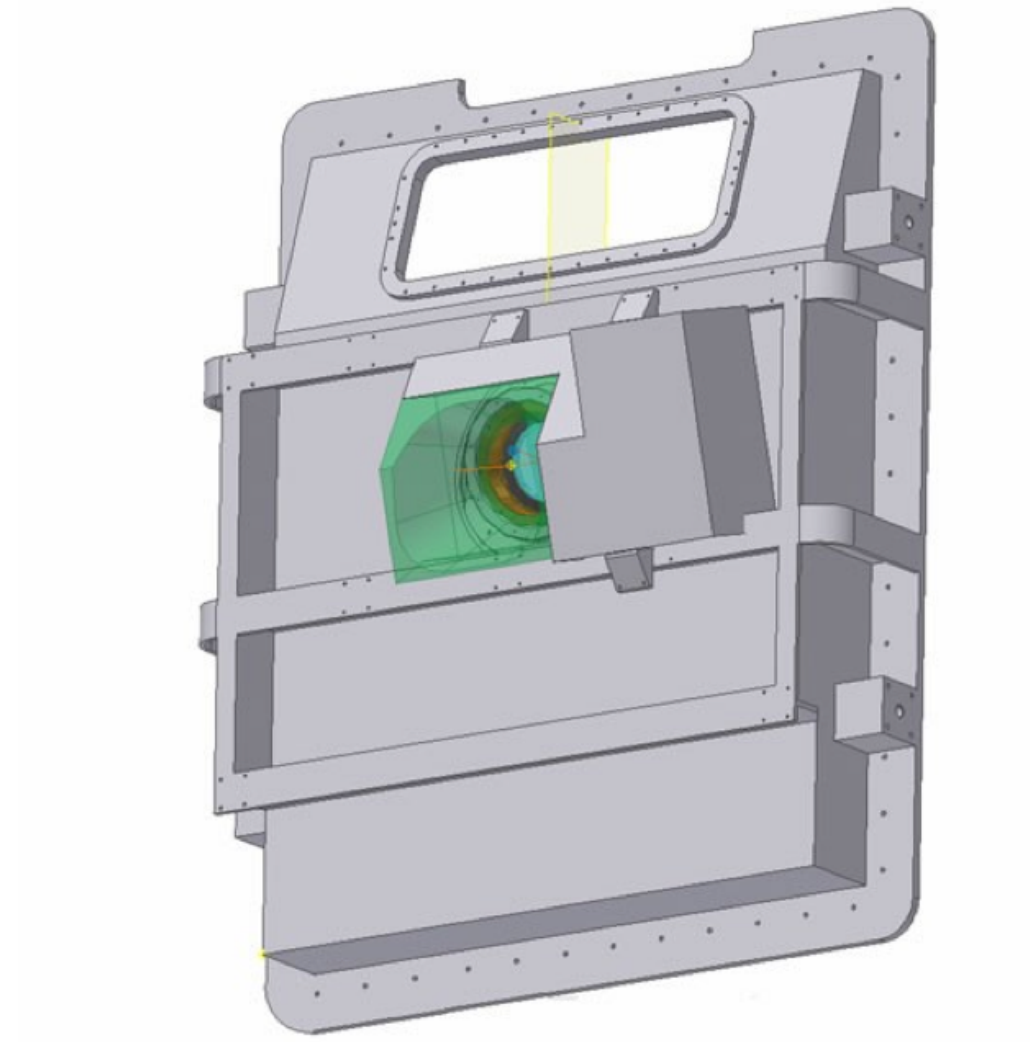

FIGURE 3.1 – Schéma de la position de POL-2 sur SCUBA-2. Le polarimètre est vissé à droite de l'entrée du faisceau de lumière. Les composantes optiques du polarimètre glissent devant cette entrée lorsque l'on observe en mode polarimétrique.

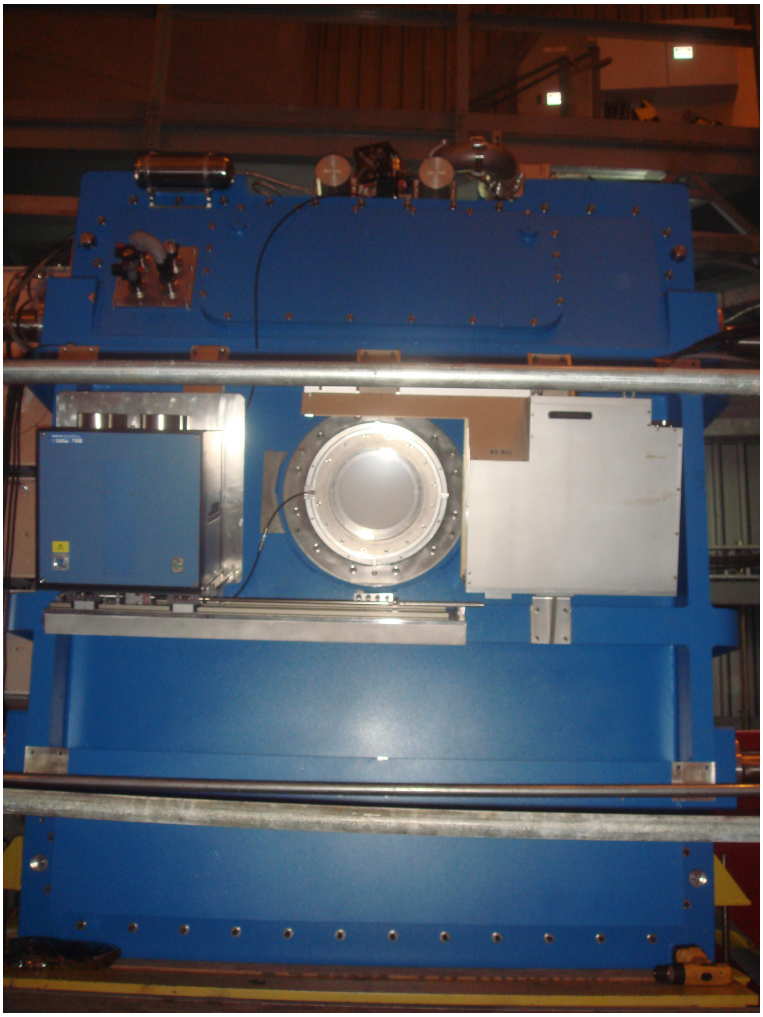

FIGURE 3.2 – Photo du polarimètre installé sur le cryostat. Le polarimètre est la boîte grise installée à droite de l'entrée du faisceau de lumière. Les composantes optiques du polarimètre glissent devant cette entrée lorsque l'on observe en mode polarimétrique.

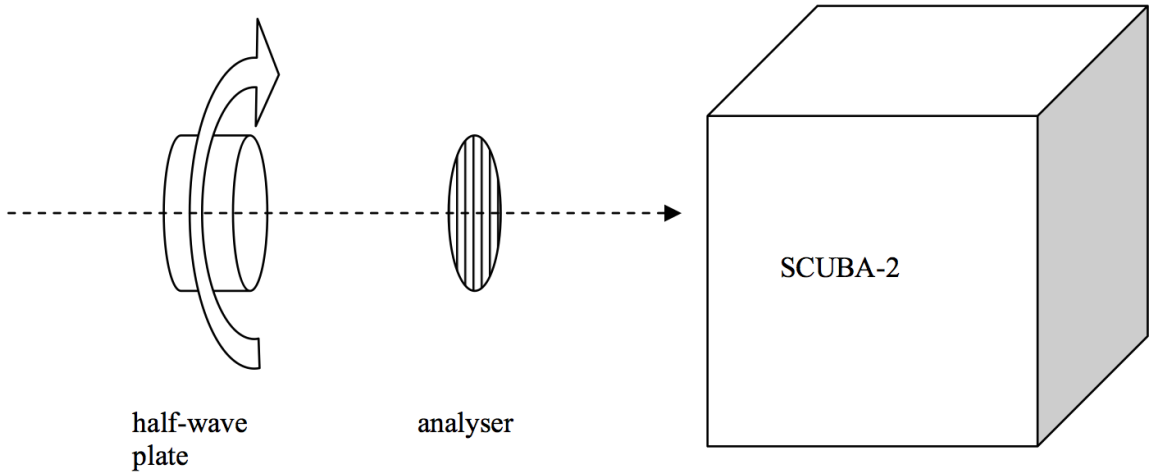

FIGURE 3.3 – Schéma du polarimètre POL-2. La lame demi-onde est placé devant l'analyseur et tourne continuellement. Le calibrateur peut glisser devant la lame en cas de besoin : pour calibrer l'instrument et pour le tester.

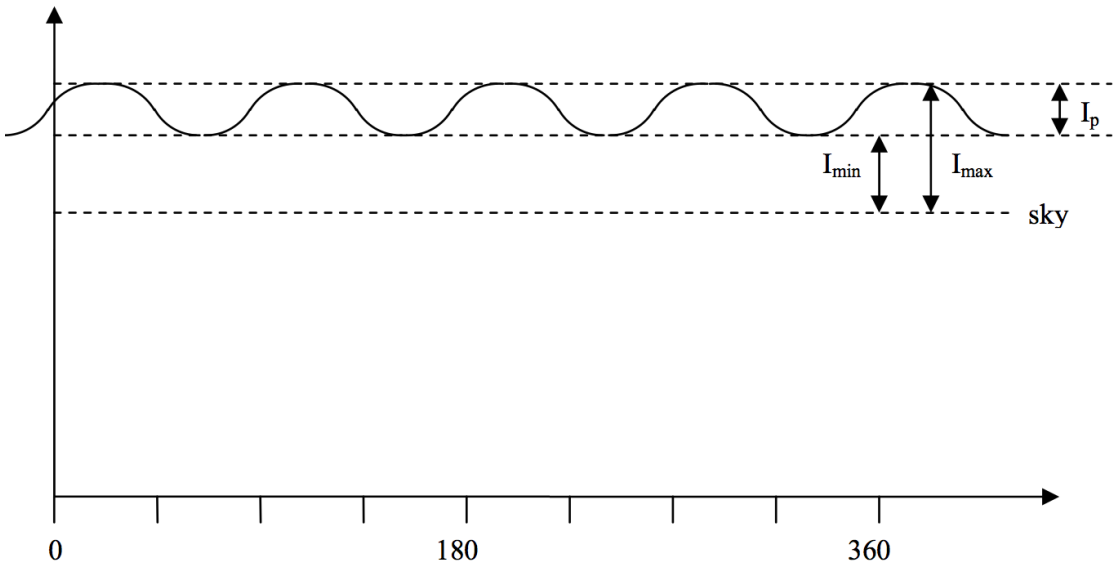

FIGURE 3.4 – Réponse de POL-2 à une lumière partiellement polarisée.

Chapitre 4

Conclusion

Nous avons effectué la première partie d'un relevé polarimétrique à 7660 Å avec l'instrument "La Belle et la Bête" à l'Observatoire du Mont-Mégantic. Nous avons observé 108 des cibles sélectionnées pour le relevé DEBRIS, ainsi que l'étoile HR 8799, particulièrement intéressante car elle possède trois planètes résolues et trois disques de débris. DEBRIS est un relevé non-biaisé des étoiles des types spectraux A, F, G, K et M, effectué par le télescope spatial Herschel dans les longueurs d'ondes sub-millimétriques (à 100 et 160 μm). Il est axé sur la recherche de disques de débris autour d'étoiles de l'environnement solaire (l'étoile la plus éloignée est à 45 pc). Les poussières de disques de débris diffusent et polarisent la lumière. Observant les mêmes cibles que DEBRIS, nous pouvons apporter des informations supplémentaires venant avec la polarimétrie (orientation du disque dans le plan du ciel, caractéristiques des grains de poussière...), particulièrement si les observations sont effectuées dans plusieurs bandes. Nous avons détecté une seule étoile polarisée (HD 115404), avec une valeur de 0.15% à 3.5σ de l'erreur. Le faible taux de détection que nous avons obtenu peut-être expliqué par plusieurs facteurs : la proportion d'étoiles possédant des disques de débris (25%), le fait que la polarisation diminue lorsque l'inclinaison augmente (un disque vu de face ne polarisera pas la lumière), l'erreur sur nos mesures (environ 0.04%) et le fait que nous intégrons la lumière non polarisée provenant de l'étoile en même temps que la lumière polarisée du disque. Des limites supérieures de la masse des disques ont pu être déterminées grâce à la théorie de diffusion de Mie. Nous avons modélisé la polarisation que nous pourrions attendre des disques

de débris de l'étoile HR 8799. Cependant, une analyse statistique comparant la polarisation d'un échantillon possédant des disques avec celui ne possédant pas d'excès dans les longueurs d'ondes infrarouges nous a permis de voir une plus grande polarisation pour les étoiles possédant un disque connu que pour celles n'en possédant pas. Ainsi, des mesures plus précises permettront d'obtenir des détections individuelles de disque de débris par polarisation. Nous étions seulement limité par le temps d'intégration sur les cibles. Pour les observations futures, nous intégrerons plus longtemps afin d'obtenir un meilleur signal sur bruit. De plus, des observations dans plusieurs bandes de HD 115404 nous permettra de vérifier la présence d'un disque et de contraindre les caractéristiques de ses grains de poussières.

La partie instrumentale de ce mémoire consistait aux tests optiques et à l'installation au télescope du polarimètre POL-2. Nous avons été aux laboratoires sub-millimétriques de l'Université de Western Ontario et de l'Université de Lethbridge, afin de vérifier que les problèmes de vibrations qui étaient présents auparavant avaient disparus grâce aux nouveaux polariseurs en grilles. Les tests optiques que nous avons effectués nous permettent de conclure que POL-2 a une réponse très stable dans le temps et qu'aucune vibration n'est détectable. Cependant, des ondes stationnaires sont présentes dans l'instrument. Grâce aux tests optiques effectués, nous sommes en mesure de quantifier l'influence des ondes stationnaires afin de bien connaître les caractéristiques réelles de l'instrument. POL-2 a passé les tests d'acceptations de la commission du JCMT et nous avons pu l'installer en juillet 2010 au télescope du JCMT au Mauna Kea (Hawaï, USA). Le polarimètre POL-2 pourra cartographier les champs magnétiques à petites et grandes échelles et permettra de répondre à de multiples questions, notamment concernant la naissance des étoiles et la prépondérance des champs magnétiques dans leur formation.

Bibliographie

Absil, O. et al. 2006, A&A, 452, 237

Aumann, H. H., Beichman, C. A., Gillett, F. C., de Jong, T., Houck, J. R., Low, F. J., Neugebauer, G., Walker, R. G., & Wesselius, P. R. 1984, ApJ, 278, L23

Backman, D. E. & Paresce, F. 1993, in Protostars and Planets III, ed. E. H. Levy & J. I. Lunine, 1253–1304

Bastien, P. 1987, ApJ, 317, 231

Beichman et al. 2005, ApJ, 622, 1160

Beichman, C. A. et al. 2006, ApJ, 652, 1674

Bhatt, H. C. & Manoj, P. 2000, A&A, 362, 978

Bryden, G. et al. 2009, ApJ, 705, 1226

Butler, R. P., Marcy, G. W., Williams, E., Hauser, H., & Shirts, P. 1997, ApJ, 474, L115

Chavero, C., Gómez, M., Whitney, B. A., & Saffe, C. 2006, A&A, 452, 921

Delsanti, A. & Jewitt, D. 2006, The Solar System Beyond The Planets, ed. Blondel, P. & Mason, J. (Springer), 267

Draine, B. T. 1985, ApJS, 57, 587

Eritsyan, M. A., Hovhannessian, R. K., & Hovhannessian, E. R. 2002, Astrophysics, 45, 25

Fischer, D. A. et al. 2008, ApJ, 675, 790

Fixsen, D. J. & Dwek, E. 2002, ApJ, 578, 1009

Gillett, F. C. 1986, in Astrophysics and Space Science Library, Vol. 124, Light on Dark Matter, ed. F. P. Israel, 61–69

Gledhill, T. M., Scarrott, S. M., & Wolstencroft, R. D. 1991, MNRAS, 252, 50P

Gomes, R., Levison, H. F., Tsiganis, K., & Morbidelli, A. 2005, Nature, 435, 466

Graham, J. R., Kalas, P. G., & Matthews, B. C. 2007, ApJ, 654, 595

Gray, R. O., Corbally, C. J., Garrison, R. F., McFadden, M. T., & Robinson, P. E. 2003, AJ, 126, 2048

Griffin, M. J. et al. 2010, A&A, 518, L3

Heap, S. R., Lindler, D. J., Lanz, T. M., Cornett, R. H., Hubeny, I., Maran, S. P., & Woodgate, B. 2000, ApJ, 539, 435

Heiles, C. 2000, AJ, 119, 923

Hough, J. H., Lucas, P. W., Bailey, J. A., Tamura, M., Hirst, E., Harrison, D., & Bartholomew-Biggs, M. 2006, PASP, 118, 1302

Ipatov, S. I. & Mather, J. C. 2006, Advances in Space Research, 37, 126

Kalas, P., Graham, J. R., & Clampin, M. 2005, Nature, 435, 1067

Kóspál, Á., Ardila, D. R., Moór, A., & Ábrahám, P. 2009, ApJ, 700, L73

Krasinsky, G. A., Pitjeva, E. V., Vasilyev, M. V., & Yagudina, E. I. 2002, Icarus, 158, 98

Krivov, A. V. 2010, Research in Astronomy and Astrophysics, 10, 383

Krivova, N. A., Krivov, A. V., & Mann, I. 2000, ApJ, 539, 424

Lazarian, A. 2009, in Astronomical Society of the Pacific Conference Series, Vol. 414, Astronomical Society of the Pacific Conference Series, ed. T. Henning, E. Grün, & J. Steinacker, 482

Leroy, J. L. 1993, A&A, 274, 203

Lestrade, J., Wyatt, M. C., Bertoldi, F., Dent, W. R. F., & Menten, K. M. 2006, A&A, 460, 733

Lucas, P. W., Hough, J. H., Bailey, J. A., Tamura, M., Hirst, E., & Harrison, D. 2009, MNRAS, 393, 229

Manset, N. & Bastien, P. 1995, PASP, 107, 483

Marcy, G. W. & Butler, R. P. 1996, ApJ, 464, L147

Marcy, G. W., Butler, R. P., Fischer, D. A., Laughlin, G., Vogt, S. S., Henry, G. W., & Pourbaix, D. 2002, ApJ, 581, 1375

Marois, C., Macintosh, B., Barman, T., Zuckerman, B., Song, I., Patience, J., Lafrenière, D., & Doyon, R. 2008, Science, 322, 1348

Matthews et al. 2010a, A&A, 518, L135

Matthews, B. C. et al. 2007, PASP, 119, 842

McArthur, B. E. et al. 2004, ApJ, 614, L81

O'Brien, D. P., Morbidelli, A., & Bottke, W. F. 2007, Icarus, 191, 434

Oudmaijer, R. D. et al. 2001, A&A, 379, 564

Phillips, N. M., Greaves, J. S., Dent, W. R. F., Matthews, B. C., Holland, W. S., Wyatt, M. C., & Sibthorpe, B. 2010, MNRAS, 403, 1089

Piirola, V. 1977, A&AS, 30, 213

Pilbratt, G. L., Riedinger, J. R., Passvogel, T., Crone, G., Doyle, D., Gageur, U., Heras, A. M., Jewell, C., Metcalfe, L., Ott, S., & Schmidt, M. 2010, A&A, 518, L1

Plets, H. & Vynckier, C. 1999, A&A, 343, 496

Poglitsch, A. et al. 2010, A&A, 518, L2

Reidemeister, M., Krivov, A. V., Schmidt, T. O. B., Fiedler, S., Müller, S., Löhne, T., & Neuhäuser, R. 2009, A&A, 503, 247

Rhee, J. H., Song, I., Zuckerman, B., & McElwain, M. 2007, ApJ, 660, 1556

Savini, G., Ade, P. A. R., House, J., Pisano, G., Haynes, V., & Bastien, P. 2009, Appl. Opt., 48, 2006

Schneider, G., Becklin, E. E., Smith, B. A., Weinberger, A. J., Silverstone, M., & Hines, D. C. 2001, AJ, 121, 525

Simmons, J. F. L. 1982, MNRAS, 200, 91

Stern, S. A. 1996, A&A, 310, 999

Su, K. Y. L., Rieke, G. H., Stapelfeldt, K. R., Malhotra, R., Bryden, G., Smith, P. S., Misselt, K. A., Moro-Martin, A., & Williams, J. P. 2009, ApJ, 705, 314

Su, K. Y. L. et al. 2005, ApJ, 628, 487

—. 2006, ApJ, 653, 675

Tamura, M. & Fukagawa, M. 2005, in Astronomical Society of the Pacific Conference Series, Vol. 343, Astronomical Polarimetry: Current Status and Future Directions, ed. A. Adamson, C. Aspin, C. Davis, & T. Fujiyoshi, 215

Tamura, M., Fukagawa, M., Kimura, H., Yamamoto, T., Suto, H., & Abe, L. 2006, ApJ, 641, 1172

Thébault, P. & Augereau, J. 2007, A&A, 472, 169

Thommes, E. W., Nilsson, L., & Murray, N. 2007, ApJ, 656, L25

Trilling, D. E. & Brown, R. H. 1998, Nature, 395, 775

Trilling, D. E., Bryden, G., Beichman, C. A., Rieke, G. H., Su, K. Y. L., Stansberry, J. A., Blaylock, M., Stapelfeldt, K. R., Beeman, J. W., & Haller, E. E. 2008, ApJ, 674, 1086

Turnshek, D. A., Bohlin, R. C., Williamson, II, R. L., Lupie, O. L., Koornneef, J., & Morgan, D. H. 1990, AJ, 99, 1243

Wiktorowicz, S., Graham, J. R., Duchene, G., & Kalas, P. 2010, in Bulletin of the American Astronomical Society, Vol. 41, Bulletin of the American Astronomical Society, 582

Williams, D. R. & Wetherill, G. W. 1994, Icarus, 107, 117

Wolstencroft, R. D., Scarrott, S. M., & Gledhill, T. M. 1995, Ap&SS, 224, 395

Wyatt, M. C. 2003, ApJ, 598, 1321

—. 2008, ARA&A, 46, 339

Wyatt, M. C. & Dent, W. R. F. 2002, MNRAS, 334, 589

Annexe A

Data Analysis of Polarization Measurements

A. Simon, P. Bastien

A.1 Introduction

We wrote this guide to help in analyzing measurements performed with the instrument "La Belle et la Bête" at the Mont-Mégantic Observatory (hereafter the B&B), though the data analysis should be applicable to any polarization measurements.

The data given by the B&B are: the polarization P'_{unbiased}, the sigma error $\sigma_{P'}$, the angle θ and its sigma error: σ_θ.
The B&B is not 100% efficient. Each night we measured a certain efficiency *Eff*. Therefore, each polarization have to be divided by this efficiency. Hence, the new polarization is:

$$P_{\text{unbiased}} = \frac{P'_{\text{unbiased}}}{Eff}$$

and

$$\sigma_P = \frac{\sigma_{P'}}{Eff}.$$

There is a bias that tends to surestimate the polarization we measure. It can be corrected with the formula: $P_{\text{unbiased}} = \sqrt{P^2_{\text{biased}} - \sigma^2_P}$. The result given by the B&B is already corrected for this bias. Then, if we want to analyze the data, we need to go back to the biased polarization which is not corrected. At the end of all the computation, we will correct for this bias again.

The polarization we use for our computation is given by: $P_{\text{biased}} = \sqrt{P^2_{\text{unbiased}} + \sigma^2_P}$.

We need to work in the $(Q,\ U)$ plane, where Q and U are the normalized Stokes parameters. Q and U are given by:

$$Q = P_{\text{biased}}\ \cos(2\theta)$$

$$U = P_{\text{biased}}\ \sin(2\theta)$$

and we need to have σ_Q and σ_U. We can't have the exact values, so we assume that the counts

on Q and on U were equals when we did the measurements. In this case, we have that

$$\sigma_Q = \sigma_U = \sigma_P.$$

(Coming from: $\sigma_P = \frac{Q^2\ \sigma_Q^2 + U^2\ \sigma_U^2}{\sqrt{Q^2+U^2}}$).

A.2 Instrumental Polarization

The instrument might not be perfectly symmetrical and might polarize a part of the light coming from a given star. In order to remedy this, we observed unpolarized standards; therefore, the polarization we measured on these stars is the polarization induced by the instrument.

Say we observed n unpolarized standards during a run of observations, we then have n measures of the intrinsic polarization of the instrument (P_{IP}).
When working in the (Q, U) plane, we compute Q_{IP} and U_{IP}:

$$Q_{IP} = \frac{\sum_{i=1}^{n} Q_i \times \frac{1}{\sigma_{P_i}^2}}{\sum_{i=1}^{n} \frac{1}{\sigma_{P_i}^2}}$$

$$U_{IP} = \frac{\sum_{i=1}^{n} U_i \times \frac{1}{\sigma_{P_i}^2}}{\sum_{i=1}^{n} \frac{1}{\sigma_{P_i}^2}}$$

$$\sigma_{Q_{PI}} = \sigma_{U_{PI}} = \sigma_{PI} = \sqrt{\frac{1}{\sum_{i=1}^{n} \frac{1}{\sigma_{P_i}^2}}}$$

The mean of P_{IP} is then given by (informative value, we won't use it since we need to work in the (Q, U) plane):

$$P_{IP} = \sqrt{Q_{IP}^2 + U_{IP}^2 - \sigma_{PI}^2}.$$

If σ_{PI}^2 is superior to $Q_{IP}^2 + U_{IP}^2$, we set P_{IP} equal to 0.

So the Q and U of a given star are:

$$Q_\star = Q - Q_{PI}$$

and

$$U_\star = U - U_{PI}.$$

Therfore, the polarization of the stars is given by:

$$P_\star = \sqrt{Q_\star^2 + U_\star^2 - \sigma_P}$$

and, if σ_P is superior to $Q_\star^2 + U_\star^2$, we set $P_\star$ equal to 0.
We have the uncertainty with:

$$\sigma_{P_\star} = \sqrt{\sigma_P^2 + \sigma_{PI}^2}.$$

A.3 Reference Angle

The measured angles are in the frame of the instrument. In order to have them in the frame of the sky, we observed polarized stars for which we know the true angle. The difference between the angle in the litterature ($\theta_{\rm cat}$) and the angle we observed ($\theta_{\rm obs}$) gives the offset between the frame of the instrument and the one of the sky.

Suppose we observed n polarized standards, the offset is given by:

$$\Delta_\theta = \frac{\sum_{i=1}^{n} (\theta_{{\rm cat},i} - \theta_{{\rm obs},i}) \times \frac{1}{\sigma^2_{\theta_i}}}{\sum_{i=1}^{n} \frac{1}{\sigma^2_{\theta_i}}},$$

where

$$\sigma_{\Delta_{\theta,i}} = \sqrt{\sigma^2_{\theta_{{\rm cat},i}} + \sigma^2_{\theta_{{\rm obs},i}}}\ .$$

In the case of the standard stars we used for the B&B, we can consider that:

$$\sigma_{\Delta_{\theta,i}} = \sigma_{\theta_{{\rm obs},i}},$$

as the angle on the standards is well constrained and therefore: $\sigma_{\theta_{\mathrm{obs},i}} \rangle\rangle \sigma_{\theta_{\mathrm{cat},i}}$

And so the error on the offset is given by:

$$\sigma_{\Delta_\theta} = \sqrt{\frac{1}{\sum_{i=1}^{n} \frac{1}{\sigma^2_{\theta_i}}}}.$$

We then have that the angle of the polarization vector is:

$$\theta = \theta_{obs} + \Delta_\theta$$

and that:

$$\sigma_\theta = \sqrt{\sigma^2_{obs} + \sigma^2_{\Delta_\theta}}\ .$$

We can test to verify that the angle is not negative, and if this is the case, we add 180°.

A.4 Averaging Mutiple Observations of the Same Star

It is essentially the same as when we averaged observations of unpolarized standard stars. Therefore, if we observed a star n times:

$$Q = \frac{\sum_{i=1}^{n} Q_i \times \frac{1}{\sigma^2_{P_i}}}{\sum_{i=1}^{n} \frac{1}{\sigma^2_{P_i}}},$$

$$U = \frac{\sum_{i=1}^{n} U_i \times \frac{1}{\sigma^2_{P_i}}}{\sum_{i=1}^{n} \frac{1}{\sigma^2_{P_i}}},$$

$$\sigma_Q = \sigma_U = \sigma_P = \sqrt{\frac{1}{\sum_{i=1}^{n} \frac{1}{\sigma^2_{P_i}}}}\ .$$

If $Q^2 + U^2 > \sigma^2_P$, then:

$$P_{\mathrm{unbiased}} = \sqrt{Q^2 + U^2 - \sigma^2_P},$$

else P

$$_{\mathrm{unbiased}} = 0,$$

and:

$$\theta = \frac{1}{2} \times \tan^{-1}(\frac{U}{Q}),$$

$$\sigma_\theta = 28.65^\circ \ \frac{\sigma(P)}{P}.$$

Annexe B

Guide to Analyze the Data of "La Belle et la Bête" Instrument of Mont-Mégantic

A. Simon

B.1 Retrieve the Information from the ".res" File and Retrieve the Standards Observed During the Run

First of all, we have to retrieve the information we are interested in the ".res" file. That is completed with the stars.pro program. The input is the name of the file, without the ".res" part. For example, for the data measured during the night of the 2nd of March 2010, you call the program "stars.pro" that way:

IDL› stars, '20100302'

The output is a file named "name_of_file.txt" ("20100302.txt" in our example). This file is a column file with:

1. The name of the star
2. The polarization (the efficiency already taken into account)
3. The sigma error on that polarization (the efficiency already taken into account)
4. The angle of polarization
5. The sigma error on that angle
6. The signal over noise ratio
7. The number of photons counted for that star
8. The duration of the integration (in minutes and without taking into account the integration on the sky)
9. Hour at the beginning of the first integration
10. Minutes at the beginning of the first integration
11. Seconds at the beginning of the integration
12. The diaphragme used
13. The date when the data were taken (in the form YearMonthDay)

Then the program will retrieve the standards you observed during the night. You will need to have the files "SNP_Turnshek.txt", "SNP_planetpol.txt" and "SP.txt" in the same folder than the program.

Be sure that the names you give for the standard stars you are observing are the exact same names as in this files.
The "stars.pro" program will compare the name of the stars you observed with the name of the standards stars. This, in order to know which star you observed because it is a standard star and which star you observed because it is a target.

The output is two files with the standards you observed during the night. The unpolarized standards will be registered in a "NP_nom_fichier.txt" file ("NP_20100302.txt" in our example). The polarized standard stars will be registered in a "SP_nom_fichier.txt" file ("SP_200100302.txt" in our example).

To be certain that this program will work in an automatic way, make sure that:

1. You give the real name of the star (be consistent if you observe the same star more than one time).
2. The name given for a standard star is the same name as in the files given to you with the lists of the standards.
3. You made the integration on a star in one go (the case where the integration is performed in two parts is not treated by this program, you will have to go manually in the data and compute the result yourself).
4. If the program closed after midnight and you opened it again, the new results won't be registered in the "date.res" file you want ("200100302.res" file in our example) but with the date when you opened the program again, the day after you began your night ("200100303.res" in our example). You can just copy and paste the parts that are not in the right file. The "stars.pro" program will need to have all the stars observed in the same night in the same file, for having the efficiency of the instrument taken into account.

5. If you do tests where the voltage on the PMTs is null and the counts are 0, the program "stars.pro" might bug. Just erase manually the lines where you did this tests.
6. If you made a mistake during the night (named the star with the wrong name...), we recommand you to correct the errors directly in the ".res" file. (But make sure you have the original files unchanged somewhere else)
7. **Don't switch the outputs of the PMTs during a run, the angle changes of 90 degrees when you do so.**

Now you have to create three files :

1. "SPobs.txt"
2. "SNPobs.txt"
3. "stars.txt"

Copy and paste the results that were in the "SPnom_fichier.txt" file in the "SPobs.txt" file, the results that were in the "NP_nom_fichier.txt" file in the "SNPobs.txt" file and the results that were in the "name_of_file.txt" file in the "stars.txt" file.

Repeat all the previous steps for all the nights of the run. In that way, all the stars of a run will be in the same file, as all the standards observed during that run.

B.2 Analysis of the Results

The lists we have created will be analysed with the "analyse.pro" program. The analysis formulae is given in : "Data analysis of polarization measurements" file. The input of "analyse.pro" is the number of the run (third run in our example). You call it this way:
IDL› analyse, 3
The results will be given in "stars_3.txt". It is a column file with:

1. The name of the star

2. The polarization of the star
3. The sigma error on the polarization
4. The ratio between the polarization and the sigma error on it
5. The angle of the star
6. The sigma error on the angle of the star
7. The signal over noise ratio
8. The number of photons counted for that star
9. The duration of the integration (in minutes and without taking into account the integration on the sky)
10. Hour at the beginning of the first integration
11. Minutes at the beginning of the first integration
12. Seconds at the beginning of the integration
13. The diaphragme used
14. If the star is a standard star, if it is an efficiency measure or if it is a star from the list you wanted to observe
15. The date when the observations were performed (in the form YearMonthDay)

B.3 Particular Cases

1. As previously mentionned, the case where the integration is done in two parts is not treated by this program, you will have to go manually in the data and compute the result yourself.
2. If you observed many times the same star, you have to do the mean of the observations with the formulae given in the "Data analysis of polarization measurements" file.
3. If the mean polarizations given by the PMTs and corrected for the overestimation of the polarization are 0, then, the program of the Beauty doesn't give you the mean of the polarization (which is 0) and the mean of the error on P (you have to compute it with the formulae given in the "Data analysis of polarization measurements" file).

Annexe C

Optical Tests of the POL-2 Polarimeter at the University of Western Ontario

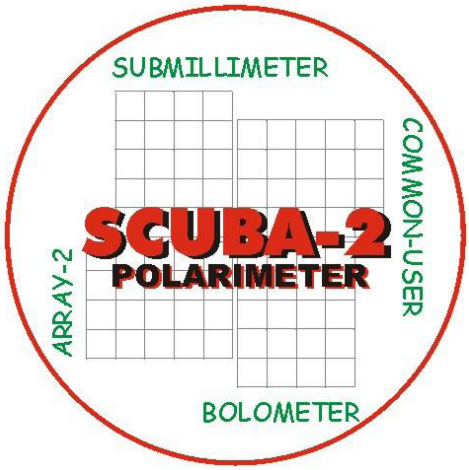

SCUBA-2 Polarimeter Project Office
Université de Montréal
Département de physique
B. P. 6128, Succ. Centre-ville
Montréal, Québec
Canada H3C 3J7

Tel: 1-514-343-5816
Fax: 1-514-343-2071

WWW: http://www.astro.umontreal.ca/~bastien/scuba2/polarimeter

Document Title: RESULTS OF OPTICAL TESTS OF POL-2 CONDUCTED AT UWO IN JUNE 2009

Document Number: SC2/POL/TST/005

Issue: Version 2.0

Date: 26 March 2010

Document Prepared By:	Amélie Simon, Pierre Bastien and Martin Houde	Signature and Date:
Document Approved By:	Michel Fich Polarimeter Project Lead	Signature and Date:
Document Released By:	Michel Fich Canadian Project Leader	Signature and Date:

Université de Montréal

Change Record

Issue	Date	Section(s) Affected	Description of Change/Change Request Reference/Remarks
0.1	16/06/2009		Section 1, first draft by AS; section 2 without fits and figures
0.2	16/06/2009		Corrections by PB
0.3	16/06/2009		Correction of orthographic errors
0.4	27/01/2010	Section 2	Fits of POL2, analyzer and calibrator
0.5	29/01/2010	Section 2	Better fits at 667 GHz (450μm)
0.6	30/01/2010	Section 2	Better fits for analyzer and calibrator
0.7	06/02/2010	Section 2	All fits done included
0.8	1-2/03/2010	Section 2	New fits with standing waves for POL-2 and HWP
0.9	10/03/2010	Section 2	New fits again!
1.0	17/3/2010	Whole document	
1.1	22/3/2010	Whole document	Take into account comments by MH
1.2	25/3/2010	Section 3	Discuss consequences of standing waves
2.0	26/3/2010	Section 3	Minor correction, version for release

Contents

Results of Optical Tests of POL-2 Conducted at UWO in June 2009

Preamble

The tests performed in the Submillimeter Astronomy Laboratory at the University of Western Ontario (UWO), London, ON in June 2007 showed that the signal is affected by vibrations which occur when the half-wave plate (HWP) is rotating continuously. The rotation mechanism has been improved and new tests were performed in April 2008 but the vibrations were still present. To solve this problem, the original lithographically etched polarizers were replaced with wire grid polarizers. We have made additional tests at the UWO on 9 – 10 June 2009 in order to find out if the vibrations still occur when the HWP rotates, and to measure the response of the new HWP and of the whole instrument.

The set up is essentially the same than in June 2007 (please refer to the report SC2_POL_TST_003 for the details; hereafter referred to as the June07 report).

1- Tests with the Half-Wave plate in Rotation

Tests with the HWP in rotation were done at 353 GHz. These tests are not quantitative. What is available is a display of the signal as a function of time (transmission on a log-scale vs. time).

Figure 1 shows the result with the analyzer in the beam and the HWP rotating at 300 RPM in front of it. No vibrations can be seen and we have a stable signal. However one sees that every second peak is higher than the other ones. This behaviour occurred only when one of the polarizers was in the beam. When only the rotating HWP is in the beam this effect is not as strong (see Figure 3). When the analyzer and the calibrator are in the beam all the peaks have more or less the same intensity.

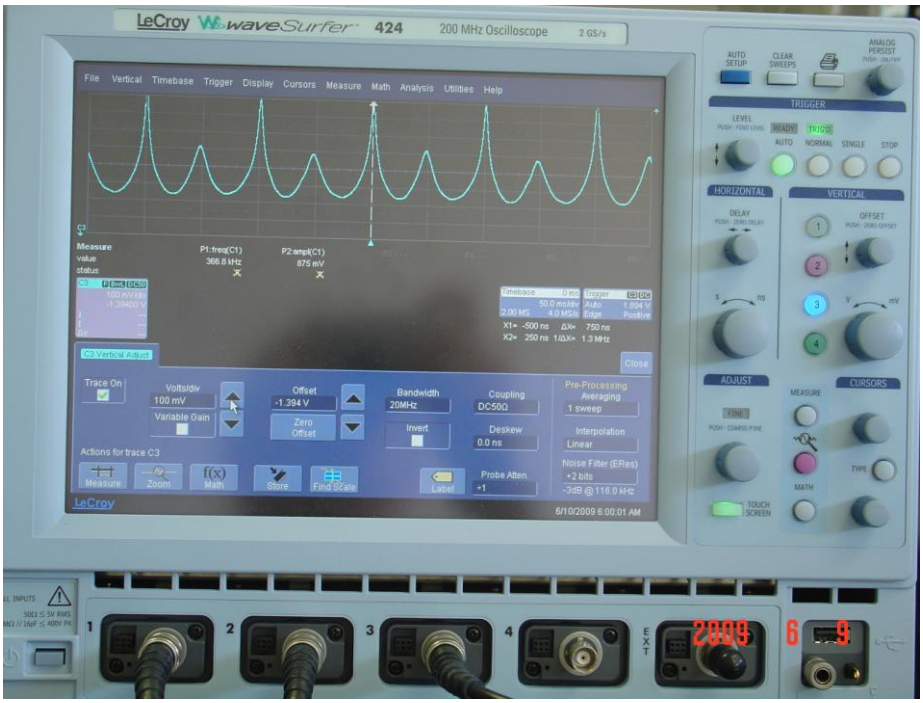

Figure 1: The signal at 353 GHz when the HWP rotates at 300 RPM with the analyzer in the beam.

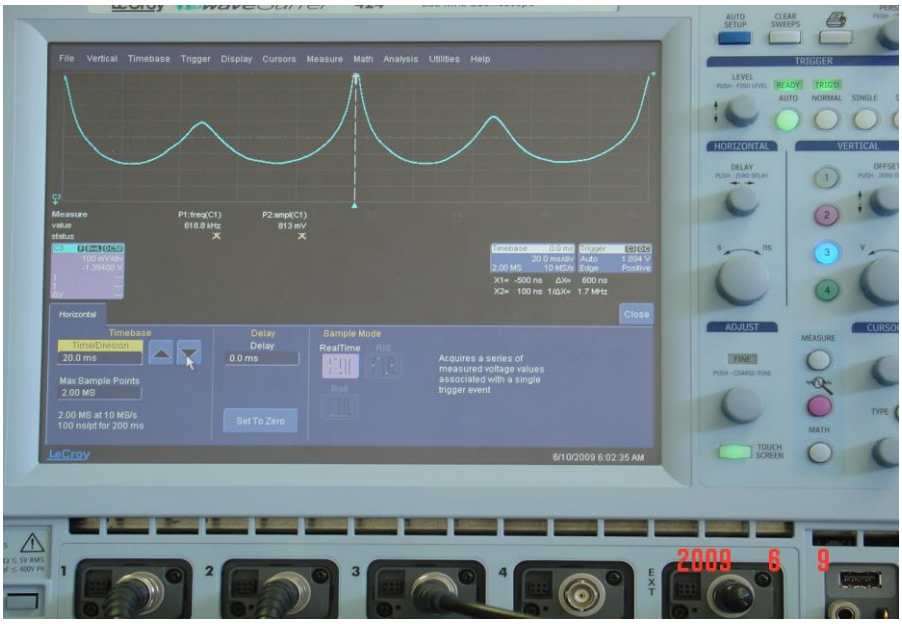

Figure 2: The signal at 353 GHz when the HWP rotates at 300 RPM, with the analyzer in the beam, with an increased time scale. The curve is smooth and no vibration effects are seen.

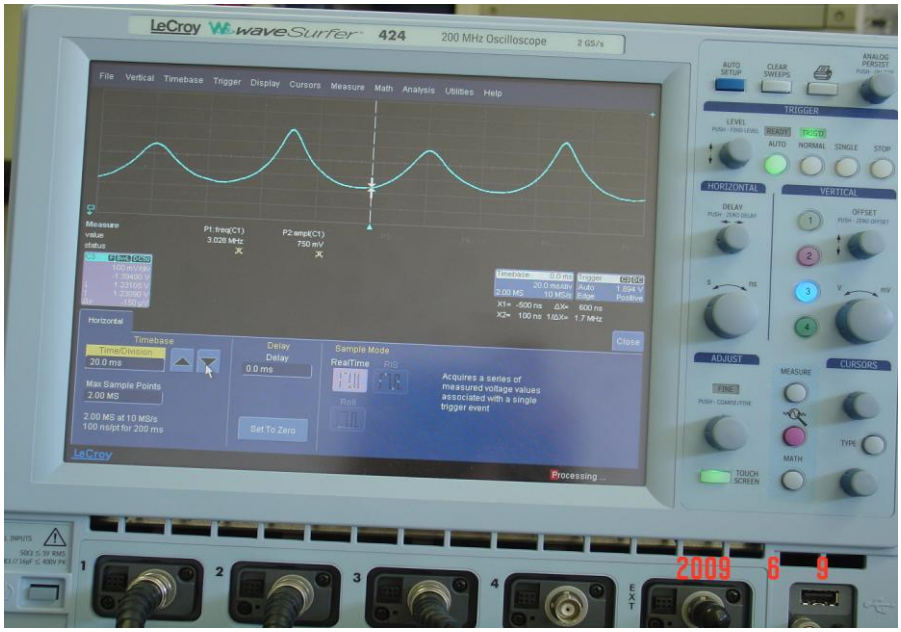

Figure 3: Signal with the HWP rotating at 300 RPM, at 353 GHz, without the analyzer and the calibrator.

We received a second HWP (named SG-HWP for science grade half-wave plate, even though it's identical to the first one); we measured the signal as a function of time with this new half-wave plate rotating (Figure 4). The response of the new HWP is as expected.

Figure 4: Signal with the new HWP rotating at 300 RPM, at 353 GHz, without the analyzer and the calibrator.

2- Tests with Fixed Optical Components

2a- Half-wave Plate

The performance of the first HWP was measured in June 2007 (see report SC2/POL/TST/003) and April 2008 (see report SC2/POL/TST/004). Details will be found in these reports.

We measured the performance of the new HWP at 353 GHz (850 μm) and 667 GHz (450 μm) using essentially the same set-up than for the tests performed in the two previous runs. We rotated the HWP every 10° and took measurements without the HWP and then with it in the beam.

A careful analysis of the results of these tests revealed that they are not as good as those of the previous runs. First, we suspect that the emitter (source) and the receiver were not aligned perfectly, i.e., their polarization axes were not in the same "vertical" plane. Therefore introducing the HWP in the beam could change the axis of polarization, and in some cases improve the throughput to give a transmission efficiency higher than 1. To take this effect into account, we normalized the data so that the maximum measured signal is 1. This normalization prevents us from determining the transmission through the new HWP at the specific frequencies of the measurements (but see Section 2b for the overall efficiency of POL-2.

However, the main effects are due to standing waves in the system. These effects are much more important than during the previous runs, with the first HWP. Simple modeling leads us to modify the fitting function to take the standing waves into account by providing a sinusoidal amplitude modulation at four-times the HWP angular position for both the incident and transmitted signals. Although the effect of standing waves probably includes higher harmonics, this simple model allows for reasonable fits to the data; the results are shown below. The function used for the fits is:

$$I(\theta) = I\left\{1 + A_{sw1}\sin\left[4(\theta - \phi_1)\right]\right\}\left\{1 + A_{sw2}\sin\left[4(\theta - \phi_2)\right]\right\}\sin\left[4(\theta - \phi_0)\right] + I_0 \quad (1)$$

The intensity I is the measured intensity of the modulated signal and I_0 is an offset. The two braces are corrections due to standing waves. The other sine factor has the 4-fold modulation introduced by rotating the HWP.

Half-wave plate at 850 μm

By taking some initial measurements, we determined the approximate position angle of the (first) maximum to be at 35°.

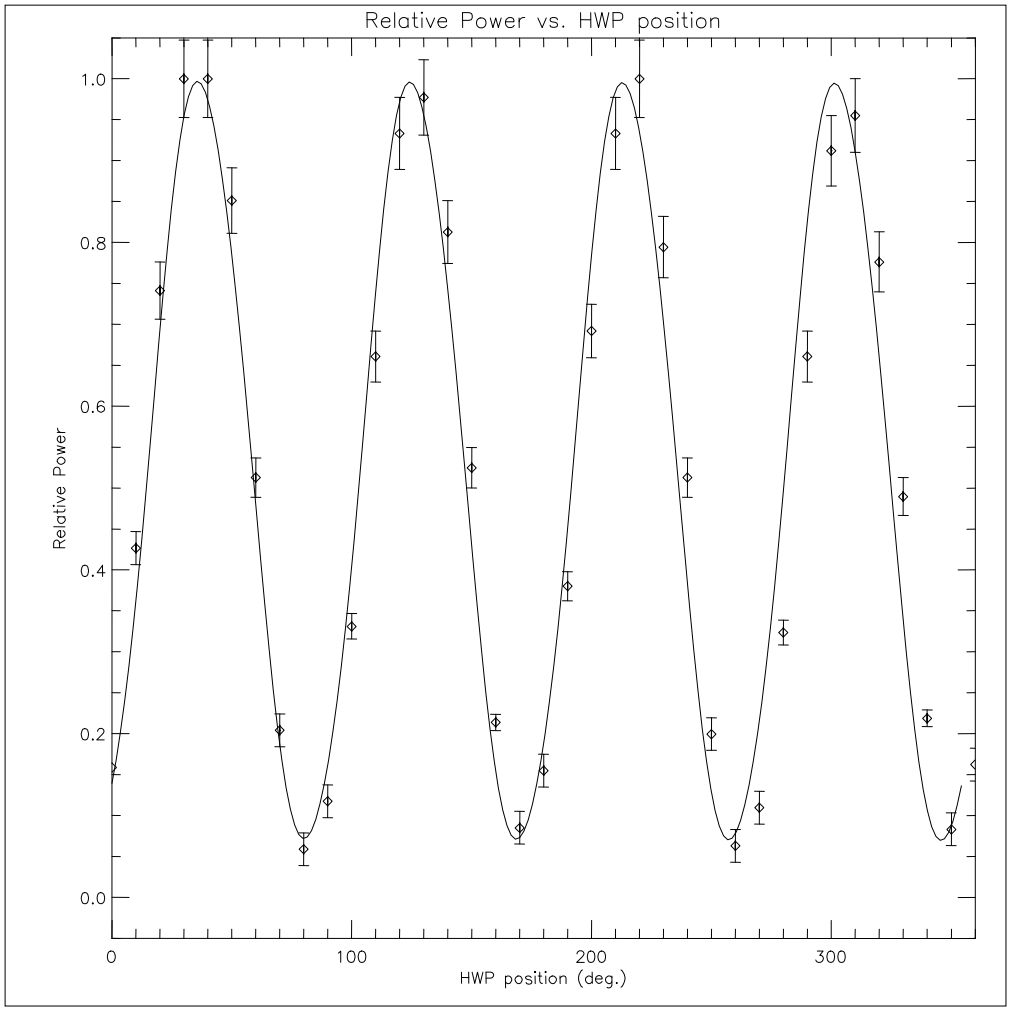

Figure 5: Transmitted signal through the HWP as a function of the position angle of the HWP at 353 GHz.

The polarization efficiency that we deduce from the fit, taking all parameters into account is 0.86 (see Table 1).

Half-wave plate at 450 μm

We repeated the same process for the HWP at 667 GHz.

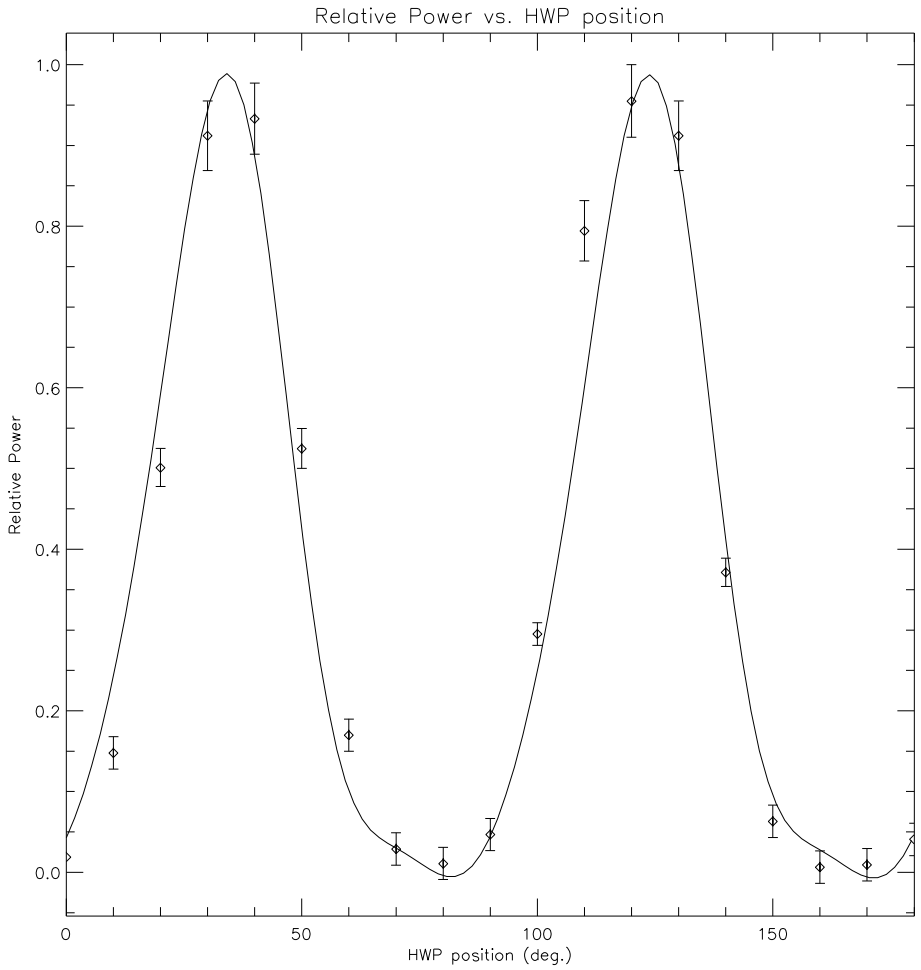

Figure 6: Transmitted signal through the HWP as a function of the position angle of the HWP at 667 GHz.

The fit yields a (formal) polarization efficiency of: 1.01.

Table 1. Parameters of the fits for the SG HWP.

Comp.	I	ϕ_0	I_0	A_{sw1}	ϕ_1	A_{sw2}	ϕ_2	Pol.Ef.
SGHWP8	0.48	14.96	0.51	-0.26	25.68	-0.29	-21.34	0.86
SGHWP4	0.49	9.75	0.24	-0.38	77.71	0.60	2.99	1.01

2b- POL-2

Finally, the polarizing efficiency of the whole instrument was measured at 353 GHz and 666.9 GHz. We rotated the HWP every 10°. Standing waves are taken into account in the fit with equation (1).

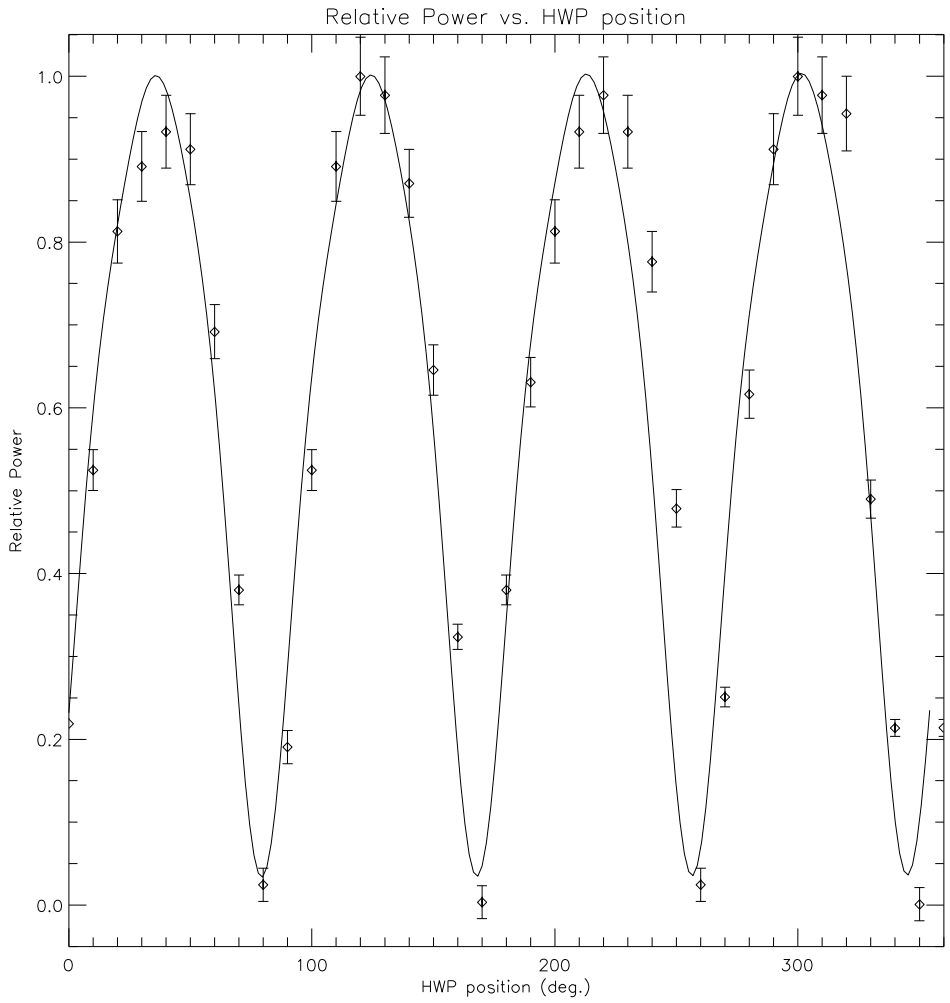

Figure 11. Transmitted signal through POL-2 as a function of the position angle of the HWP at 353 GHz.

The fit yields a polarization efficiency of 94%.

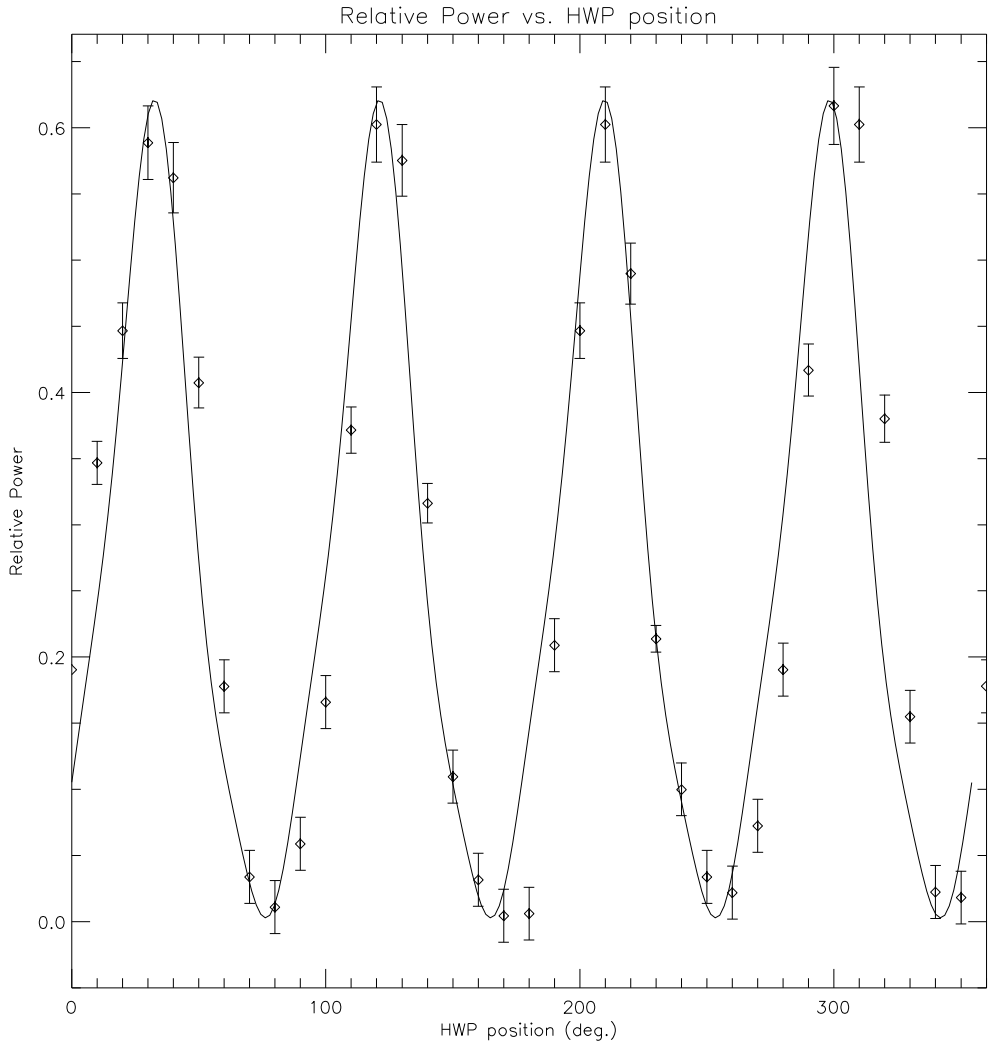

Figure 12. Transmitted signal through POL-2 as a function of the position angle of the HWP at 667 GHz.

The fit yields a polarization efficiency of 99%.

Table 3. Parameters of the fits for POL-2.

Comp.	I	ϕ_0	I_0	A_{sw1}	ϕ_1	A_{sw2}	ϕ_2	Pol.Ef.
POL2-8	0.47	13.57	0.69	-0.53	-4.51	-0.50	30.15	0.94
POL2-4	0.31	8.51	0.22	0.58	-5.10	0.58	32.01	0.99

Summary.

Table 4. Parameters for all the fits.

Comp.	I	ϕ_0	I_0	A_{sw1}	ϕ_1	A_{sw2}	ϕ_2	Pol.Ef.
SGHWP8	0.48	14.96	0.51	-0.26	25.68	-0.29	-21.34	0.86
SGHWP4	0.49	9.75	0.24	-0.38	77.71	0.60	2.99	1.01
POL2-8	0.47	13.57	0.69	-0.53	-4.51	-0.50	30.15	0.94
POL2-4	0.31	8.51	0.22	0.58	-5.10	0.58	32.01	0.99

$$I(\theta) = I\left\{1 + A_{sw1}\sin\left[4(\theta-\phi_1)\right]\right\}\left\{1 + A_{sw2}\sin\left[4(\theta-\phi_2)\right]\right\}\sin\left[4(\theta-\phi_0)\right] + I_0 \quad (1)$$

3- Summary and Conclusions

The so-called vibrations problem has been resolved with the new polarizers. No effects due to vibrations can be detected to our level of sensitivity. The mechanical improvements and particularly the replacement of the first polarizers with wire-grid polarizers have been instrumental to achieve this.

Unfortunately, the new measurements with the new HWP and wire grids are affected by standing waves. These effects have been modeled as much as possible and the polarization performance of the components has been determined. Despite the problems encountered, the new HWP and the instrument as a whole perform as expected.

Table 5. Results for the polarization efficiencies of the SG HWP and the whole instrument.

Device	353 GHz	667 GHz
SG HWP	86%	101%
POL-2	94%	99%

The measurements performed during this period of tests show that standing waves are more important with the new optical components (wire-grid polarizers and the SG HWP) than they were with the previous ones (lithographically-etched polarizers and the first HWP).

A comparison with the measurements taken at Lethbridge (see the SC2_POL_TST_006 report) will show that standing waves are less important in those, but are nevertheless still present. The most likely reason is probably that since the Lethbridge measurements were made in wide bands (the SCUBA-2 filters), then the effects of standing waves are thus attenuated through averaging across the signal bandwidth. Clearly, these effects will have to be evaluated in the telescope environment before the instrument is used for scientific observations.

We thank Talayeh Hezareh for help with setting up the instrument and taking the measurements in the lab.

-.-.-.-.-

Annexe D

Optical Tests of the POL-2 Polarimeter at the University of Lethbridge

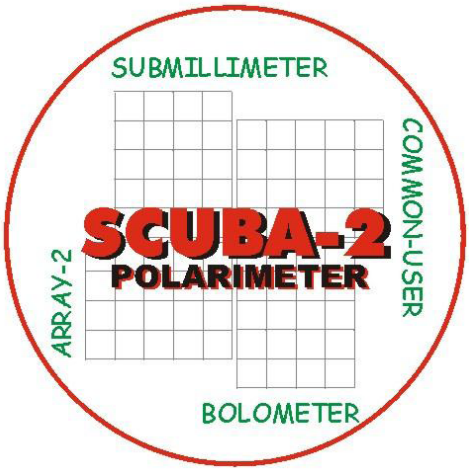

SCUBA-2 Polarimeter Project Office
Université de Montréal
Département de physique
B. P. 6128, Succ. Centre-ville
Montréal, Québec
Canada H3C 3J7

Tel: 1-514-343-5816
Fax: 1-514-343-2071

WWW: http://www.astro.umontreal.ca/~bastien/scuba2/polarimeter

Document Title: RESULTS OF OPTICAL TESTS OF POL-2 CONDUCTED AT UOL IN SEPTEMBER 2009

Document Number: SC2/POL/TST/006

Issue: Version 1.2

Date: 14 April 2010

Document Prepared By:	Amélie Simon, Pierre Bastien	Signature and Date:
Document Approved By:	Michel Fich Canadian Project Lead	Signature and Date:
Document Released By:	Michel Fich Canadian Project Leader	Signature and Date:

Université de Montréal

Change Record

Issue	Date	Section(s) Affected	Description of Change/Change Request Reference/Remarks
0.1	06/02/2010		
0.2	11/03/2010		New plots
0.3	14/03/2010		Corrections made by Pierre
0.4	14/03/2010		Plots for HWPs rotating
0.5	17/03/2010		Plot with the standing waves
0.6	22/3/2010		Pictures
0.7	25/03/2010	2	New fits
0.8	29/03/2010	1, 2	New section 1 with instrumental set up
0.9	31/03/2010	1, 3	Filter description, new table and new plots
1.0	01-05/04/2010	All	Add discussions, non-linearity, conclusions, formatting ... Version for internal distribution
1.1	10-12/04/2010	1, 2, 3	Integrate comments from BG, MH, info from Savini
1.2	14/04/2010	Add new 3.2	New subsection to present a comparison with the Savini paper

Contents

Results of Optical Tests of POL-2 Conducted at UOL in September 2009

Preamble

The tests performed in the Submillimeter Astronomy Laboratory at the University of Western Ontario (UWO), London, ON in June 2007 showed that the signal is affected by vibrations which occur when the half-wave plate (HWP) rotates continuously. The rotation mechanism has been improved and new tests were performed in April 2008 but the vibrations were still present. To solve this problem, the original lithographically etched polarizers were replaced with wire grid polarizers. We have made additional tests at the UWO in June 2009 in order to find out if the vibrations still occur when the HWP is rotating, and to measure the response of the new HWP and of the whole instrument. The vibrations are no longer visible (see report SC2/POL/TST/005 for more details). But the set-up in UWO did not permit us to register the signal while the half-wave plate (HWP) rotates. In order to have these measurements, we carried out additional tests at the University of Lethbridge, AB, in September 2009 in the laboratory of Prof. David Naylor. Brad G. Gom carried out the tests for us on the 16th of September and David Naylor and Locke Spencer on the 19th of September, as we were not able to do them when we were there.

1. Instrumental Set Up

The detector used for the tests is a He3 cooled bolometer system which was used by the University of Lethbridge FTS at the JCMT. The detector was placed on the SCUBA-2 side of the polarimeter (see Figure 1), and a 'Pegasus' calibrated blackbody source and optical chopper (Figure 2) were placed on the other side. HDPE lenses were used to collimate the blackbody beam and focus it on the detector after going through the POL-2 optical components. However, Figures 1 and 2 show the initial set up where the bolometer is replaced with a room-temperature Pyroelectric detector, and a 320 GHz line source.

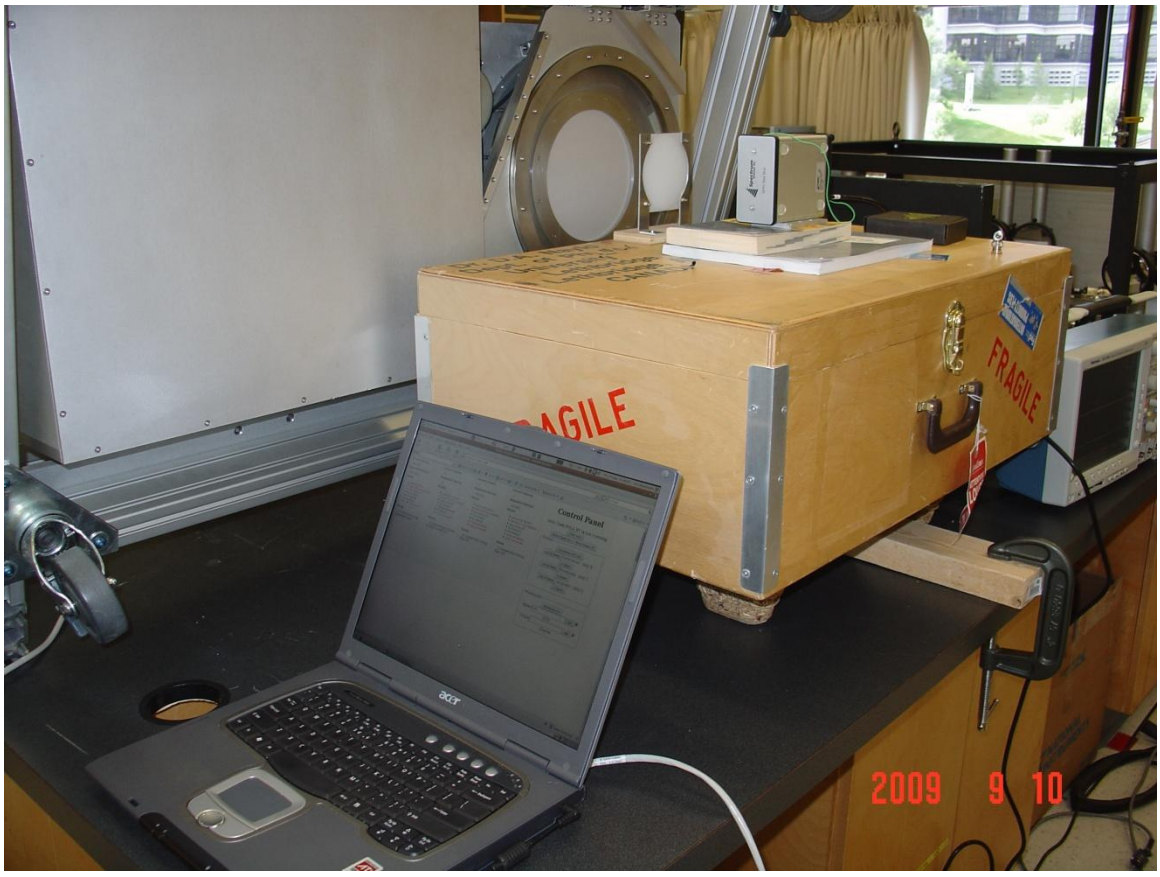

Figure 1. The receiver side. One can see from left to right, the HWP inside its mounting ring, the lens to focus the beam and the detector, a room-temperature Pyroelectric detector.

For the polarizer tests, chopped signal intensity was recorded as a function of the calibrator and analyzer position angles. For the HWP tests, the plate was spun at 2 different speeds, 120 and 300 rpm, while the signal was recorded on a digital oscilloscope.

The band centered around 450 μm that we used corresponds approximately to the wide band that was supposed to be used by SCUBA-2 originally (hereafter, 450w). The actual filter that will be used at the telescope has a narrower bandwidth than the filter we used for the tests. The only exceptions are a few measurements with the optical components fixed that were made with all 3 filters. In particular, all measurements with both HWPs in rotation (Section 3) were made with the 450w filter. The band centered around 850 μm is the same one as the one mounted on SCUBA-2.

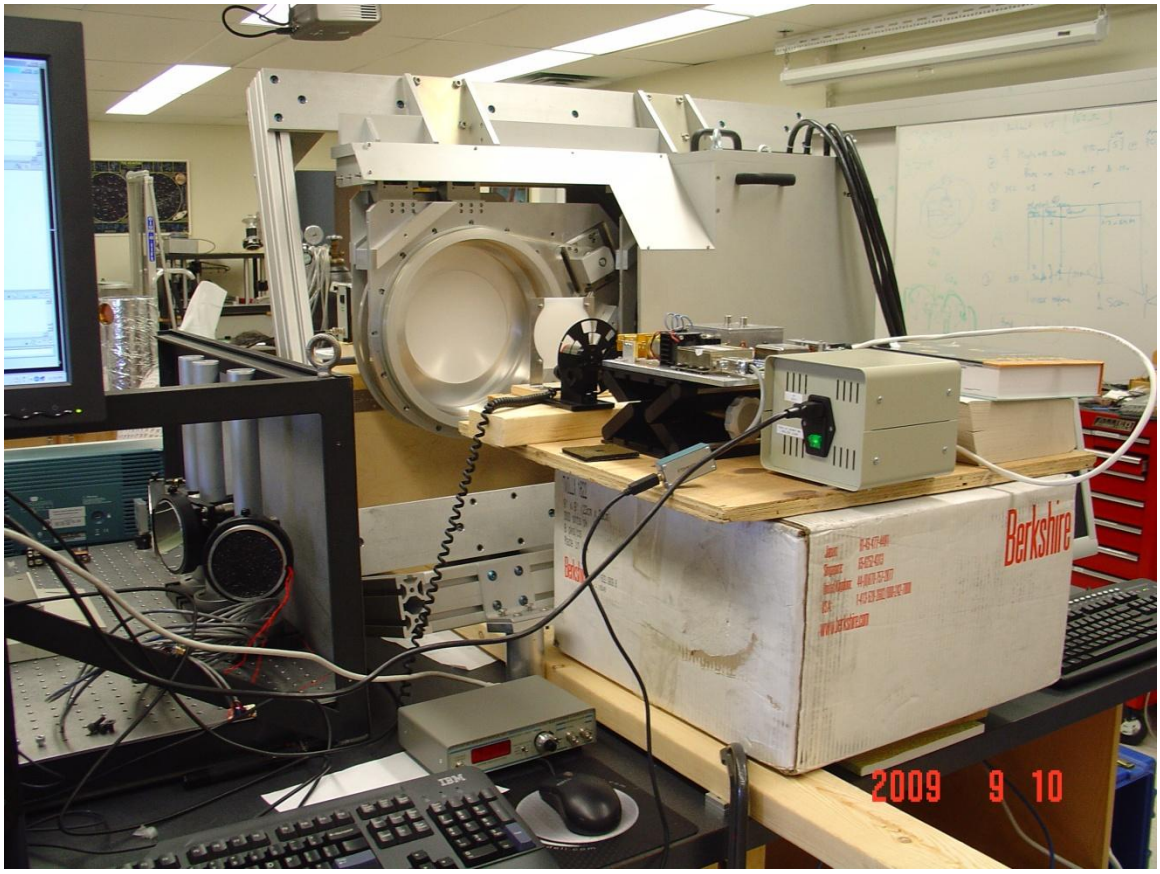

Figure 2. The emitter side of the instrumental set up. One can see from left to right the HWP, the collimating lens, the chopper and a 320 GHz line source. For the tests, a Pegasus black-body source was used instead.

2. Tests with Fixed Optical Components

2.1 Transmittances

The power was measured with and without the two polarizers in the beam, in order to have their transmittances in the two SCUBA-2 band passes. Unfortunately, these tests were not done with the half-wave plates.

Table 1. Transmittances of the polarizers

	450w	850
Calibrator (W102)	0.527 +/- 0.002	0.529 +/- 0.002
Analyzer (W101)	0.517 +/- 0.002	0.499 +/- 0.002

The transmittance should be 50% for ideal polarizers, but we obtained values which are often superior to what they should be. However, wire grid polarizers are fairly common now and when they are well designed (which is the case here), they are nearly perfect, with a polarization very close to 100%. The only particularity of the three POL-2 polarizers (calibrator, analyzer and a spare one) is their size, 300 mm in diameter, which is rather uncommon.

2.2 Polarizers

Figure 3 shows the signal measured in the band centered around 450 µm when the analyzer is fixed and the calibrator is rotated by steps of 22.5°. The calibrator polarizes the signal and this signal goes through the analyzer, which is an identical grid to the calibrator. This set-up therefore should follow Malus' law.

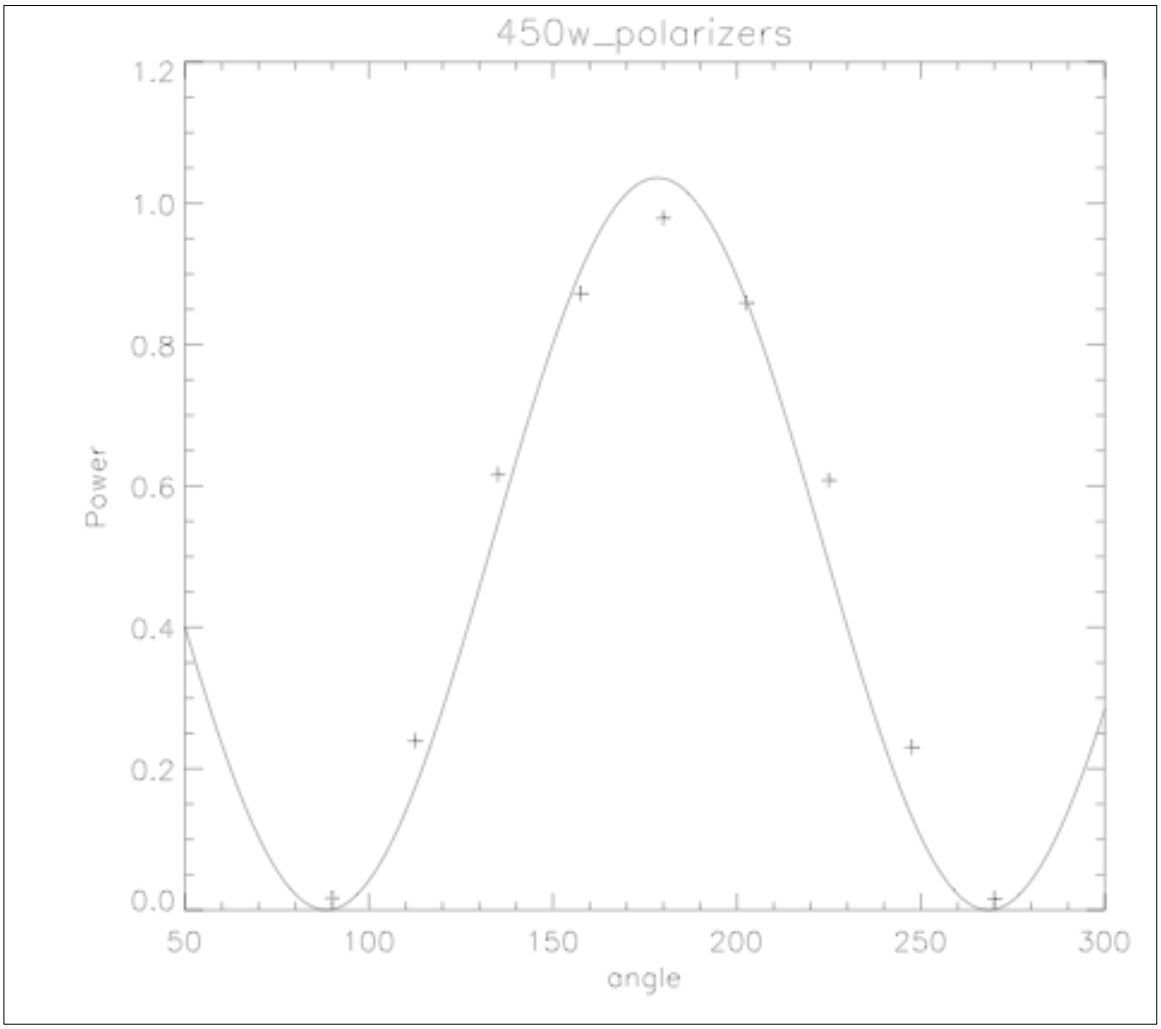

Figure 3: Signal in the 450 µm band recorded by the oscilloscope with respect to the calibrator position angle. The analyzer is kept fixed.

The y-axis represents the signal recorded by a digital oscilloscope. Since no reference level was measured before and after placing the optical components in the beam, the measurements are on a relative scale, i.e., they are not calibrated in terms of absolute power. However, we would expect zero in case of zero signal, and the scale is linear, as demonstrated below.

The fit yields $I(\theta) = 1.04\cos^2(\theta + 1.58°)$

Figure 4 is the same as Figure 3 but at 850 μm.

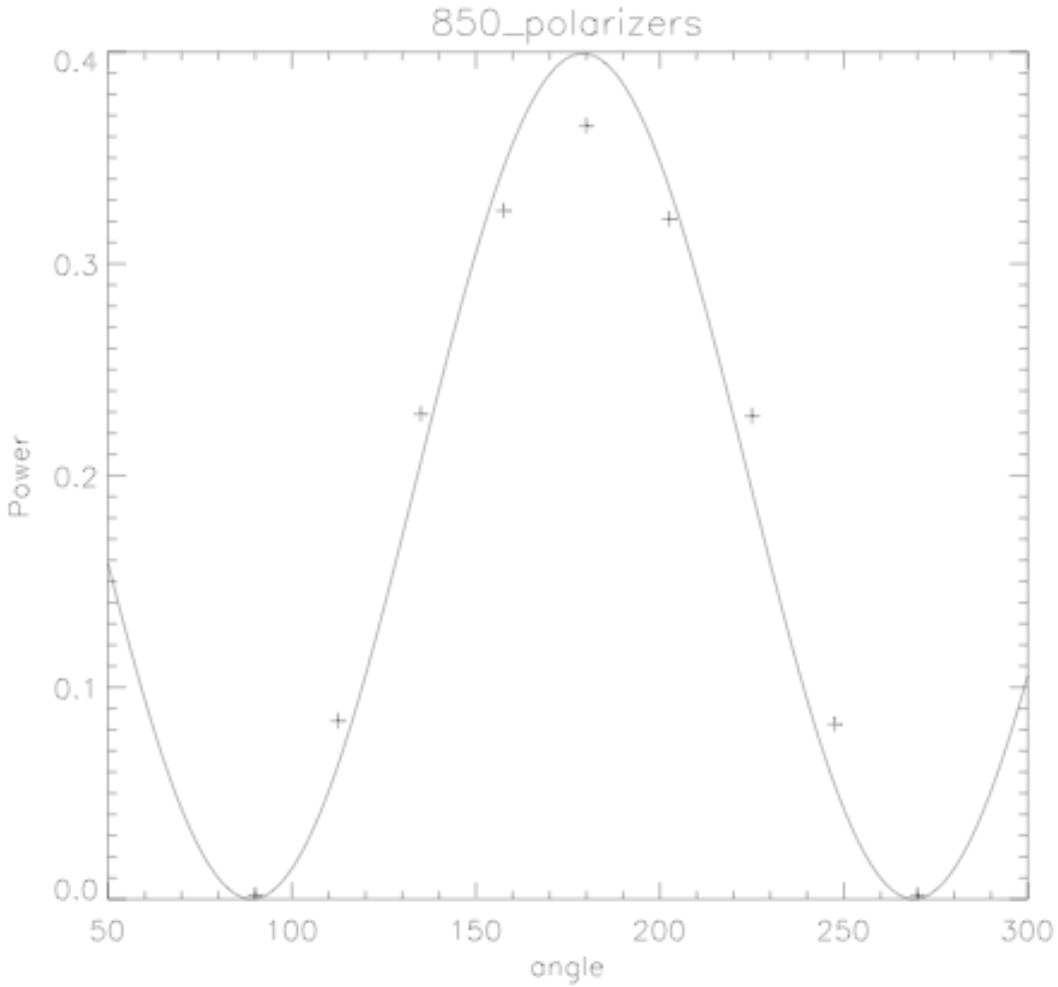

Figure 4: Signal recorded in the 850 μm band by the oscilloscope with respect to the calibrator position angle while the analyzer is kept fixed.

The fit yields $I(\theta) = 0.40\cos^2(\theta + 0.95°)$. We note that the offset in the origin of the two polarizers is very similar in the two band passes, as expected. Deviations from Malus' law are due to standing waves. However, the deviations are not as large as they were in the UWO tests in June 2009. We interpret this difference as being due to the averaging of the signal which is done across the two SCUBA-2 band passes, which reduces the effect.

Effects due to a possible nonlinearity of the detector output were eliminated. To quote an e-mail from Brad Gom dated 5 March 2010:
"The last image (Figure 5) shows the prototype HWP stationary at 0 degree, with an optical chopper modulating the beam at 30 Hz, where you can see that the signal is symmetrical. The speed is faster for the chopped measurement, but this does not affect the signal shape. In each plot, the red trace is the same data as the white trace except inverted and shifted by 180 deg."

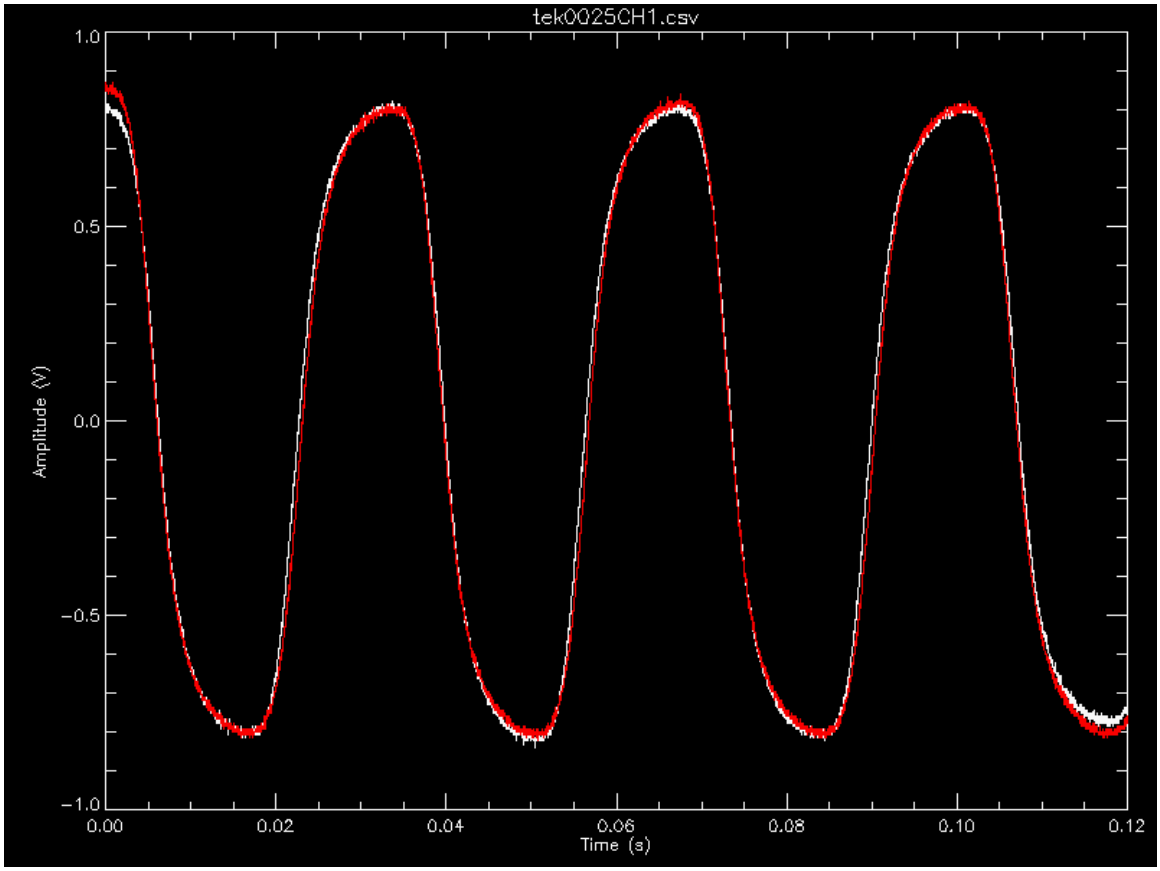

Figure 5. This figure shows that the detector response was linear and non-linearity did not cause the responses measured. See text above for details.

3. Tests with the Half-Wave Plates in Rotation

The two HWP were tested: the science-grade HWP, received from the manufacturer in May 2009, and the first HWP. The science grade HWP was supposed to be an improved version of the HWP (hence the name). In the end, it was not possible to improve on the original recipe for the coatings of the (first) HWP, therefore this is an equivalent version of the HWP, but we kept the SG HWP name nonetheless.

3.1 Science Grade Half-Wave Plate

Two sets of data were registered for each band and each HWP rotation speed: when the calibrator and the analyzer are aligned and when they are perpendicular to each other. Between these two cases, there is a position angle difference of $\pi/4$ for the HWP to have the maximum signal going through. But since we do not know at which position angle the HWP is at the time the data begins to be collected[1], we cannot use this information. Consequently, these two sets of data can be considered as representing the same experiment. We verified each time that the results of the fit of the data for experiments with the same set-up were coherent; it is the case up to 0.5% (see also section 3.2 below).

Here again, a reference signal was not measured just before and after putting the components in the beam, as a consequence, the y-axis represents the signal recorded by the oscilloscope and not a measured fraction of the incoming signal.

We first fitted the data with the function $I\sin\left[4(\theta+\phi_0)\right]+I_0$. The actual function that should be fitted, determined with the Mueller matrices for perfect polarizers and an ideal HWP is $I\cos\left[4(\theta+\phi_0)\right]+I_0$. But the two functions are obviously equivalent. This fit is not satisfactory as can be seen in Figure 6.

[1] However, this will not be the case at the telescope. The observing software will communicate with the POL-2 computer and record the position of the HWP whenever the detector is read. This position will be recorded in the header of the image file.

We then tried to fit the data with the Fourier series:

$$I(\theta) = \sum_i P_i \cos\left[i(\theta + \phi_i) \right], \quad i \in [0,16]. \tag{1}$$

SG HWP at 450 μm

We present here the data taken with the SG HWP, in the wide band centered at about 450 μm and the different fits done.

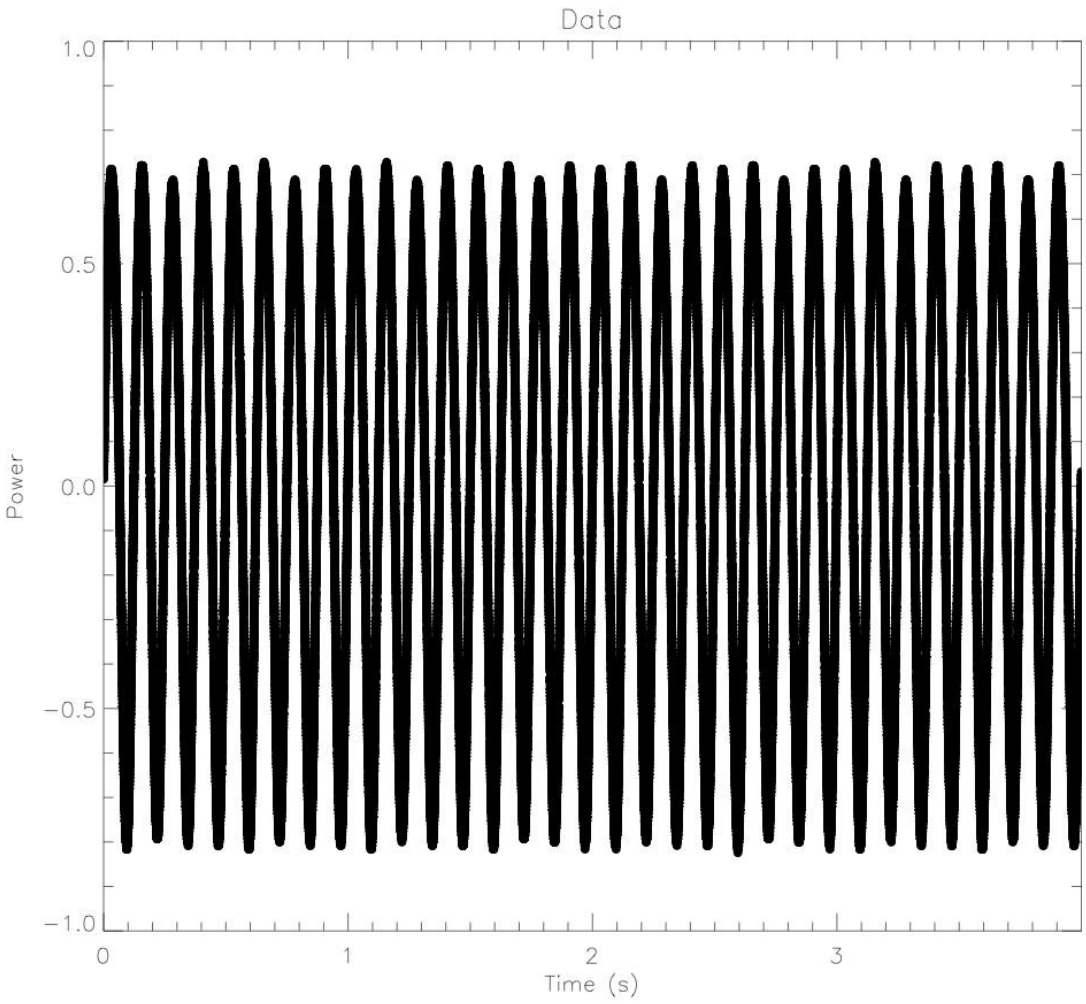

Figure 6: Data for the SG HWP rotating at 120 rpm, recorded in the band centered around 450 μm, when the calibrator and the analyzer are

perpendicular to each other. All the data points obtained during the 4-second integration are shown.

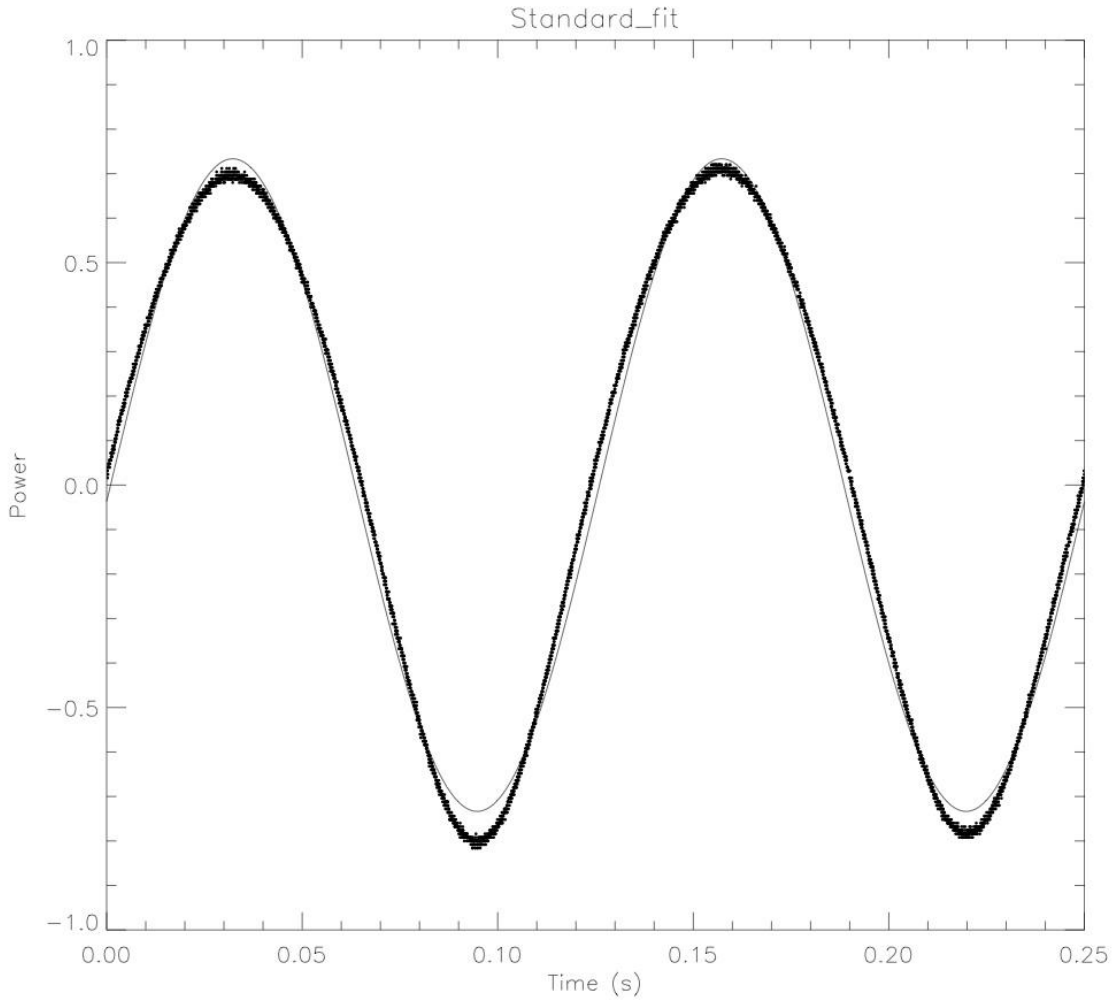

Figure 7. Zoom on the fit of the data for the SG HWP rotating at 120 rpm, recorded in the 450 μm band, when the calibrator and the analyzer are perpendicular to each other. The function fitted to the data is the function for a perfect half-wave plate.

The fit function is $I \sin\left[4(\theta+\phi_0)\right]+I_0$, where:

$I = 0.734$

$\phi_0 = -0.00100$

$I_0 = 0.00850$

We see deviations from the behaviour for an ideal HWP which has only the 4th harmonic of the rotation speed. The result of taking all harmonics from 0 (the constant offset) to 4 is shown in Figure 8.

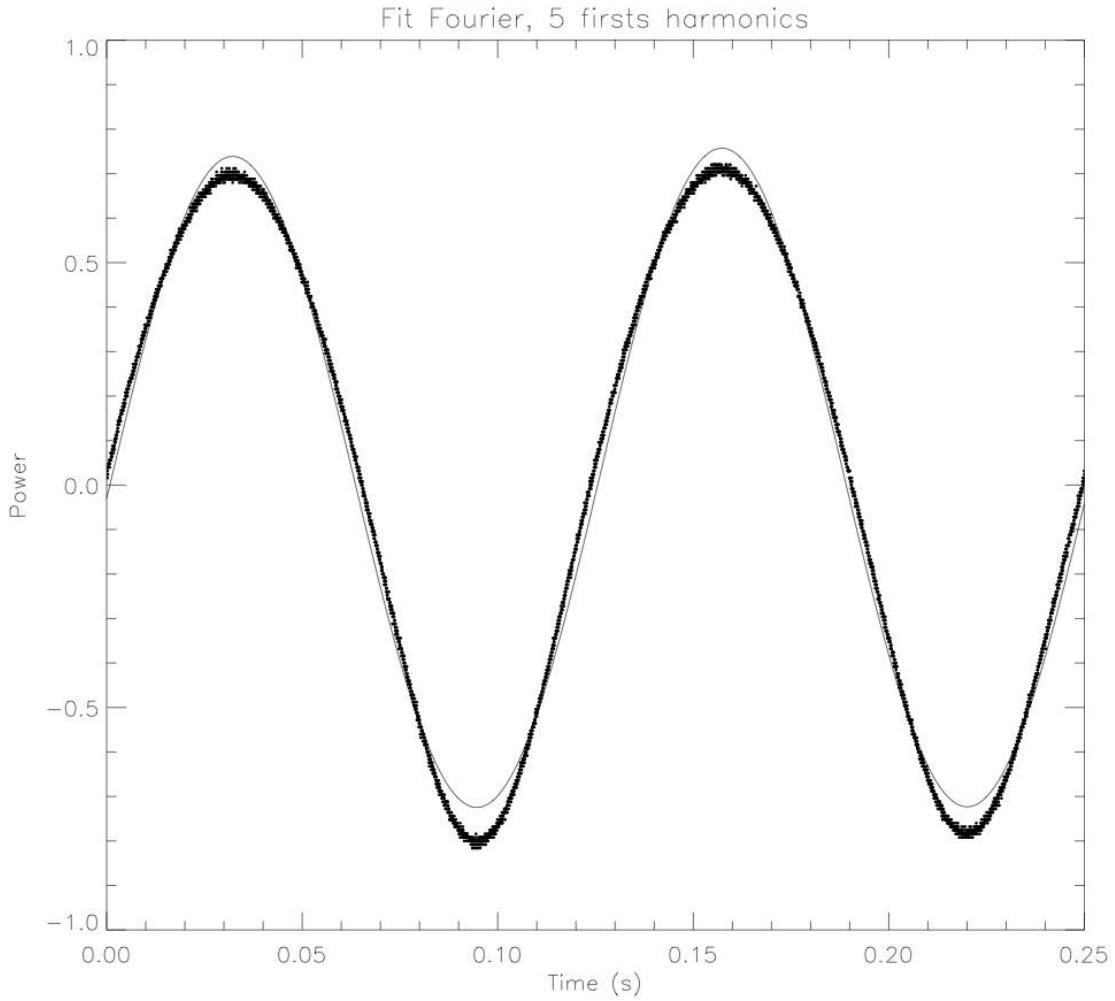

Figure 8: Same data as in Figure 7, this time with a cosine Fourier series with the first five harmonics.

This fit is not satisfactory but we present it here nonetheless in order to compare with the fit done by Savini et al (2009)[2]. This comparison is shown below in Tables 2 and 3 for the two bands. The fit is better than the fit

[2] Savini, G., Ade, P. A. R., House, J., Pisano, G., Haynes, V., & Bastien P. 2009, App. Optics, 48, 2006-2013. *Recovering the frequency dependent modulation function of the achromatic half-wave plate for POL-2: the SCUBA-2 polarimeter.*

presented in Figure 7 (the sides of the curve are closer to the expected curve).

To learn more about the behaviour of the SG HWP, we made another fit with 17 harmonics in a cosine Fourier series (equation 1). This time the fit is essentially perfect, as can be seen in Figure 9 below. We found out that after the 4th harmonic, expected from a perfect HWP, the next dominant harmonic is the 8th one, then the 12th, and the second. The values of the parameters are given in Table 2 below.

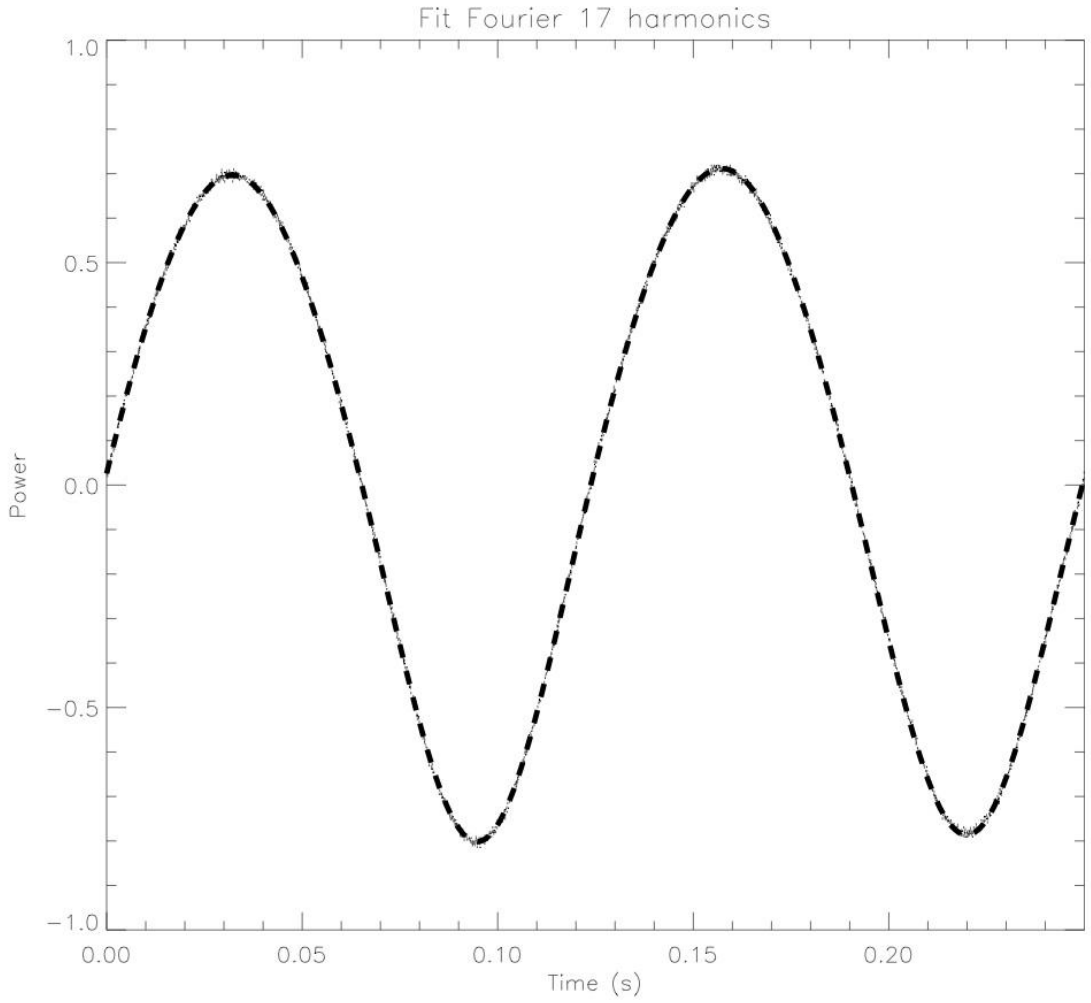

Figure 9: Same data as in Figure 7, this time with a cosine Fourier series with the first seventeen harmonics. The little dots are the data; the thick dashed line is the fit.

SG HWP at 850 μm

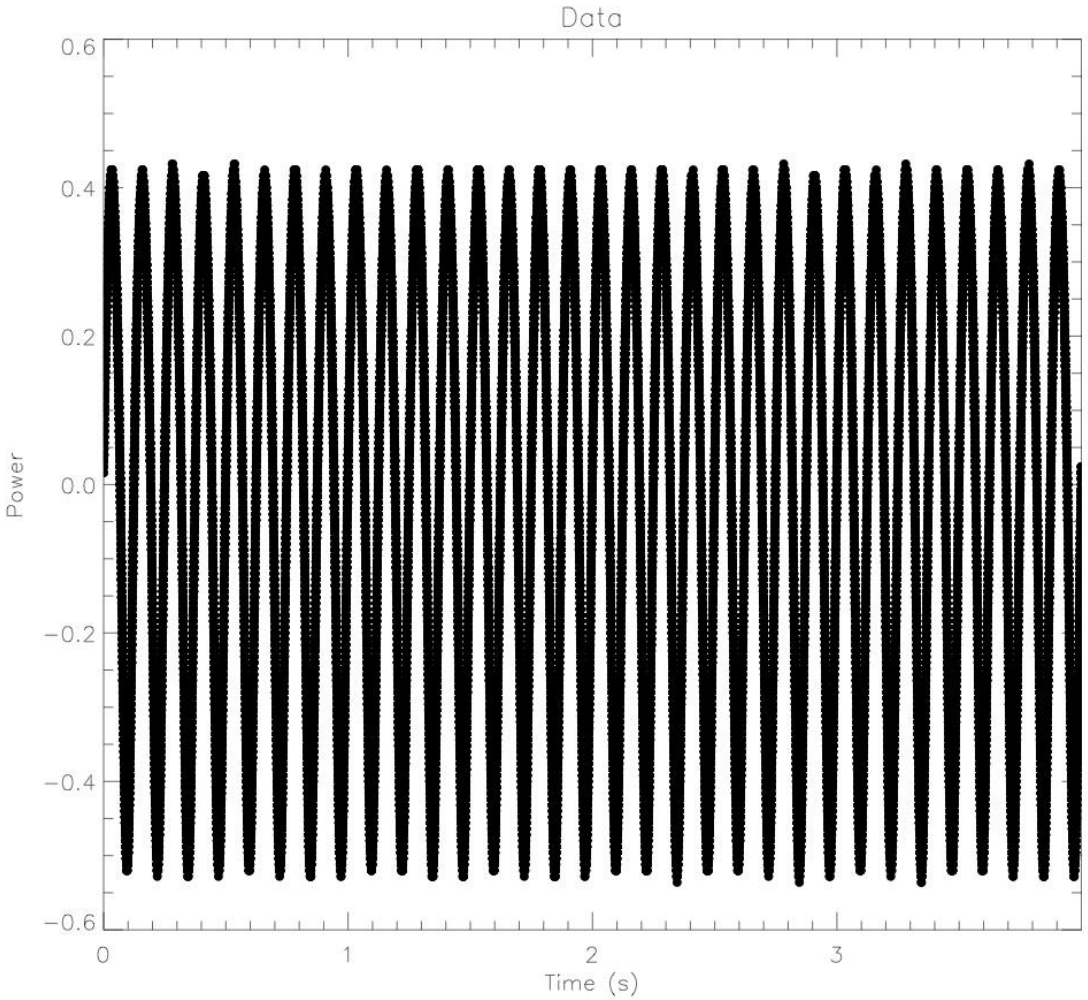

Figure 10: Data for the SG HWP rotating at 120 rpm, recorded in the 850 μm band, when the calibrator and the analyzer are perpendicular to each other.

A fit with the 4th harmonic component for a perfect HWP is given in Figure 11.

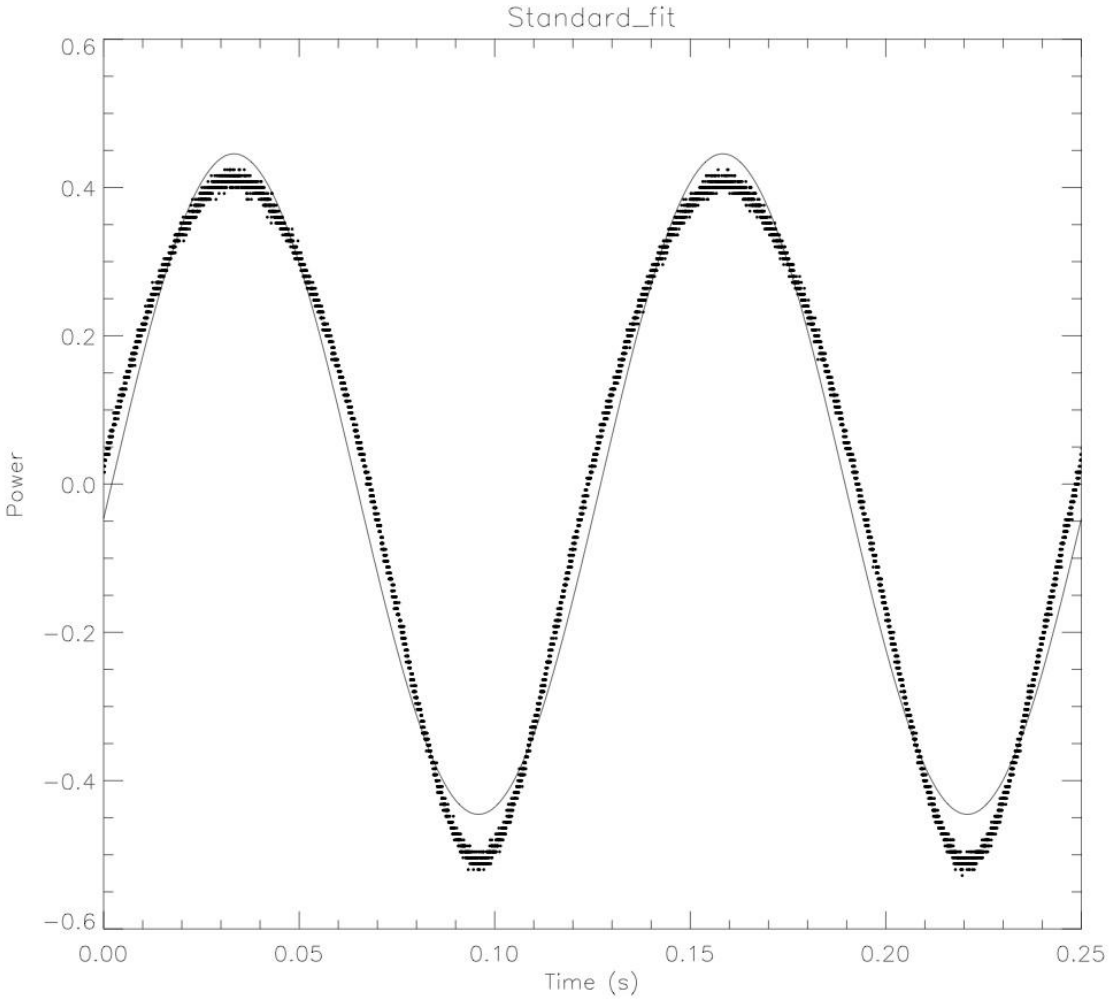

Figure 11: Zoom on the fit of the data for the SG HWP rotating at 120 rpm, recorded in the 850 μm band, when the calibrator and the analyzer are perpendicular to each other. The function for a perfect half-wave plate has been fitted to the data. Compare to Figure 7 for the 450 μm band.

The fit function is $I\sin\left[4(\theta+\phi_0)\right]+I_0$, where:

$I = 0.45$

$\phi_0 = -0.00208$

$I_0 = 0.0088$

A cosine Fourier series with 17 harmonics (equation 1) has been fitted to the 850 μm data and can be seen in Figure 12. The parameters of the fits in both 450 and 850 μm bands are given in Table 2. The columns give respectively the no of the harmonic, and for the two bands, its amplitude (P_i), the ratio of

the amplitude of each harmonic to the amplitude of the 4th harmonic (for a perfect HWP) (P_i/P_4), and finally the phase of the harmonic in degrees.

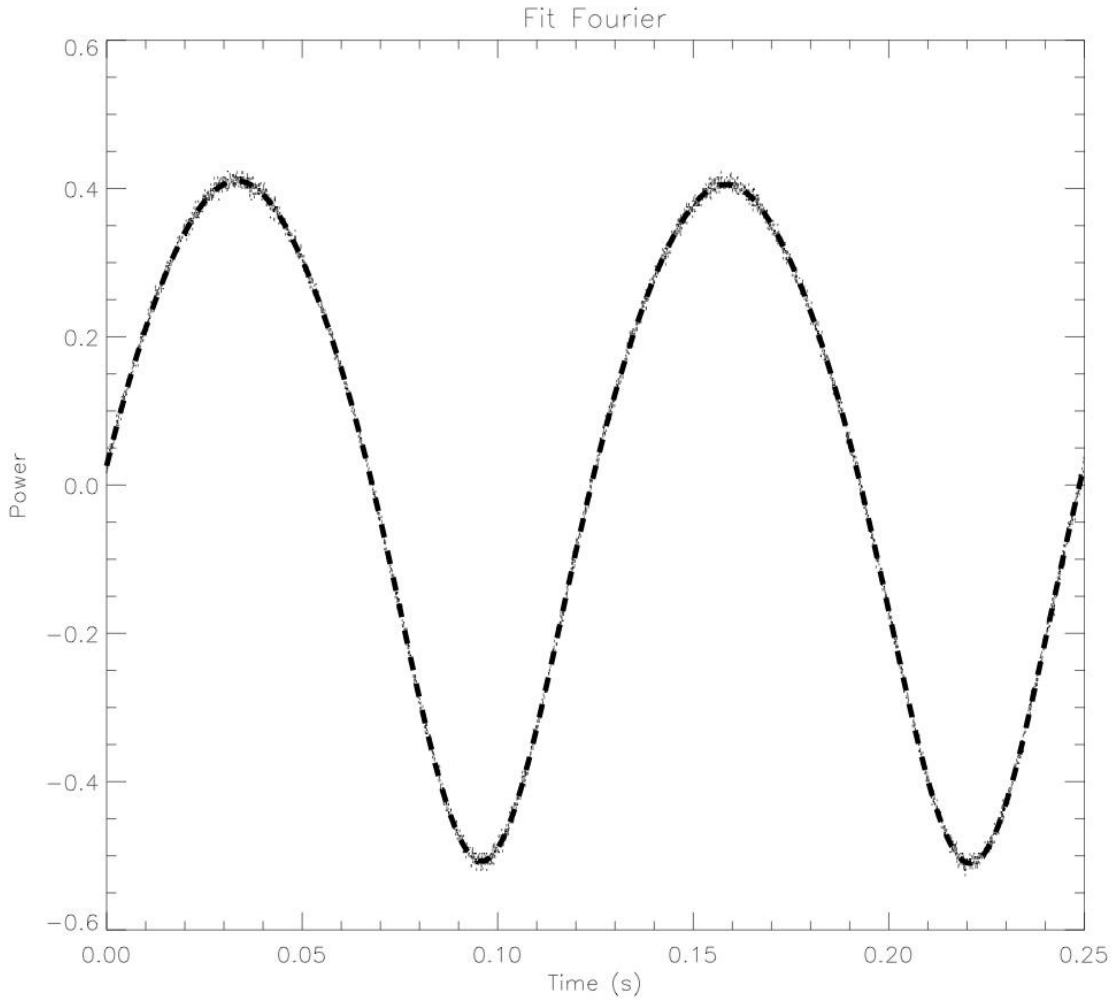

Figure 12: Same as Figure 11 with a Fourier series with the firsts seventeen harmonics. The little dots are the data; the thick dashed line is the fit.

We can see that the phases are essentially all the same for all harmonics and for the two bands. The order of importance of the harmonics is 4, 8, 12 and 2 for both 450 and 850 μm. Harmonics 8 and 12 at 850 μm are approximately twice as much as those at 450 μm. This is in agreement when we compare visually the fits in Figure 12 (850) and Figure 7 (450). However, the ratio is higher for the second harmonic at 450 than at 850 μm.

Table 2: Parameters the cosine Fourier series fitted to the data with the SG HWP rotating at 120 rpm. The firsts seventeen harmonics were taken into account. The amplitude ratios listed as 0 below are equal or less than 0.04%.

n° harmonics	450 μm			850 μm		
	P_i	P_i / P_4 (%)	ϕ	P_i	P_i / P_4 (%)	ϕ
0	8.5e-3	1.2		8.8e-3	2.0	
1	4.9e-3	0.7	0.00°	1.1e-3	0.2	0.00°
2	-1.2e-2	1.6	1.00°	2.5e-3	0.6	1.04°
3	-4.3e-3	0.6	0.98°	1.2e-3	0.3	0.98°
4	0.73	100	1.02°	0.45	100	0.80°
5	-5.2e-3	0.7	0.98°	9.5e-4	0.2	0.98°
6	1.0e-3	0.1	1.00°	-1.4e-4	0	0.95°
7	-3.8e-5	0.0	1.00°	-2.7e-4	0	1.00°
8	5.7e-2	7.8	1.00°	0.06	13.4	1.07°
9	1.6e-3	0.2	1.00°	-1.6e-4	0	1.00°
10	1.0e-3	0.1	1.01°	-1.9e-4	0	0.99°
11	3.5e-4	0.0	1.00°	-1.7e-5	0	1.01°
12	1.2e-2	1.6	1.00°	0.014	3.1%	1.00
13	1.7e-4	0.0	1.00°	-3.5e-6	0	1.00°
14	-2.7e-4	0.0	1.00°	-2.0e-4	0	1.00°
15	-2.6e-5	0.0	1.00°	1.4e-5	0	1.00°
16	-4.5e-4	0.0	1.00°	3.1e-4	0	1.00°

When the half-wave plate is rotating at 300 rpm, the results are essentially the same than those at 120 rpm. Therefore, they are not given here.

3.2 Comparison with the Data from the Savini Paper

The SG HWP was measured in great details in the lab in Cardiff by the manufacturer. The set up insured that all reflections and standing waves were absorbed by a special absorbing material. These measurements are presented in synoptic figures in a published paper by Savini et al. (2009). The instrumental setup is displayed in their Figure 1. The goal of that paper was to present a new method to take into account in the data reduction of polarimetric data the precise characteristics of the HWP (any HWP) instead of assuming as is customary that it behaves like a perfect HWP with only the 4^{th} harmonic component being non-zero. Such a different behaviour is expected of from all achromatic HWPs since for those, the manufacturer tries to produce one-half wave retardation over a significant wavelength range by using many single HWP. In our case, 5 single blades were selected from a total of 12, and assembled with the proper orientation. Cement with the appropriative index of refraction was used, and the whole was coated in order to minimize losses.

We present figures to make a visual comparison of the measured values at 450 μm for the SG HWP rotating at 120 rpm with the standard fit of a single 4^{th} harmonic, the same as in Figure 7 above, but we now add also the curve determined by Savini et al (2009) using the many individual measurements made with their special set up. Measurements were taken at various frequencies and integrated across the two band passes. The case where the two polarizers are perpendicular to each other is used. The data over a full rotation of the HWP is presented in Figure 13. Figures 14 and 15 show a zoom of the same figure (13) so that details can be seen well. The Savini data have not been fitted to the Lethbridge measurements, but simply scaled and shifted in order to get a "good" fit by eye.

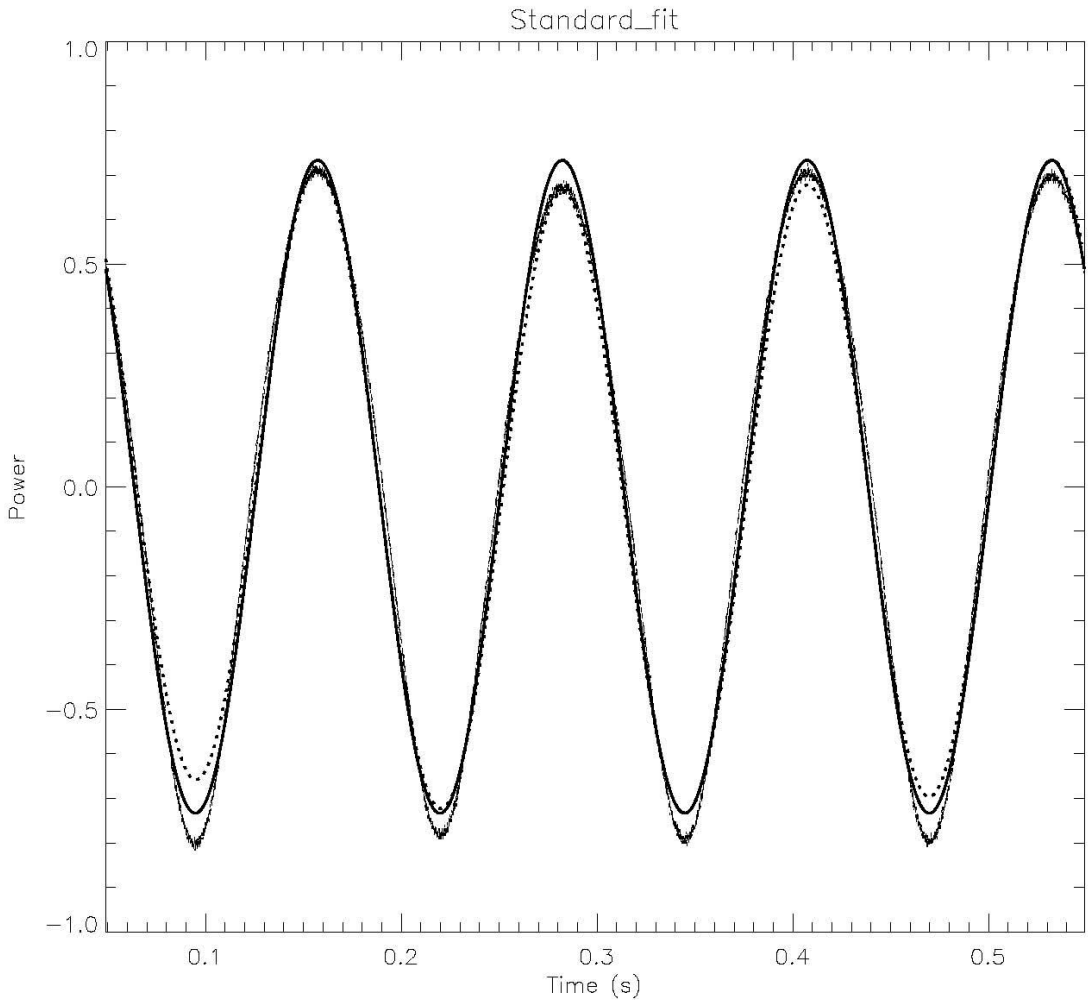

Figure 13. Same as Figure 7 for the SG HWP at 450 μm rotating at 120 rpm. The data points are the Lethbridge measurements, the full line is the standard 4th harmonic only fit, and the dotted line is the Savini curve as described in the text.

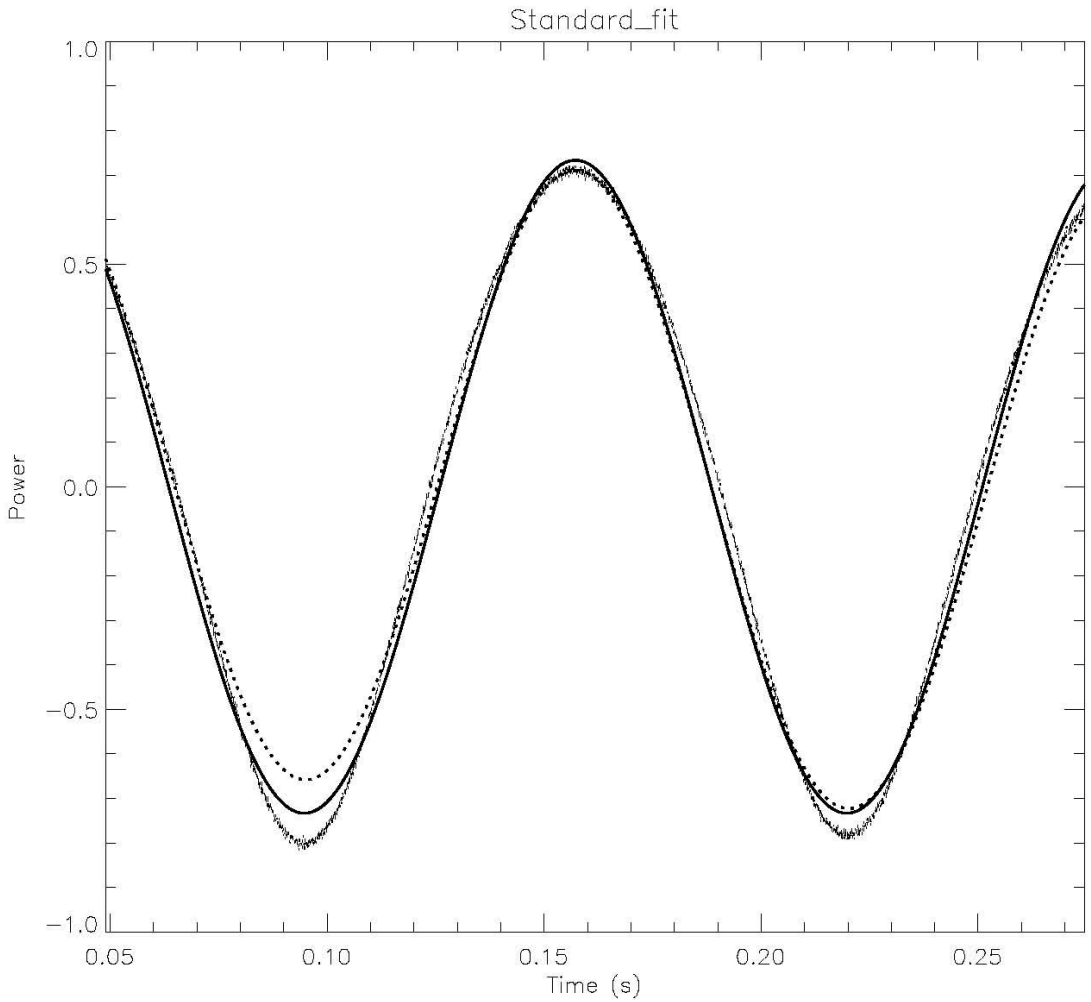

Figure 14. Enlarged view of a portion of Figure 13.

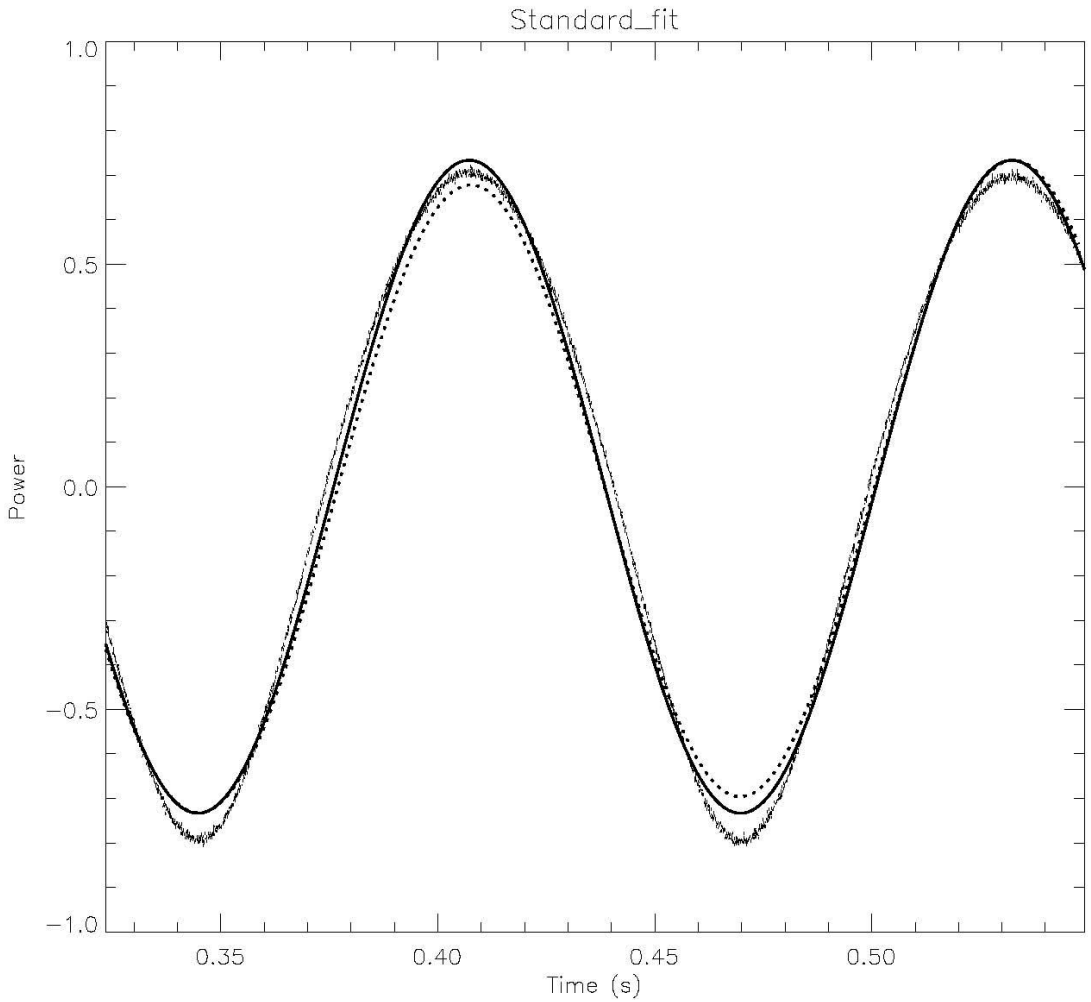

Figure 15. Enlarged view of another portion of Figure 13.

Figure 13 – 15 show that the deviations from the Lethbridge measurements are comparable for the standard fit and for the Savini data. In other words, the measurements in the lab in Lethbridge while the SG HWP was rotating give a reasonable representation of the real properties of the HWP as given by the Savini measurements.

We also compare the Savini measurements obtained with two polarizers when they are perpendicular and parallel to each other at 450 μm in Figure 16, and at 850 μm in Figure 17.

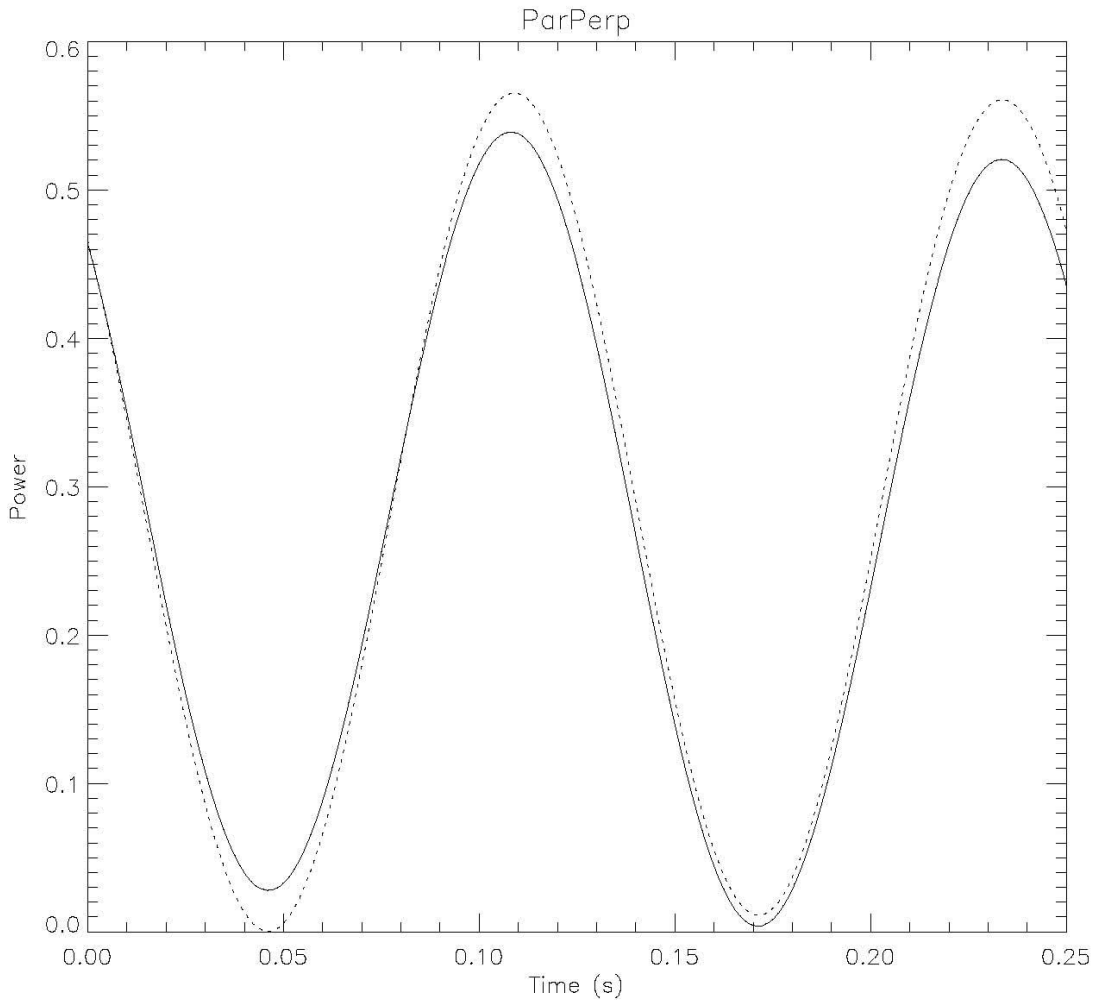

Figure 16. Comparison between the two Savini curves for the SG HWP between two polarizers which are parallel and perpendicular to each other, at 450 μm.

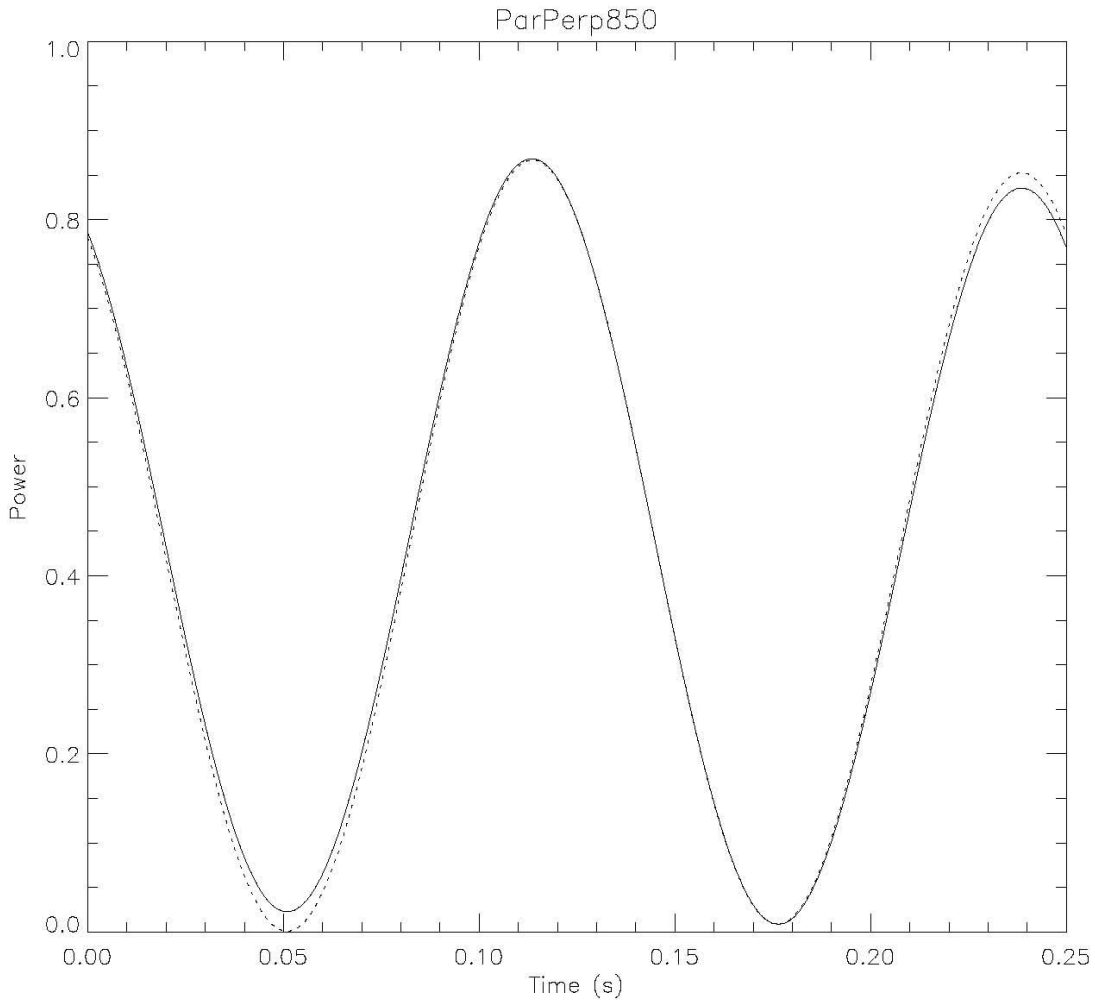

Figure 17. Same as Figure 12, but at 850 μm.

Figures 16 and 17 show that the SG HWP is not exactly symmetric. For example, the last two peaks (3 and 4) are not a reproduction of the peaks 1 and 2. This point is clearly visible on Figures 6 (450) and 10 (850). A perfect HWP would show two curves that coincide exactly.

In order to compare with the paper of Savini et al (2009) for the SG HWP, we fitted the data with the first five harmonics. This fit is plotted in Figure 8 for the 450 μm band. The parameters of the fits are given in Tables 3 and 4.

Table 3. Table 2 of Savini et al with the parameters for the first five harmonics, except the third one which was not included because it is not expected theoretically.

Table 2. Harmonic Fit Parameters for the Two SCUBA-2 Bands for a Polarized Source Aligned to the Detector Polarization

Parameter	450 μm	850 μm
P_0	0.2855	0.4304
P_1	4.2e-3	3.1e-3
P_2	6.2e-3	7.6e-3
P_4	0.2777	0.4273
ϕ_1	+257.0°	+245.3°
ϕ_2	+40.6°	+44.2°
ϕ_4	+56.7°	+53.2°

Table 4. Parameters of the fits that we determined, for comparison with the Savini results in Table 3 above. These fits have been done for the first 5 harmonics only.

Parameter	450 µm	850 µm
P_0	8.5e-3	8.8e-3
P_1	4.9e-3	1.1e-3
P_2	-1.2e-2	2.4e-3
P_3	4.3e-3	1.2e-3
P_4	-0.734	-0.45
ϕ_1	0.07°	3.63°
ϕ_2	0.04°	0.03°
ϕ_3	0.44°	-0.16°
ϕ_4	-0.03°	-0.03°

To help make a better comparison, we present the ratios of the amplitudes in Table 5.

Table 5. Ratios of the amplitudes.

Ratios	450 Savini	450 Lethb.	850 Savini	850 Lethb.
P_1 / P_4	1.52%	0.68%	0.73%	0.24%
P_2 / P_4	2.23%	1.63%	1.78%	0.53%
P_3 / P_4	-	0.59%	-	0.27%

We see that similar values are obtained for the amplitudes and their ratios for the different lower harmonics. However, the main difference between our results and those of Savini remain the difference in phases that Savini determined whereas our fits always gave essentially the same phase for all harmonics that were fitted, for fits with 5 and 17 harmonics.

The main difference in the instrumental setups concerns standing waves. Our setup is influenced by them, but not the Savini one which absorbs all reflections. The precision of the Savini measurements is probably somewhat higher than that of ours.

The 450 μm band used by Savini corresponds to the new, narrow 450 μm band used by SCUBA-2. The Lethbridge data presented here is for a 450 μm wide band which approximates the original 450 μm SCUBA-2 band. However, we do not expect any significant difference due to these similar, but not exactly the same, bands.

3.3 Half-Wave Plate

The results of Fourier fits with up to 17 harmonics in both pass bands are given in Table 6 for the first HWP. The figures are not given since they look very similar to those for the SG HWP. We note that harmonics 8 and 12 are more important for the HWP, just as for the SG HWP. However, after those, harmonics 1 (more at 450), 2, 3, 5 (more at 450), 6, 7 contribute to similar levels.

Table 6. Parameters of the cosine Fourier series fitted to the data with the HWP rotating at 120 rpm. The firsts seventeen harmonics were taken into account. The amplitude ratios listed as 0 below are less than 0.02%.

	450 μm			850 μm		
	P_i	P_i / P_4	ϕ	P_i	P_i / P_4	ϕ
0	0.47	116%		0.52	122%	
1	-3.1e-3	0.77%		-4.8e-4	0.11%	0.00°
2	1.7e-3	0.43%	0.00°	1.5e-3	0.36%	1.04°
3	-3.1e-3	0.78%	1.00°	-1.4e-3	0.33%	0.98°
4	-0.40		0.98°	0.43		0.80°
5	-2.7e-3	0.68%	1.02°	7.3e-4	0.12%	0.98°
6	1.6e-3	0.39%	0.98°	-9.6e-4	0.22%	0.95°
7	-1.2e-3	0.29%	1.00°	3.8e-4	0.90%	1.00°
8	-0.03	8.7%	1.00°	0.06	14%	1.07°
9	-8.9e-4	0.22%	1.00°	-9.24e-6	0%	1.00°
10	5.2e-4	0.13%	1.00°	-3.4e-4	0.08%	0.99°
11	-4.2e-4	0.11%	1.01°	-1.3e-5	0%	1.01°
12	7.1e-3	1.8%	1.00°	0.015	3.5%	1.00
13	-2.3e-4	0.06%	1.00°	9.3e-5	0.02%	1.00°
14	2.4e-4	0.06%	1.00°	-9.6e-5	0.02%	1.00°
15	-1.83e-6	0%	1.00°	-1.2e-5	0%	1.00°
16	-2.8e-4	0.07%	1.00°	9.7e-4	0.23%	1.00°

A comparison of Tables 2 (SG HWP) and 6 (HWP) shows that the two HWP have very similar characteristics. Harmonics 8 and 12 are the largest ones, after harmonic 4.

Summary and Conclusions

Thanks to this experiment, we can confirm that the vibrations problem does not appear anymore in the instrument. The response of the half-wave plate is very stable over time in all the tests that were made. The curves that were obtained are all very smooth and do not show any irregular bumps that characterized the vibrations noticed in 2007 and 2008.

Although the polarizers performed as expected, since we were able to carry out our tests with the two HWP, we were not able to determine quantitatively their properties. Unfortunately, we cannot also determine the transmission of the half-wave plates and the polarization efficiency of POL-2, due to the set-up of the experiment.

By comparing with a sine curve, we realize that standing waves are present to some level. This level is smaller than in the UWO June 2009 tests essentially because of averaging across the pass bands.

By fitting with a cosine Fourier series, higher harmonics than the expected 4^{th} harmonic for a perfect HWP, were found. Harmonics 8 and 12 are nearly two times smaller for the 450μm band than for the 850μm band. The separation of the effects of standing waves and of the real properties of the two HWP cannot be done in a reliable way. However, a comparison with the Savini paper, which was done with a set up which absorbs all reflections (therefore without standing waves), shows very similar results for harmonics up to 4 for the SG HWP. The other HWP shows very similar properties to those of the SG HWP and therefore can be a very good spare HWP.

The many Fourier series fits done with the tests data reported here, and the comparison with the Savini paper for the SG HWP, show clearly that it would be advantageous in the data reduction process to take into account the real characteristics of the achromatic SG HWP, instead of assuming, as is usually done, that it behaves like a perfect HWP.